Brno University of Technology
Faculty of Mechanical Engineering
Institute of Machine and Industrial Design

Vysoké učení technické v Brně
Fakulta strojního inženýrství
Ústav konstruování

EXPERIMENTAL INVESTIGATION OF THE ROLLING CONTACT FATIGUE BEHAVIOR OF TOROIDAL BEARINGS USING ACOUSTIC EMISSION

EXPERIMENTÁLNÍ VÝZKUM ÚNAVOVÉHO CHOVÁNÍ TOROIDNÍCH LOŽISEK PŘÍ VALIVÉM KONTAKTU S VYUŽITÍM AKUSTICKÉ EMISE

Eng. Housam Mohammad
Author
Autor práce

doc. Ing. Pavel Mazal, CSc.
Supervisor
Vedoucí práce

Dissertation Thesis
Dizertační práce

Brno 2024

Brno University of Technology
Faculty of Mechanical Engineering
Institute of Machine and Industrial Design

Vysoké učení technické v Brně
Fakulta strojního inženýrství
Ústav konstruování

EXPERIMENTAL INVESTIGATION OF THE ROLLING CONTACT FATIGUE BEHAVIOR OF TOROIDAL BEARINGS USING ACOUSTIC EMISSION

EXPERIMENTÁLNÍ VÝZKUM ÚNAVOVÉHO CHOVÁNÍ TOROIDNÍCH LOŽISEK PŘÍ VALIVÉM KONTAKTU S VYUŽITÍM AKUSTICKÉ EMISE

Eng. Housam Mohammad
Author
Autor práce

doc. Ing. Pavel Mazal, CSc.
Supervisor
Vedoucí práce

Dissertation Thesis
Dizertační práce

Brno 2024

STATEMENT

I hereby declare that I have written the PhD thesis “Experimental investigation of the rolling contact fatigue behavior of toroidal bearings using acoustic emission” on my own according to the advice of my supervisor doc. Ing. Pavel Mazal, CSc. and using the sources listed in the references.

Brno …… ……

Ing. Housam Mohammad

BIBLIOGRAPHICAL REFERENCE

MOHAMMAD, Housam. *Experimental Investigation of the Rolling Contact Fatigue Behavior of Toroidal Bearings Using Acoustic Emission*. Brno, 2024. 90 p., PhD thesis. Brno University of Technology, Faculty of Mechanical Engineering, Institute of Machine and Industrial Design. Supervisor doc. Ing. Pavel Mazal, CSc.

ACKNOWLEDGEMENT

I would like to express my deepest appreciation to my supervisor, doc. Ing. Pavel Mazal, CSc. for his invaluable guidance, support, and encouragement throughout this journey. His insights and expertise have been instrumental in shaping this dissertation.
I am also grateful to my colleagues at the Institute of Machine and Industrial Design, especially those who have become much more than colleagues, such as dr. Frantisek Vlasic, with whom I have now a lifelong relationship in my personal and professional life. Your collaboration, support, and encouragement have made this journey more enriching and fulfilling.

My heartfelt thanks go to my mother, father, and brothers for their unwavering support and understanding. Your encouragement and support have been a constant source of strength for me along the way. Lastly, a special big thanks to my wife and daughter. Your presence in my life, your patience, and your love have been my greatest support. This achievement would not have been possible without you.
Thank you all.

ABSTRACT

Bearings are an essential part of most types of machines and their failure is the main reason for the machines' failure. The failure of a bearing when it is properly mounted, aligned, lubricated, maintained and not overloaded is attributed to the so-called rolling contact fatigue, which is a degradation phenomenon as a result of cyclic, localized loading. It results in early fatigue damage called crack-like flaws, which takes the shape of surface originated pitting and/or subsurface originated spalling.

This work concentrated on a specific type of bearing that has gained increased popularity since its introduction, which is the Toroidal Roller bearing. The main advantage of this type of bearing is its ability to accommodate axial misalignment and angular tilting together. The successful application of toroidal bearings on the main shaft of wind turbines was one of the leading incentives to study this type of bearing experimentally in a laboratory and on-site using acoustic emission as a primary nondestructive testing technique.

There is a big body of research that documents the use of acoustic emission as a successful NDT tool for detecting and predicting the initiation of defects in bearings. Most of the studies used time-domain feature extraction in AE, which was proved to be useful to a certain extent. In the early stage of this work, time-domain parameters were used for comparison reasons, as well as vibration and temperature. More concentration was then put on the frequency-domain of AE signal, especially the use of dominant frequency of AE hits as a parameter, since it has been proven recently, by many studies in geotechnical engineering field, to give close correlation with the defects in the monitored material.

The condition monitoring of toroidal bearing was not confined to laboratory tests, but extended to long measurements on-site where they were installed. For that purpose, a wireless remote condition monitoring system was developed. For better visual representation of the dominant frequency representation, the concept of DF maps was introduced, and a number of Matlab snippets codes were developed to automate and facilitate its creation. Collecting DF maps in a single graph for specific time intervals and the ability to statically analyze them gave an opportunity to quantify the defects, which would be a solid foundation for any future work.

KEYWORDS

Acoustic Emission, Non-Destructive Testing, Condition Monitoring, Toroidal Roller Bearings, Rolling Contact Fatigue, Dominant Frequency.

ABSTRAKT

Ložiska jsou nezbytnou součástí většiny mechanismů a jejich selhání je hlavní příčinou poruch strojů. Poškození ložiska, pokud je správně namontováno, seřízeno, mazáno, udržováno a není přetěžováno, se připisuje vzniku tzv. kontaktní únavy, což je degradační proces vznikající v důsledku cyklického, lokalizovaného zatížení. Jejím důsledkem může být poškození, které má podobu důlků vzniklých na povrchu, nebo dalších strukturních defektů, vznikajících pod zatěžovaným povrchem.

Tato práce se soustředila na specifický typ ložiska, který si od svého zavedení do praxe získal zvýšenou popularitu, a to toroidní válečkové ložisko. Hlavní výhodou tohoto typu ložisek je jejich schopnost současně vyrovnávat axiální nesouosost a případné úhlové naklápění. V důsledku vysokých zatížení (momentů) na hlavní hřídeli a náhlým poruchám ložisek bylo jedním z hlavních podnětů k experimentálnímu studiu tohoto typu ložiska v laboratoři a v provozu s využitím akustické emise jako primární metody nedestruktivní diagnostiky.

Existuje velké množství výzkumů, které dokumentují použití akustické emise jako úspěšného nástroje nedestruktivního zkoušení pro predikci a detekci iniciace defektů v ložiscích. Většina studií používala pro znázornění časové průběhy základních parametrů signálu AE, která se ukázala být do jisté míry užitečná. V počáteční fázi této práce byly z důvodů porovnání použity parametry v časové oblasti společně s měřením úrovně vibrací a změny teploty. Větší pozornost pak byla věnována charakteristikám AE ve frekvenční oblasti, zejména použití dominantní frekvence (DF) hitů AE, protože se v poslední době mnoha studiemi v oblasti geotechnického inženýrství prokázalo, že poskytuje úzkou korelaci s aktivními defekty ve sledovaném materiálu.

Hodnocení stavu toroidních ložisek se neomezilo pouze na laboratorní zkoušky, ale rozšířilo se na dlouhodobá měření přímo v provozu, kde byla toroidní ložiska instalována. Za tímto účelem byl vyvinut bezdrátový systém dálkového monitorování stavu. Pro lepší vizuální znázornění zastoupení DF byl zaveden koncept DF map a pro automatizaci a usnadnění jejich tvorby byla vyvinuta řada kódů v Matlabu. Shromáždění map DF do jednoho grafu pro určité časové intervaly a možnost jejich statistické analýzy poskytly rozšířené možnosti hodnocení technického stavu ložiska a v případě dalšího výzkumu také predikci zbývající životnosti.

KLÍČOVÁ SLOVA

Akustická emise, nedestruktivní testování, monitorování stavu, toroidní válečková ložiska, kontaktní únava, dominantní frekvence.

CONTENTS

1 INTRODUCTION

For the last two decades, toroidal roller bearings (TRBs) have been getting an increasing amount of attention especially after the end of the patent of their main introducer, SKF ©, where TRB was invented. Many companies started production and development of this type of bearing that provides properties no other bearing can offer, thanks to its unique design. The main advantage of TRB is its ability to tolerate axial with angular misalignment at the same time, which makes it ideal for applications where high-magnitude vibration is a real concern. Since TRB can accommodate large scale loads, it found attractive applications in many heavy industries like paper production and casting, but more recently it has proved efficient in its application as a non-locating bearing on the main shaft of wind turbines. On the other hand, the fact that TRBs cannot take pure axial loading led to some restrictions and limitations to its use.

For more than half a century, the term Rolling Contact Fatigue (RCF) has been used to represent the phenomenon that expresses the failure driven by crack propagation caused by near-surface alternating stress field, which it is a very unfavorable phenomenon. RCF occurs in surface layers by repeated contact of two non-conformal surfaces where contact bodies are contacted by mutual contact at a point, on a straight line or along a curve. Since the surfaces of the bodies meet in a small area, highly localized contact pressures occur. In pure rolling, the main stresses are compressive. Shear stresses reach their maximum at a certain depth below the surface. In these places, cracks arise and grow, which penetrate the surface and lead to peeling or crumbling of small volumes of material. This creates small cavities, which are collectively referred to as pitting, while the subsurface initiated RCF leads to the so-called spalling.
The main parameters influencing contact fatigue include Hertz stress, number of cycles, surface quality, hardness, temperature, and presence of lubricants.

Many methods have been suggested and used over the years for detecting and predicting the defects in bearings that are results of RCF. Most of them are non-destructive methods because of the many advantages they offer and because of their availability.
One of the newest and most sophisticated NDT methods is Acoustic Emission technique (AE) which depends on capturing and processing acoustic transient waves. Those are elastic stress waves caused by local changes in the material during loading. Acoustic waves propagate from the place of origin of the defect to the surface of the material, so we can locate the defects and monitor the course of their origin by fixing an AE sensor (transducer) on the surface.

AE has been one of the main NDT techniques proven to be very effective in detecting and even predicting RCF in bearings. However, most of the AE parameters used to prove that were time-domain parameters. There has been an increase focus on the use of AE's frequency-domain parameters recently, but not in mechanical applications, and certainly not in bearings. To compensate for that gap, the focus in the second half of this work was directed towards the frequency-domain parameters, especially the dominant frequency of AE hits. Building upon what has been achieved in other fields for the application of AE on CM of TRBs has showed promising results, which can form the basis of a new way of approaching this subject.

2 STATE OF THE ART

The problem of RCF in bearings has been one of the main subjects of research for the last half century, since it has been identified as the main source of defects in bearings if the bearing is properly mounted, aligned, lubricated, maintained and not overloaded [1]. RCF appears through subsurface originated spalling and/or surface originated pitting and micro-pitting [2].
There are several conditions where RCF differs from classical fatigue [3]:

1. The state of stress is governed by the Hertzian contact theory is complex because the nature of non-conformal contacts is multiaxial.
2. In the case of non-conformal contacts, there is also a high hydrostatic (volumetric) stress component, which contains uniaxial stresses, but not shear stresses.
3. There is a non-proportionality in the loading history at a point below the surface. Which means that the stress components do not rise and fall with time in the same proportion.
4. RCF is much localized, i.e., it occurs in a very small volume of stressed material. Typical contact sizes are of the order of 200–1000 µm.
5. The development of residual stresses and localized plastic deformation play a crucial role in the fatigue damage.

There are many methods that have been developed to capture failure information with the help of a wide variety of sensors and equipment. Those methods are called data acquisition techniques [4]. One of the most popular ones is vibration. The signal is collected using accelerometers, velocity sensors and displacement sensors. Its biggest advantages are the wide frequency range, which is about [1-30 kHz], and it is cheap and easy to use. One of the problems with vibration is that when the monitored system has fast pressure pulses with a period of around 5 µs, the normal accelerometers may not react accurately because their natural frequencies are not high enough. Here comes the second technique, which is acoustic emission, where the AE transducer works in the frequency range from 20 kHz to 1 MHz. AE acquisition depends on the phenomenon of radiation of elastic wave generation in solids under stress. The fast release of strain energy is transmitted in the form of elastic waves which can be collected by the AE transducer [5]. This is considered a big advantage of AE over vibration in the CM of bearings.
Other techniques include Lubricant analysis (or debris analysis), microscopic analysis, shock pulse meter (SPM), ultrasonic testing, temperature monitoring, sound analysis and jerk measurement, with each of them has its pros and cons.
For this literature review, the focus will be first on AE as the NDT method of choice for this work, because of the many advantages it can provide, and because of its suitability for this specific investigation. The use of AE in RCF detection will be explored, then the new trend of using AE frequency-domain parameters, especially the dominant frequency, and finally the place of toroidal roller bearings in the literature.

2.1 Acoustic Emission

Historically, it has been considered that AE history started in 1950 with the publication of Kaiser's dissertation (1950). Kaiser, J. tested tensile specimens of metallic materials, recording AE signals. He discovered a famous irreversibility, which is now called the Kaiser effect. Then B. H. Schofield reexamined Kaiser's work, and published his pioneering work entitled "Acoustic Emission" in 1961. This is the first use of the terminology of Acoustic Emission in history. Following Schofield's study, A. T. Green and H. L. Dunegan were known to develop standard procedures and devices [6].

In 1982 Yoshioka T. and Fujiwara T. published their famous paper on the use of AE source locating system for the study of RCF [7]. And even though it was a short communication paper it is one of the most cited papers in this field because of its importance. They introduced an AE source locating system and confirmed the coincidence between positions of AE sources and the sources of failure. They concluded that the system was able to locate failure positions precisely. They both published another work in 1987 [8], where they measured the propagation initiation and the propagation time of RCF using AE and vibration. They reported that AE parameters can identify bearing defects before they appeared in the vibration acceleration range. Since then, many studies have been dedicated to study RCF defects, especially in bearings, using AE.

Physically, failure takes place due to the release of stored strain energy, nucleating cracks and generating elastic waves. Elastic waves due to crack nucleation are detected as AE waves, which propagate inside the material and are detected by an AE sensor on the surface. Although recent AE devices are fully digitized, detection systems are basically of analog type [6] [9].

Acoustic emission (AE) is the phenomenon of transient elastic wave generation in materials under stress. When the material is subjected to stress at a certain level, a rapid release of strain energy takes place in the form of elastic waves which can be detected by transducers placed on its surface. Plastic deformation and growth of cracks are among the main sources of acoustic emission in metals [6] [5] [10].

AE monitoring has an added advantage that it can even detect the growth of sub-surface cracks whereas vibration monitoring can normally detect a defect when it appears on the surface [10]. Since AE signals are weak, they are normally amplified by pre-amplifier and main amplifiers. The signal-to-noise ratio of equipment shall be low, and the amplifiers often provide more than 1000 times gain. Lately, it is set to normally 100 times or so. As discussed above, the band-pass filter is successfully employed to eliminate the noises. In engineering materials, the band width from several kHz to 1 MHz is recommended in the measurement [6].

Acoustic emission (AE) was originally developed for non-destructive testing of static structures, however, over the years its application has been extended to health monitoring of rotating machines and bearings.

The many research works of Jacobs L. J. et al. [9] [11] [12] at the beginning of the 1990s have also influenced the advancement of AE experimental usage and helped in defining its analytical characterization. They were able to verify their suggested analytical procedure, and they validated the effectiveness of the integral equation method that they used by confirming the agreement with the experimentally measured AE signals.

As the stress waves propagate from the AE source they are influenced by a variety of factors. These factors include propagation velocities, attenuation, reflection, refraction, discontinuities and the geometry of the material. When the stress waves reach the surface, they cause it to vibrate, and the vibration can be measured. The small surface displacements are measured using sensitive transducers which respond to surface displacements to the order of several picometers ($=10^{-12}$ m). Several types of transducers can be used for this: piezoelectric, capacitance, electromagnetic and optical. The last two are non-contact, but electromagnetic transducers are considerably less sensitive than piezoelectric transducers. Optical sensors, e.g. laser, are free of resonance and can be absolutely calibrated by measuring the correct amplitude of the AE [13].

Piezoelectric transducers are the most popular and are either of a broadband or a resonance type. The sensitivity spectra of them is determined by the ISO standard 24543:2022 [14].

The transducers are made from special ceramic, usually Porous Lead Zirconate Titanate (PZT). Figure 1 shows a schematic view of a piezoelectric transducer and how an AE is converted into an electric representation. The transducers are fixed firmly on the surface of the material and the micro vibration is transmitted to the PZT element inside the transducer through a wear plate. The PZT element generates an electric signal when it vibrates. So, the transducer's signal is a voltage-time representation of the displacement-time wave that it detects.

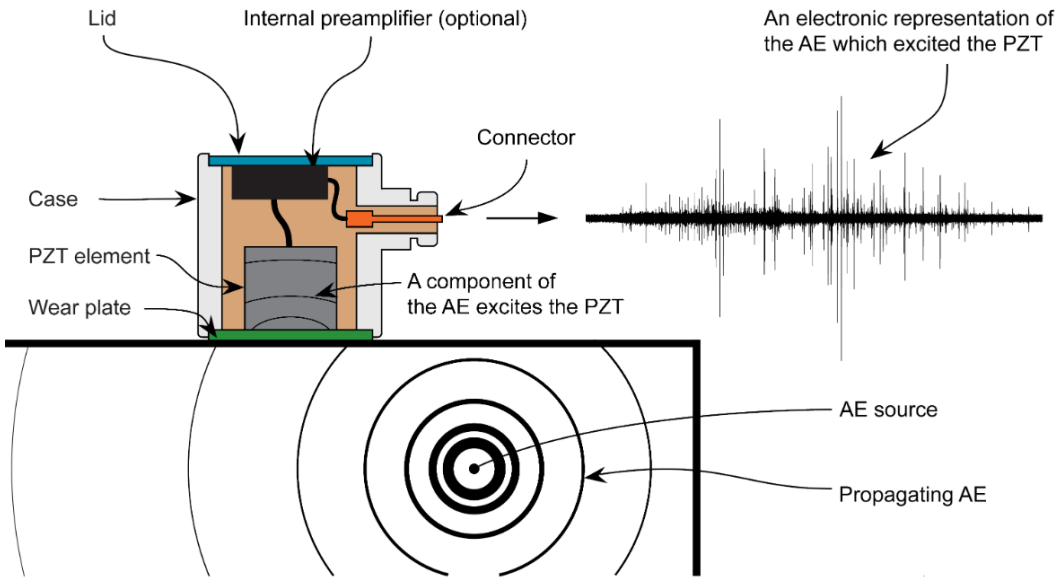

Figure 1. An illustration of a typical resonant piezoelectric AE transducer and how an AE is converted into an electric representation [15]

Because of its importance and the continuous increase of its vital use in NDT, AE has been addressed by the International Standardization Organization (ISO) in many standards, including the Vocabulary standard [16], where most of AE parameters' definitions are specified. The number of AE methodology and general evaluation criteria for testing different types of materials is increasing every year. This includes standards, such as ISO 18249:2015, ISO 19835:2018, ISO 16836:2019, and ISO 19016:2019.

2.1.1 Basic features/parameters of AE Signal

The total activity of AE, or the number of "hits" that are recorded by AE sensor, is indicative of the phenomenon that is being monitored. In addition, the shape of the waveform yields important information relative to the source of the emission. The early AE systems, not having the capacity for recording full waveforms of thousands of points, extracted only a set of features indicative of the waveform shape which were also powerful for source characterization. Therefore, many parameters are used for the quantification of the waveform. The basic ones are shown in Figure 2 and are defined below.

First, we define two important terms:

The Threshold: It is a predefined voltage that must be overpassed by the incoming waveform in order to trigger the acquisition. It also helps to avoid low amplitude noise signals.

AE Hit: a signal that exceeds the threshold and causes a system channel to record data.

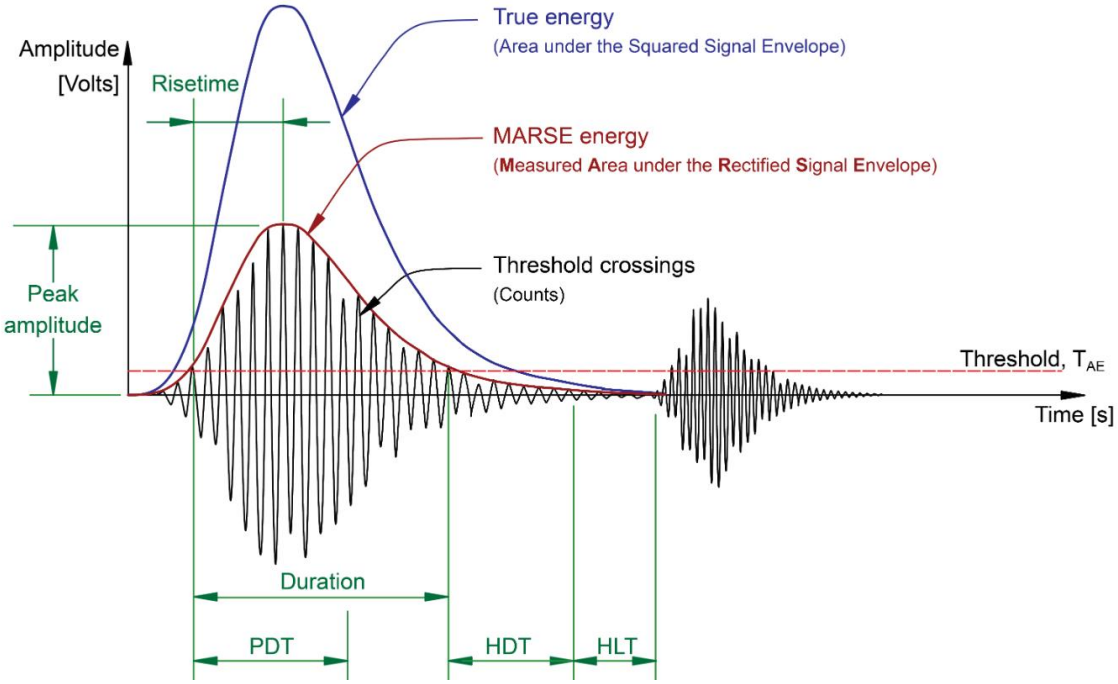

Figure 2. Features of an AE Burst [17]

Where HDT is Hit Definition Time, HLT is Hit Lockout Time, and PDT is the Peak Definition Time. The HDT specifies the maximum time between threshold crossings, so if no crossing occurs during this time then the hit will be considered as ended. If the HDT is set too high, then the system may consider two or more hits as one. The PDT specifies the time allowed, after a hit has been detected, to determine the peak value. If the PDT is set too high, false measurements of peak value are likely to occur. The HLT specifies the time which must pass after a hit has been detected before a new hit can be detected. If the HLT is set too high then the system may not capture the next AE and if it is set too low then the system may capture reflections and late arriving component of the AE as hits [18] [13].

Some of the basic AE parameters are:

2.1.1.1 Amplitude

The amplitude is the greatest measured voltage of the signal, corresponding to the greatest surface displacement, and is closely related to the magnitude of the source event.

2.1.1.2 Ring Down Counts

Ring down counts (sometimes simply referred to simply as counts) are a count of the number of the times during a single event the signal exceeds the threshold. The number of counts depends upon the transducer frequency, the damping characteristics of the transducer, the damping characteristics of the structure and the pre-defined threshold.

2.1.1.3 MARSE

The Measured Area of the Rectified Signal Envelope (MARSE) is a regularly used parameter in acoustic emission testing. MARSE represents the energy content of a signal although different system suppliers use variations in the method of calculation.

2.1.1.4 Duration

Duration is measured as the period between the first and last threshold crossings. In a similar manner to Counts, the duration can be used to differentiate between sources of acoustic emissions and therefore act as a filter.

2.1.1.5 Rise Time

The rise time is a measure of the time difference between the first threshold crossing and the peak amplitude. It can be used to classify the type of fracture or, as with counts and the duration, eliminate noise signals.

2.1.1.6 Decay Time

It is simply the measure of time difference between the peak amplitude of the signal and the final threshold crossing.

2.1.1.7 Energy

AE energy is generally defined as a measured area under the rectified signal envelope (MARSE). The term “signal strength” is defined the same way. The energy is preferred to interpret the magnitude of source event over counts because it is sensitive both to the amplitude and the duration, and less dependent on the voltage threshold and operating frequencies. The “Absolute energy” comes from the integration of the rectified waveform envelope squared, is measured in “attoJ” and is considered analogous to the actual energy freed from the source:

$$E_{abs} = \int_0^{t_1} V^2(t)dt \qquad (1)$$

Where the waveform starts at time t_0 and ends at t_1.

2.1.1.8 Average Frequency

It is calculated in time domain as the ratio of the total number of counts over the duration of the waveform in kHz.

AE waveforms can be recorded readily as well as the parametric features. Thus, waveform-based features as peak frequency (PF) and frequency centroid or central frequency (CF) are additionally determined in real time from the fast Fourier transform (FFT) of recorded waveforms. AE parametric features are thus extracted and provide useful information to correlate with the failure behavior of materials. The first (PF) is the frequency with the highest magnitude in the FFT and the latter (CF) is the centroid of the FFT. Which is given by:

$$CF = \frac{\int_0^f fH(f).df}{\int_0^f H(f).df} \tag{2}$$

Where f is the frequency, and $H(f)$ the magnitude of the FFT.

2.1.2 Brief Definition of AE signal features:

Most of the features used to describe AE signal are denoted by the extreme values, derived from the signal in time-domain or frequency-domain. For example, the root mean square of the signal "AE_{RMS}" and the average signal level "AE_{ASL}" values are used in the same way as in are used in electrical engineering, where they are used to describe the effective voltage within a characteristic time interval. In the frequency domain, the "Frequency centroid" can be understood as additional information on the characteristic average frequency of the signal and is not equal to the "Peak/Dominant Frequency" as shown in Figure 3. The Dominant Frequency is highly efficient feature for discrimination of AE signals, since it is very discrete [18].

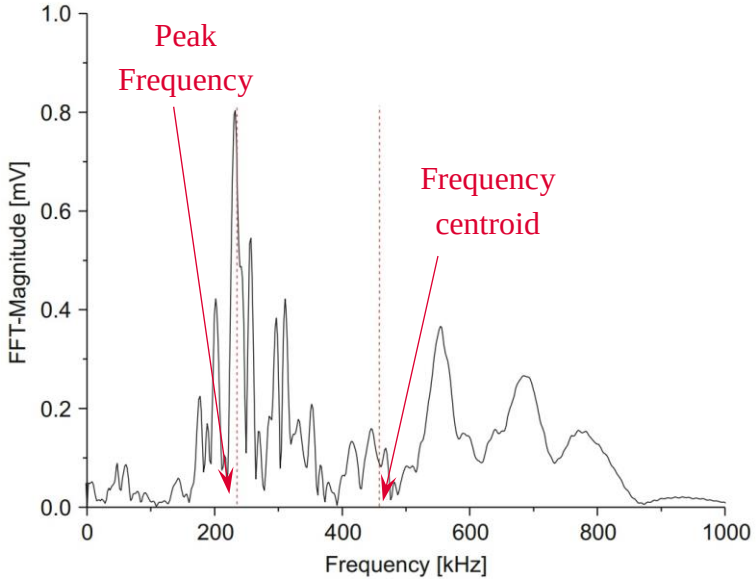

Figure 3. The frequency spectrum of an AE hit [18].

Feature	Definition	Unit
Amplitude	$\mathrm{dB}_{AE} = 20\log(U_{\max}/1\mu\mathrm{V}) - \mathrm{dB}_{\mathrm{preamplifier}}$	[dB]
Counts	N_{AE}	[#]
Duration	t_{AE}	[µs]
Rise time	$t_0 - t_{\mathrm{peak}}$	[µs]
Counts to peak	N_{peak}	[#]
Root mean square (RMS)	$\mathrm{RMS} = \sqrt{\frac{1}{T_{\mathrm{RMS}}}\int_{t_0}^{t_0+T} U^2(t)\mathrm{d}t}$ with a characteristic time T_{RMS} for averaging ranging from 10 to 1000 ms	[mV]
Average signal level (ASL)	$\mathrm{ASL} = \sqrt{\frac{1}{T_{\mathrm{ASL}}}\int_{t_0}^{t_0+T} \left(20\log(U(t)/1\mu\mathrm{V}) - \mathrm{dB}_{\mathrm{preamplifier}}\right)\mathrm{d}t}$ with a characteristic time T_{ASL} for ranging from 10 to 1000 ms	[dB]
Average frequency	$\langle f \rangle = N_{\mathrm{AE}}/t_{\mathrm{AE}}$	[Hz]
Reverberation frequency	$f_{\mathrm{rev}} = \frac{N_{\mathrm{AE}} - N_{\mathrm{peak}}}{t_{\mathrm{AE}} - t_{\mathrm{peak}}}$	[Hz]
Initiation frequency	$f_{\mathrm{init}} = \frac{N_{\mathrm{peak}}}{t_{\mathrm{peak}}}$	[Hz]
Rise angle	$\phi_{\mathrm{rise}} = \tan\left(\frac{U_{\max}}{t_{\mathrm{peak}}}\right)$	[rad]
Decay angle	$\phi_{\mathrm{decay}} = \tan\left(\frac{U_{\max}}{t_{\mathrm{AE}} - t_{\mathrm{peak}}}\right)$	[rad]
Absolute energy	$W_{\mathrm{AE}} = \int_0^{t_{\mathrm{AE}}} \frac{(U(t))^2}{10\mathrm{k}\Omega}\mathrm{d}t$ with 10kΩ input impedance of the recording equipment	[aJ]
Peak frequency	f_{peak}	[Hz]
Frequency centroid	$f_{\mathrm{centroid}} = \frac{\int f \cdot \tilde{U}(f)\mathrm{d}f}{\int \tilde{U}(f)\mathrm{d}f}$	[Hz]
Weighted peak frequency	$\left\langle f_{\mathrm{peak}} \right\rangle = \sqrt{f_{\mathrm{peak}} \cdot f_{\mathrm{centroid}}}$	[Hz]
Partial power	$\int_{f_1}^{f_2} \tilde{U}^2(f)\mathrm{d}f / \int_{f_{\mathrm{start}}}^{f_{\mathrm{end}}} \tilde{U}^2(f)\mathrm{d}f$ Frequency range of interest $[f_1;f_2]$ Frequency range of investigation $[f_{\mathrm{start}};f_{\mathrm{end}}]$	[%]

Where:

Feature	Definition	Unit
t_0	Time of first threshold crossing (arrival time)	[s]
N_{AE}	Number of threshold crossings	[#]
t_{AE}	Time between first and last threshold crossing of signal	[µs]
U_{max}	Maximum signal voltage	[mV]
t_{peak}	Time of maximum signal voltage	[µs]
f_{peak}	Frequency of maximum signal contribution	[Hz]
N_{peak}	Number of threshold crossings between t0 and t_{peak}	[#]

2.1.3 AE Modes

Acoustic emission signals can be characterized as continuous, burst or a combination of both sometimes referred to as mixed emission; this distinction was first made by Kaiser in his influential work on AE.

2.1.3.1 Continuous Emission

Continuous emissions are typically low energy emissions which occur when friction mechanisms or dislocation movements occur on or within a structure and do not display any visually obvious features in the time domain. The amplitude of the emission increases with applied load. Noise can also be a component attributing to a signal exhibiting continuous emission. The monitoring of continuous emission is suited to the detection and analysis of signals produced by plastic deformation in ductile materials, stress corrosion cracking and creep. It has been suggested that this type of emission is best measured with RMS or energy rate measuring circuitry; parameters which are calculated over the entire signal for a predefined period.

2.1.3.2 Burst Emission

Burst emission signals have definite start and end points with distinct peaks of significantly larger amplitude than the background noise. Such bursts tend to be no longer than a few hundredths of a second long. Deformation mechanisms which tend to exhibit burst type emissions include the fracture of non-metallic inclusions, breakage of corrosive products or crack propagation in brittle materials. Impact, which is particularly relevant when monitoring bearing damage, can also be a source of burst emissions. Situations may occur where burst and continuous emissions are present creating mixed emissions.

2.1.4 AE Source Location Techniques

2.1.4.1 Multi-Channel Source Location Techniques:

Locating the source of significant acoustic emissions is the main goal of an inspection. Although the magnitude of the damage may be unknown after AE analysis, follow up testing at source locations should provide the answers. Most AE systems are capable of using multiple sensors/channels during testing, allowing them to record a hit from a single AE event. The AE systems can be used to determine the location of an event source. As hits are recorded by each sensor/channel, the source can be located by knowing the velocity of the wave in the material and the difference in hit arrival times among the sensors, as measured by hardware circuitry or computer software. By properly spacing the sensors in this manner, it is possible to inspect an entire structure with relatively few sensors.

Source location techniques assume that AE waves travel at a constant velocity in a material. However, various effects may alter the expected velocity of the AE waves (e.g. reflections and multiple wave modes) and can affect the accuracy of this technique. Therefore, the geometric effects of the structure being tested, and the operating frequency of the AE system must be considered when determining whether a particular source location technique is feasible for a given test structure.

2.1.4.2 Linear Location Technique

Several source location techniques have been developed based on this method. One of the commonly used computed-source location techniques is the linear location principle shown in Figure 4. Linear location is often used to evaluate struts on truss bridges.

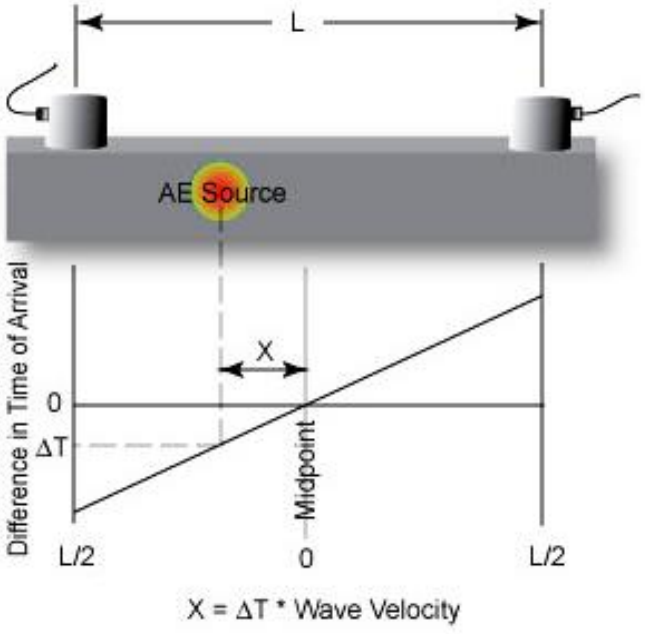

Figure 4. The principle of linear location technique of AE source [6]

When the source is located at the midpoint, the time of arrival difference for the wave at the two sensors is zero. If the source is closer to one of the sensors, a difference in arrival times is measured. To calculate the distance of the source location from the midpoint, the arrival time is multiplied by the wave velocity. Whether the location lies to the right or left of the midpoint is determined by which sensor first records the hit. This is a linear relationship and applies to any event sources between the sensors.
Because the above scenario implicitly assumes that the source is on a line passing through the two sensors, it is only valid for a linear problem. When using AE to identify a source location in a planar material, three or more sensors are used, and the optimal position of the source is between the sensors. Two categories of source location analysis are used for this situation: zonal location and point location.

2.1.4.3 Zonal Location Technique

As the name implies, zonal location aims to trace the waves to a specific zone or region around a sensor. This method is used in anisotropic materials or in other structures where sensors are spaced relatively far apart or when high material attenuation affects the quality of signals at multiple sensors. Zones can be lengths, areas or volumes depending on the dimensions of the array. A planar sensor array with detection by one sensor is shown in the upper right figure. The source can be assumed to be within the region and less than halfway between sensors.

2.1.4.4 Point Location

In order for point location to be justified, signals must be detected in a minimum number of sensors: two for linear, three for planar, four for volumetric, as shown in Figure 5. Accurate arrival times must also be available. Arrival times are often found by using peak amplitude or the first threshold crossing. The velocity of wave propagation and exact position of the sensors are necessary criteria as well. Equations can then be derived using sensor array geometry or more complex algebra to locate more specific points of interest.

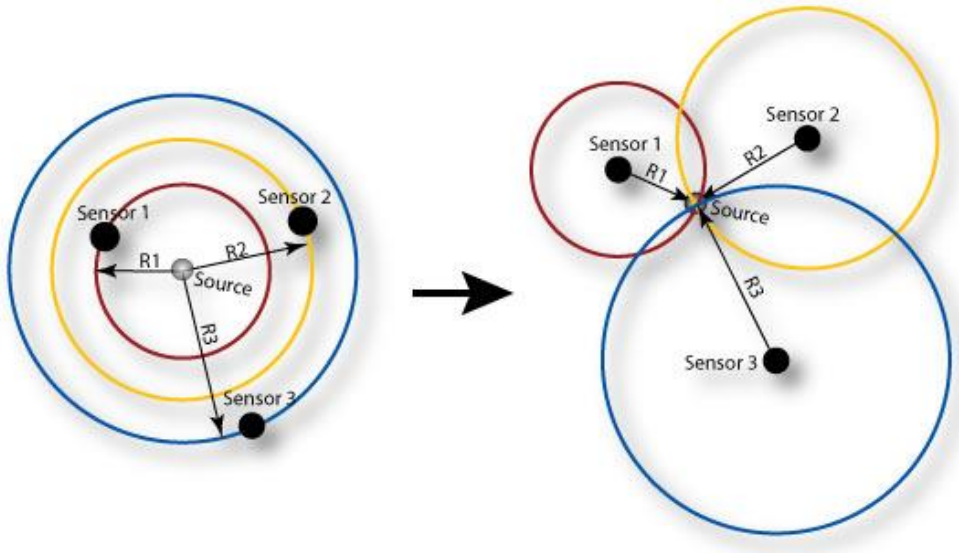

Figure 5 - Two geometrical methods to locate the source point in a plane using 3 sensors [13].

2.2 Application of AE in RCF detection

As mentioned before, the first research attempt to apply AE successfully in the detection of rolling contact fatigue in bearings was carried out by Yoshioka T. and Fujiwara T. [7] where they introduced a new AE source locating system. They concluded that AE can be used successfully to detect RCF process that is related to bearing fatigue failure. In 1987 they published their second paper [8] with this regard, where they studied the propagation initiation and propagation time of RCF cracks by observations from the AE signal combined with vibration signal. Other research attempts started to increase since the beginning of the 1990s.
Yoshioka T. and Mano H. [19] then studied the relationship between AE source position and spalling (which is the advanced level of pitting where bigger pits appear on the raceways) position in radial rolling bearings. The method that they used was able to locate the AE source positions within ± 1 address of the spalling positions. And in another paper Mano, Yoshioka et al. [20] investigated the relationship between growth of RCF cracks and load distribution using AE. They concluded that the fatigue cracks have tendency to propagate in narrow areas and deviate to the entrance side of the rotational direction within the loading zone in the early stage of its growth and then the area spreads to the exit side when the growth process is advanced.

Choudhury A. and Tandon N. [21] in one of the most cited works in this field investigated the changes in AE signal for different sizes of simulated defects on the inner race and a roller of radially loaded cylindrical roller bearings. They concluded that the method of ringdown counts of AE has been found to be a very good parameter for the detection of defects in both the inner race and roller of the tested bearings. The sharp rise in the value of AE counts for the smallest defect size tested indicates that this may serve as a good parameter for incipient fault detection in bearings. Distributions of events by ringdown counts and peak amplitudes are also found to be good indicators of bearing defect detection.
In a fundamental study on the impact of surface integrity by hard turning on rolling contact fatigue [22], Schwach D. and Guo Y. tried to answer the long-standing question of how residual stress and the white layer affect Rolling Contact Fatigue (RCF) using AE technique. They claimed that the white layer induced by hard turning is very detrimental to RCF. They concluded that early fatigue damage and fatigue failure can be accurately captured by the AE amplitude and that compressive surface residual stress with a negative slope of residual stress profile in the near-surface can significantly increase RCF life. However, the depth and magnitude of the maximum compressive residual stress in the subsurface seems to be non-critical.

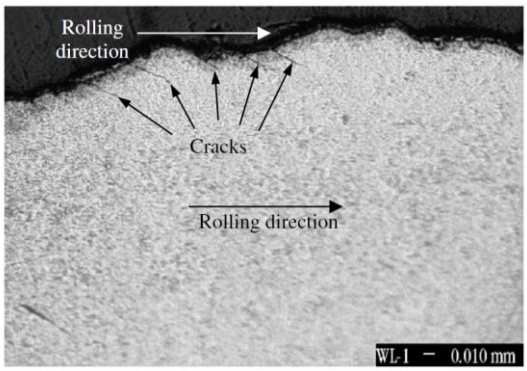

Figure 6. Sub-surface fatigue crack orientation at initiation stage for white layer surface [22].

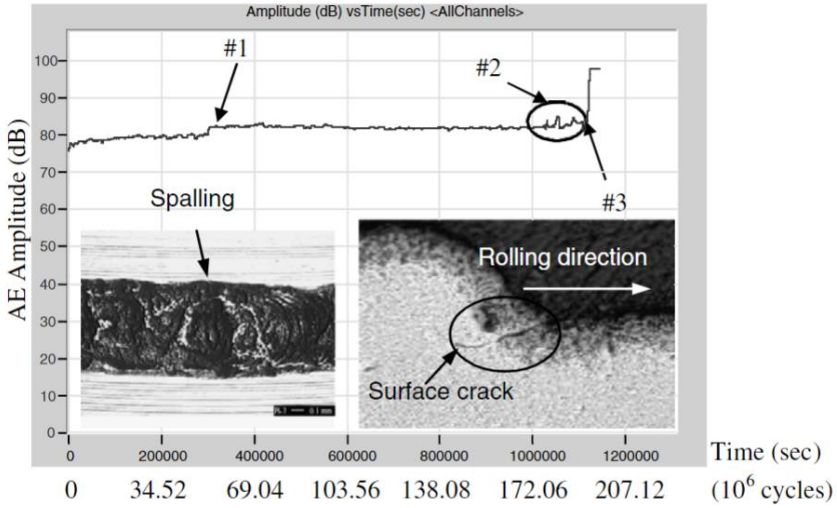

Figure 7. AE amplitude, RCF life, spall, and subsurface crack [22]

The test results of this study have shown that the AE amplitude is most consistent and sensitive to fatigue damage than other AE parameters. And that the surface integrity affects RCF through the mechanism of near surface damage rather than subsurface damage.

In a study on the incipient damage monitoring in RCF process using AE [23], the authors (Rahman M., Yoshioka T. et al) aimed to clarify the potentiality of the AE technique as a useful diagnostic tool for the CM of gears in detecting and locating early damage of rollers during contacts. They assumed that combining the AE monitoring and the AE source locator can be used to detect the incipient damage and to forecast the position of the damage in rollers, and this technique could allow the monitoring of the deterioration rate of the rolling elements.

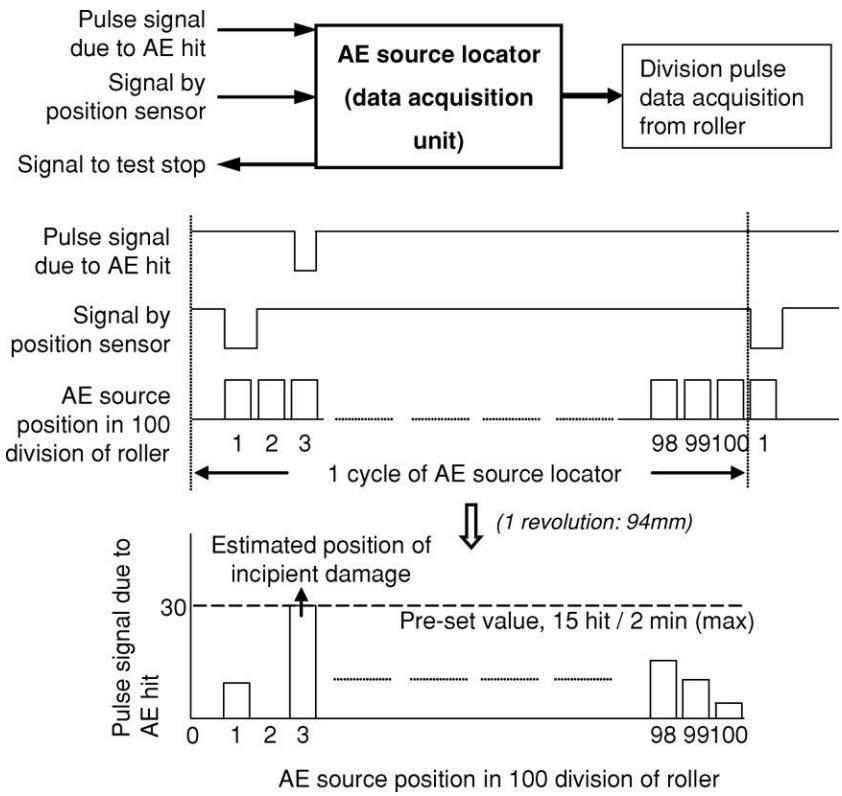

Figure 8. AE source locator data acquisition and estimation of damage position [24].

They found out that typical AE features, amplitude and energy, were employed to identify and classify AE signatures. Figure 8 displays AE hit counts rate (number of AE hit counts per 1 min) and its corresponding acceleration in vibration with time during in RCF test. Initially, the AE hit counts rate increased gradually because of interaction of the initial surface roughness and plastic deformation of two rollers. This state is termed as "running-in state" This region prevailed up to 27 h (N=1.3×106 cycles), and then decreased and continued until incipient damage occurs. The subsequent drop in the AE signal level might be attributed to the phenomenon known as "healing". The term is applied to the smoothing of the sharp edges of the initial surface roughness due to plastic deformation and/or wear by continued rolling contact. From this study, we see that AE hit counts rate is a very important parameter to reflect the incipient damage. The combination of the AE source locator and the AE data analyzer could be used as a useful tool for determining the incipient damage with its position of occurrence.

In a later study Rahman Z. a Yoshioka T et al. [24] confirmed their previous results, and insisted on AE hit count rate as an important parameter to define an incipient damage, its detection and the size of the damage during the damage propagation. The AE measurement unit that they used was found to be capable of providing real damage information at the initial stage.

In their monitoring of wear mechanisms of bearing steel using AE, Sun J. et al [5] found good correlation between AE RMS and friction signals in all their tests.

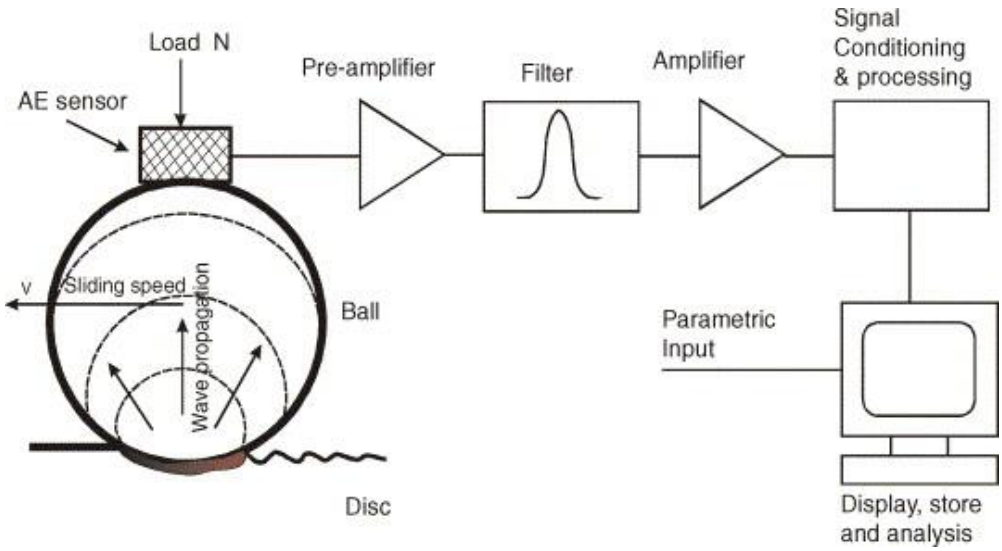

Figure 9. Schematic of the AE monitoring system for a ball on flat sliding tribo-contact [5].

They distinguished the three wear regimes through the tests as running-in, delamination and oxidation, and among their findings were distinct AE RMS features for each wear regime which has a different dominant wear mechanism. They found out that AE RMS is sensitive to different aspects of contact breakdown during dry sliding wear, and concluded that integrated AE RMS is highly sensitive to running-in and oxidation wear. Those were important and dependable findings for many other subsequent research efforts in this area.

A big contributor in this area of research was also Mba D., who for the last two decades authored and coauthored many research works that investigated the use of AE in monitoring bearing condition and for the detection of RCF in general. In one of his early and most cited papers [10] he validated the use of AE parameters such as RMS and Counts as a robust technique for detecting bearing damage. More importantly his research showed that the relationship between bearing mechanical integrity and AE counts is independent of the chosen threshold level. In another work with Al-Ghamd A. [25], they presented a relationship between the AE burst duration and the defect length. They also showed that AE RMS maximum amplitude and kurtosis have all been shown to be more sensitive to the onset and growth of defects than vibration measurements.
Mba D. with Elforjani M. in different papers [26] [27] [28] [29] [30] [31] investigated the crack initiation and propagation in slow speed bearings using AE. They concluded that sub-surface initiation and subsequent crack propagation can be detected using a range of data analysis techniques such as spectrum analysis and information entropy on AE signal generated from natural degrading bearings. One of the results of their investigations showed that whilst measurements on operational bearings cannot be achieved, the method of identifying the onset of crack propagation can be employed as a quality control tool for bearing manufacturers particularly for testing bearing material homogeneity. They also demonstrated in [27] the ability to determine the size of natural defects on bearings using AE technology, which was a breakthrough at that time. And again showed that there is a clear correlation between increasing AE energy levels and the natural propagation and formation of bearing defects.

In [28] and [30] they concluded that AE parameters such as energy, amplitude, counts and ASL have been validated as reliable, robust and sensitive to the detection of crack propagation and rubbing between cracked surfaces in slow-speed bearings. They observed an important correlation between the increasing AE levels and the natural degradation of the shaft.
After that Yoshioka T. and Shimizu S. [32], introduced a new compound diagnostic system detecting vibration and AE for monitoring ball bearing operation under grease lubrication. They concluded that even under grease lubrication their developed compound information system was able to diagnose rolling contact of the bearings. Another important finding was that combining both the basic statistical values of AE and vibration does not only appear to advance toward reliability but also clarifies the possibility to forecast the appearance of the damage.

Widodo A. et al. [33] also diagnosed the faults of low-speed bearings based on AE signal and multi-class relevance vector machine and support vector machine, which are pattern classification methods. They changed the original statistical features into component analysis and conducted fault diagnosis using the two mentioned classification techniques, then they compared the classification accuracies between original features and extracted features through component analysis which gave promising results that this technique can improve the performance of classification. They also highlighted the importance of specific signal processing techniques for fault diagnosis of the slow speed bearings, which leads to high accuracy in fault detection.
In a similarly important effort, Hase A. et al. [34] aimed at recognizing the wear mechanisms by means of AE monitoring technique and to find the correlation between the two.
They suggested that the difference between AE signals detected during adhesive wear in the high-frequency region and the AE signals detected during abrasive wear in low-frequency region permits the recognition of wear mechanisms. They stated that AE signals are produced when elastic stress waves are generated as a result of deformation and fracture of the material.

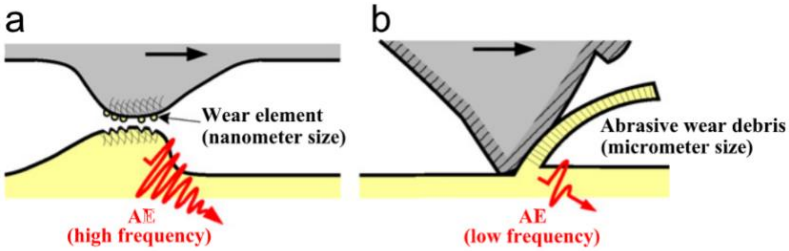

Figure 10. Schematic of sources of AE in (a) adhesive wear and (b) abrasive wear [34].

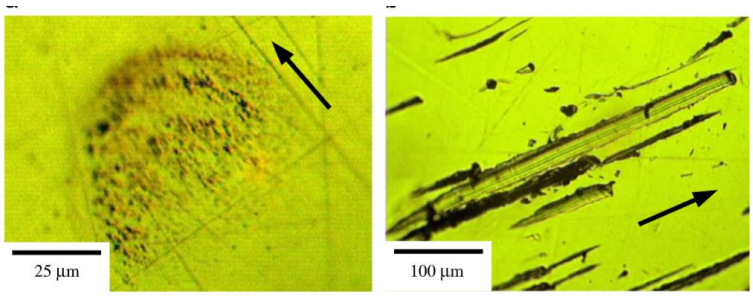

Figure 11. Micrographs of wear tracks for pin specimens:

(a) Adhesive wear (Fe/Fe, dry); and (b) abrasive ear.
(b) The arrow in each micrograph indicates the direction of sliding [34].

They produced a well-constructed figure that was cited by many research papers, shown here in Figure 12 which illustrates a correlation map for the AE frequency spectrum (<=>: frequency band, ↑: frequency peak) for several phenomena associated with deformation and fracture. The vertical axis represents the amplitude of the AE signal, and the horizontal axis represents its frequency. In the figure, the magnitude of the AE signal on the vertical axis is sequenced roughly because this shows marked changes depending on the type of AE sensor, AE filters, the experimental system (the distance and propagation paths of the waves from the respective AE sources to the sensors), and experimental conditions.

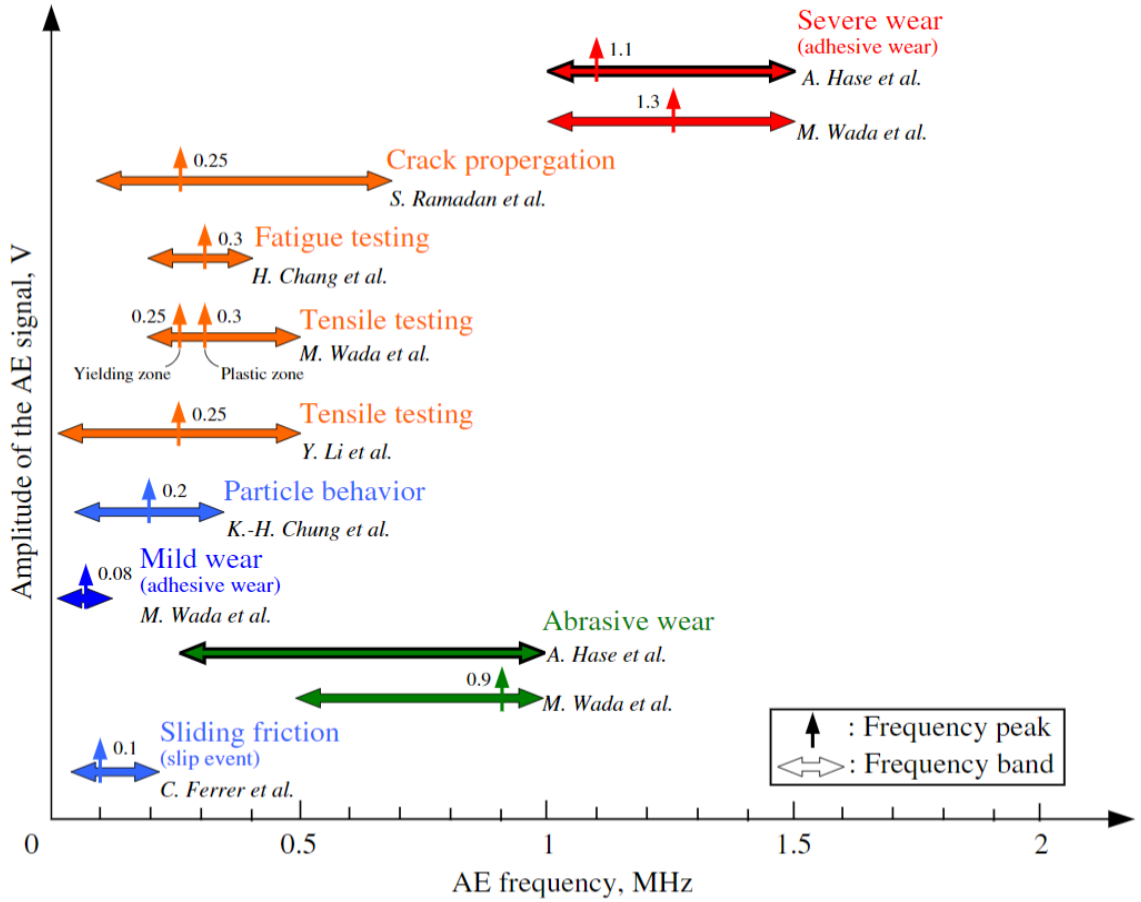

Figure 12. Correlation map of AE frequency spectra for phenomena involving deformation and fracture (<=> frequency band, ↑ frequency beak) [34]

The AE signals detected during adhesive wear showed a large peak in the high-frequency region, whereas AE signals detected during abrasive wear showed a few peaks in the low-frequency region.

Their conclusion approved the hypothesis, and it stated that mechanisms of wear can be recognized from the features of the AE frequency spectrum. Also, the AE signals that correspond to particular wear mechanisms can be discriminated. Their correlation map, in Figure 12, makes clear that the distribution of the AE frequency changes depends on the mode of deformation and fracture. Each wear mechanism produces its own type of AE frequency spectrum, which is not dependent on the nature of the materials involved.

Chacon, L. et al. [35] proposed a novel approach for incipient defect detection in rolling bearings using AE where they propose an AE signal envelope analysis method that is able to identify localized defects in an incipient stage, in which the signal-to-noise ratio (SNR) is extremely low. The method combines Wavelet packet for AE signal de-noising, the Hilbert Transform (HT) for envelope extraction, and autocorrelation function, to find patterns in the AE signal.

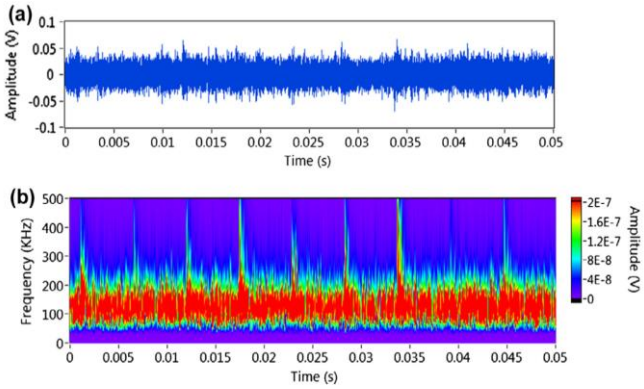

Figure 13. AE signal from defected bearing in (a) time domain and (b) scalogram [35].

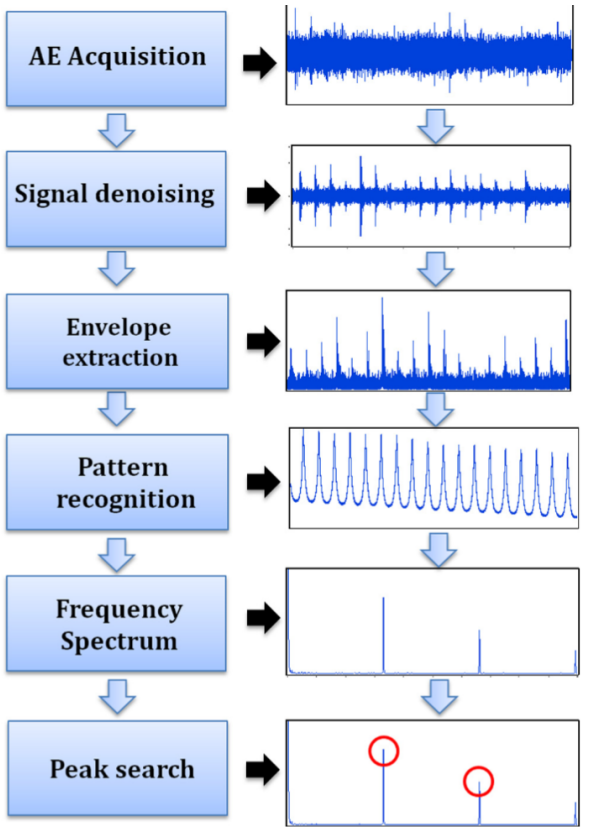

Figure 14. Flow chart of the proposed method [35].

The proposed method was able to detect the defect with 9 dB lower SNR than the traditional method. This scenario, in which the SNR is low, is typically present in defects at an early stage, which would be very beneficial for later studies.

Another interesting finding of this paper is the fact that the high frequency spectrum of AE provides most of the information regarding the seeded defect.

Then as a continuation of the efforts of Mba, D. and others to detect the faults in low speed bearings, Van Hecke B. et al. [36] presented a new methodology where the used resampling approach was able to segment the AE signal according to shaft crossing times to compute a single spectral average, which is used to extract features and evaluate condition indicators for bearing fault diagnosis. This AE based technique starts with sampling the AE signals at a rate comparable to vibration centered methodologies. Then, the sampled AE signal is time synchronously resampled to account for possible fluctuations in shaft speed and bearing slippage. This approach can segment the AE signal according to shaft crossing times to compute a single spectral average, which is used to extract features and evaluate condition indicators for bearing fault diagnosis. The approach computes only one average for all bearing fault types. They began with a heterodyne technique that allows AE signals to be sampled at a rate comparable to vibration based approaches.

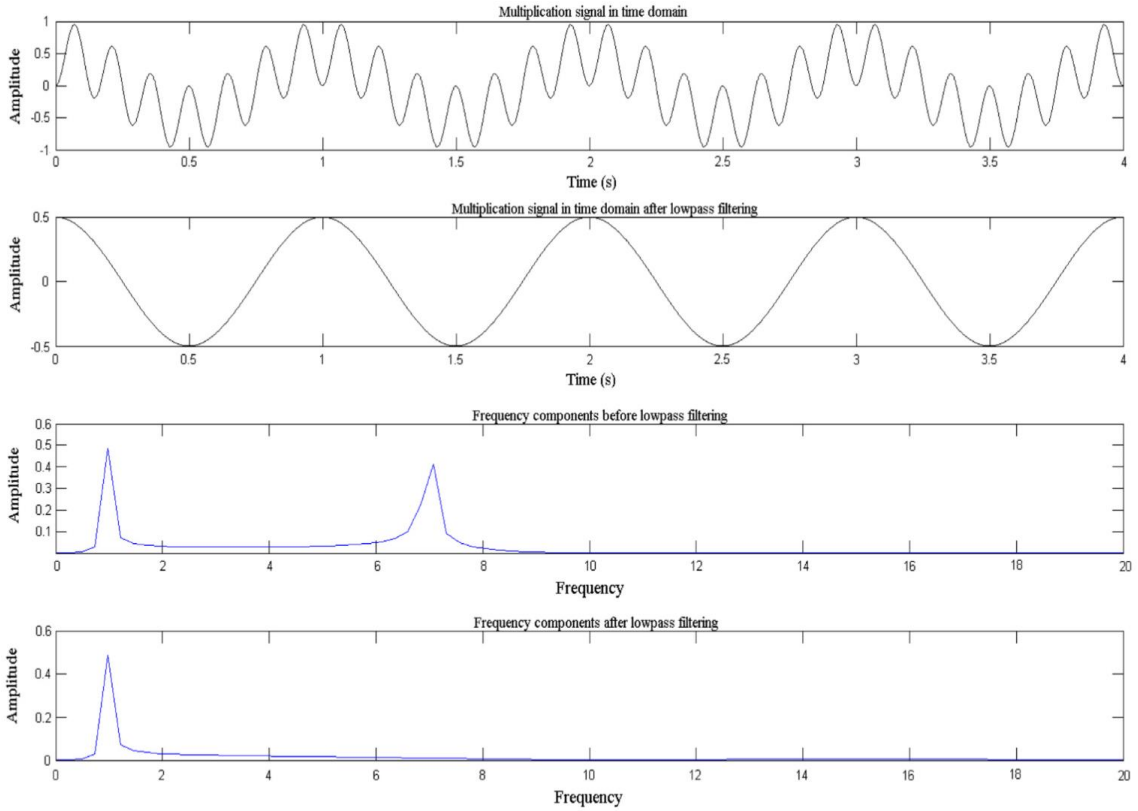

Figure 15. Extracting the heterodyned signal by frequency domain filtering [34]

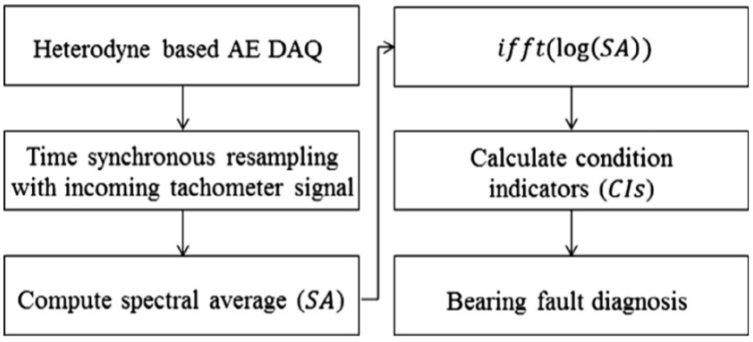

Figure 16. Overview of the methodology [36].

For the condition indicator Shannon's entropy, the separation of the bearing faults increases with decreasing shaft speeds. This indicates the potential of the methodology to diagnose bearing faults at shaft speeds lower than what was presented in the paper.

The results in this paper indicate that the low sampled AE signals in combination with the presented approach can be utilized to diagnose the types of bearing faults at low shaft speeds as low as 10 Hz, and supposedly, these results would be beneficial for this dissertation work..

At the same time Cockerill A. et al. [37] investigated of the effects of increased speed and load on the generation of AE within cylindrical roller bearings, where they suggested that the increase in speed has a higher effect on RMS of the signal than the increase in loading. The AE_{RMS} level increased significantly with increasing speed whereas increasing load had a far weaker effect. This work showed that the excitation of the bearings resonant frequencies was responsible for an increase of energy in the frequency range of 20–60 kHz.

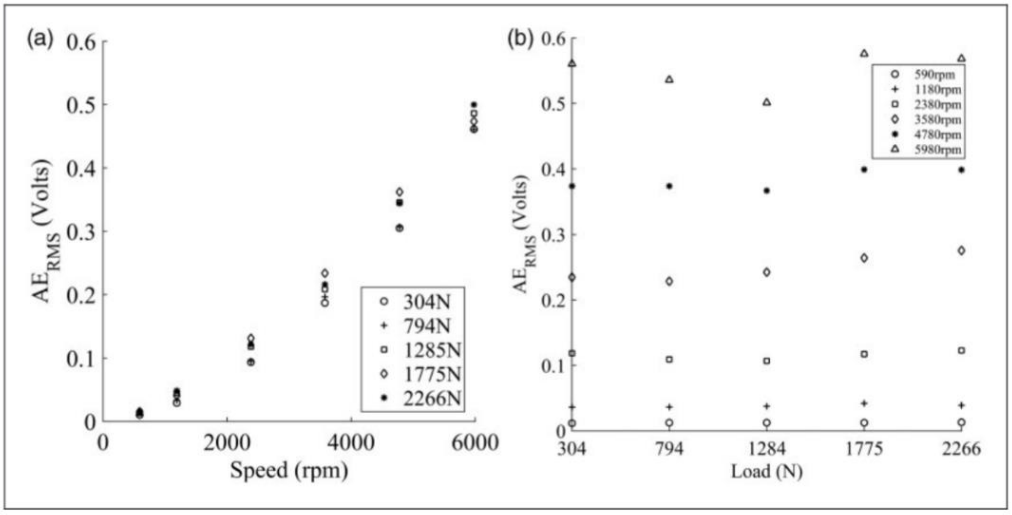

Figure 17. (a) AE_{RMS} vs. Speed and (b) AE_{RMS} vs. Load [37]

Initial analysis determined a strong correlation between speed and AE_{RMS} and a far less significant effect due to increasing load. By studying the frequency response with respect to time, it was shown that the lower frequency range, 20–60 kHz, was highly sensitive to speed and is associated with the bearing's natural resonant frequencies. Whereas load has little effect on the frequencies lower than 60 kHz, the energy released at 330 kHz (the sensor's resonant frequency) increases as load is increased, this is due to increased stresses within the contact zone and hence a greater release of strain energy and increased likelihood of plastic deformation occurring.

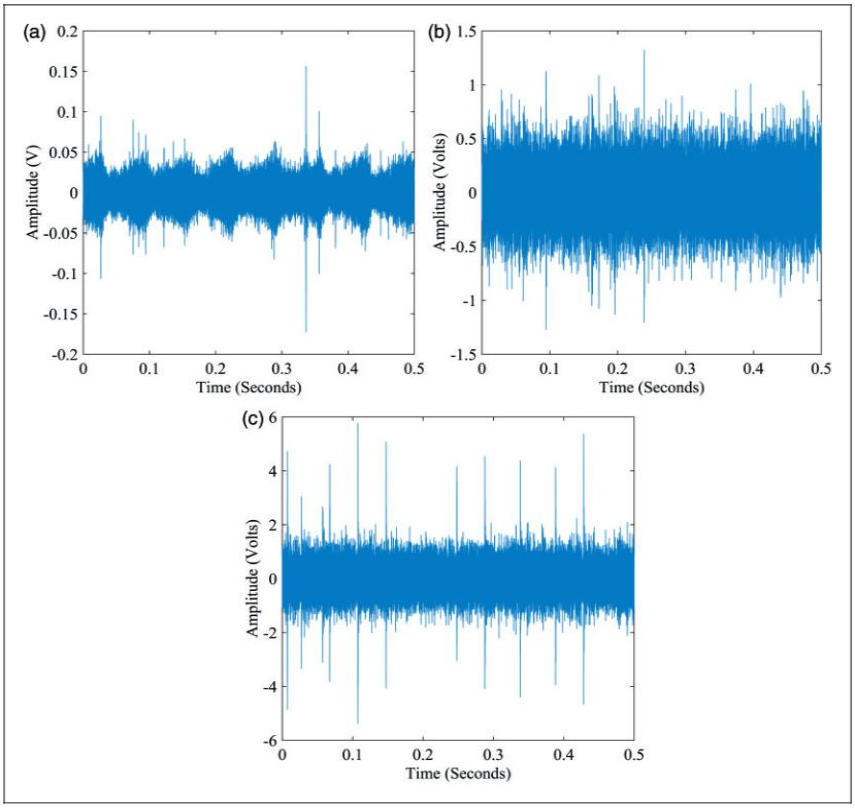

Figure 18. Raw AE waveforms at (a) 590 r/min, (b) 2980 r/min and (c) 5980 r/min [37].

The results demonstrated the sensitivity of AE to both bearing operating conditions and to bearing failure, therefore its great potential for use in bearing monitoring systems.
An advanced version of this work then was presented by Rycerz P. et al [38] when they studied the growth of RCF cracks before they develop into surface pits, in an attempt to better understand crack propagation mechanisms in bearing steel. The authors proved that the crack initiation occurs in early in total life, and there are two distinct stages of crack growth in RCF, and contact pressure and crack size are the main parameters controlling the crack propagation rate. The two distinct stages of crack growth in RCF are: stage 1, where cracks grow at a slow and relatively steady rate, consumed most of the total life; and stage 2, reached at a critical crack length, within which the propagation rate rapidly increases.

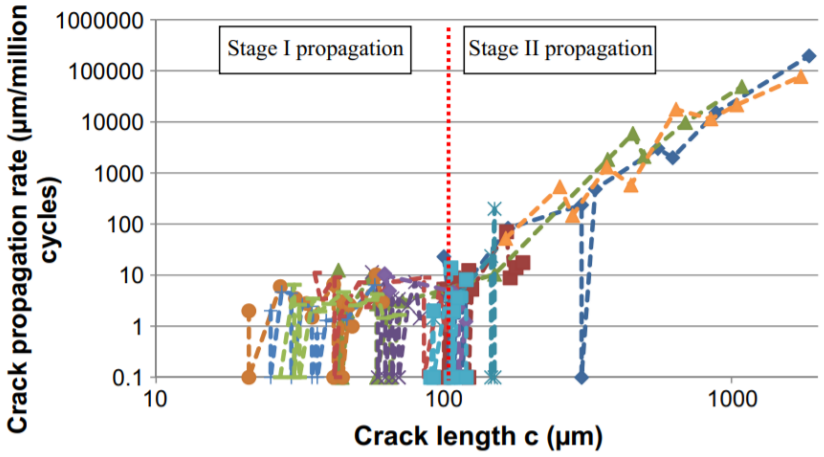

Figure 19 - Crack propagation rate across the surface (dc/dN) as a function of instantaneous surface crack length [38].

Stage I of crack propagation was associated with cracks up to about 100 µm in length, cracks show discontinuous growth with long periods of crack arrest. The average rate of crack growth was relatively low.
In stage II propagation, reached once cracks exceeded the length of about 100 µm, propagation rate increases exponentially with crack length so that cracks extend much faster and eventually lead to pitting. Growth of the stage II RCF cracks can be described by a Paris-type power law, where the rate of crack growth across the surface is proportional to the contact pressure raised to a power of approximately 7.5.
Observations about crack behavior from the experiments:

- Cracks display a V-shaped propagation pattern when viewed at the surface.
- Crack growth occurs in the direction opposite to the direction of the applied friction force.
- In parallel section view cracks have an initial angle of inclination to the surface of 20–30º.
- Secondary cracks form and grow to break the surface, eventually causing a pit to form.

Those observations show that the failure mode is representative of the generally accepted mechanisms of surface initiated RCF cracks. It also provided new quantitative data on crack propagation rates within a wide range of crack lengths and at different contact pressures.

Then Sharma R. and Prey A. [39] introduced a modelling of AE generated in rolling element bearing, where they developed a mathematical model to understand the influences of operating parameters on energy of AE generated in the bearing. They tried to prove that a mathematical model that represents the actual physical mechanism in the bearing can be developed and can explain the experimental results. The theoretical model was developed on the bases of asperities interaction between surfaces of inner race, outer race and rolling element of bearing using Hertzian contact approach, statistical concepts, contact load distribution during the load zone, and lubrication effects. Their model has been validated with experiments.

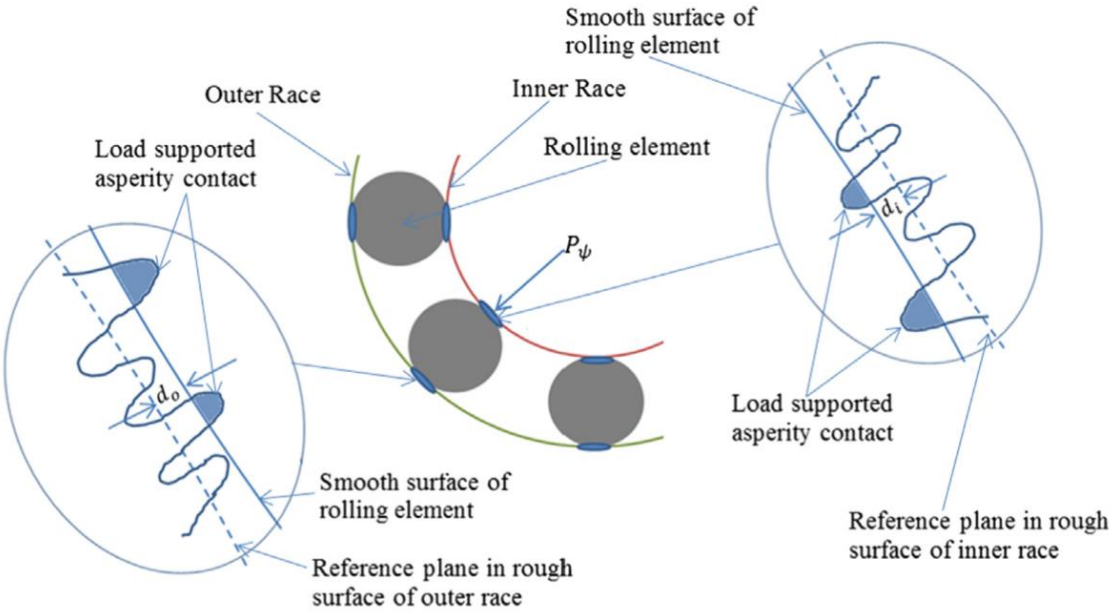

Figure 20. Deformation of asperities during contact between smooth surface and rough surface in rolling element-races contacts [39].

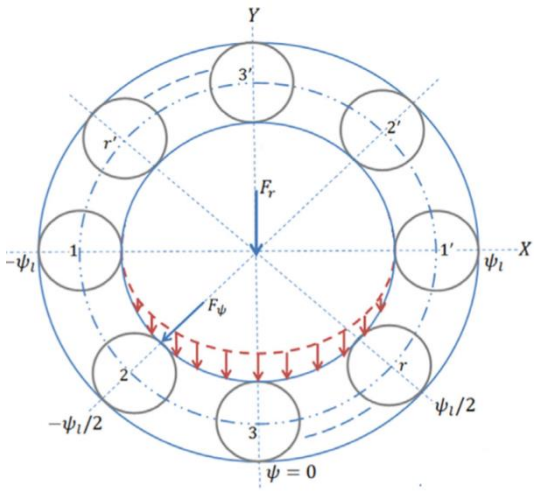

Figure 21. Radial load distribution for $\epsilon = 0.5,\ \Delta_r = 0$ [39]

The results of the developed model demonstrate that the level of AE is influenced by the load, rotational speed, defect size, number of asperity contacts, bearing element surface topographic characteristics and specifications/profile of bearing. The developed model correlates AE to bearing operating parameters, and it shows the potential of this model to understand the AE generated during the bearing operation which is an important factor in the condition monitoring of rolling element bearings. The developed model was validated on the bases of experimental studies conducted by other researchers in other papers.

The detection of plastic deformation in rolling element bearings by AE was studied by Schnabel S. et al [40] where they noticed that transient force signals dominate the AE signal of a rolling element bearing at increased rotational speeds, while at low rotational speed plastic deformation is detected by AE. Their work showed a dominance of transient force signals at high rotational speeds. It also showed the detectability of plastic deformation in rolling element bearings caused by particle contamination depends on the ratio between signals caused by plastic deformation and transient force signals. The contribution of transient force signals decreases with the decrease of rotational speed. Eventually the contribution of transient force signals is so weak that plastic deformation can be detected with decreased rotational speed.

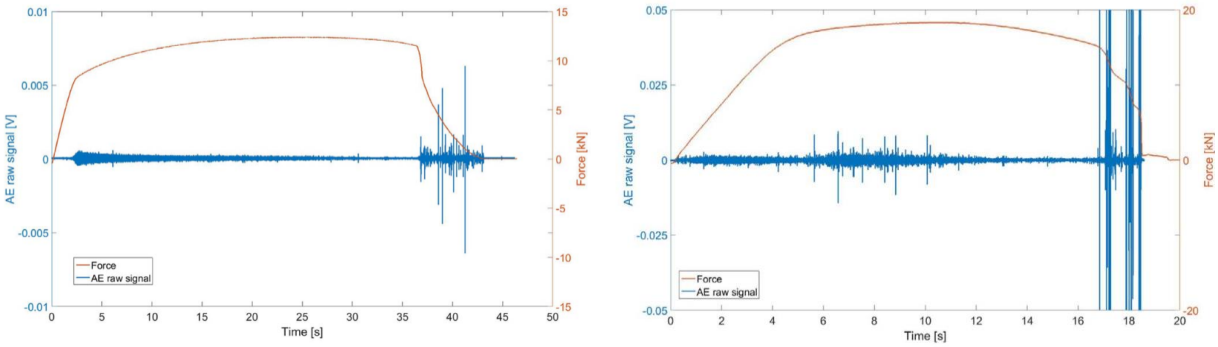

Figure 22. Acoustic emission measurements of a tensile test (Figures a and b are in different scales) [40]

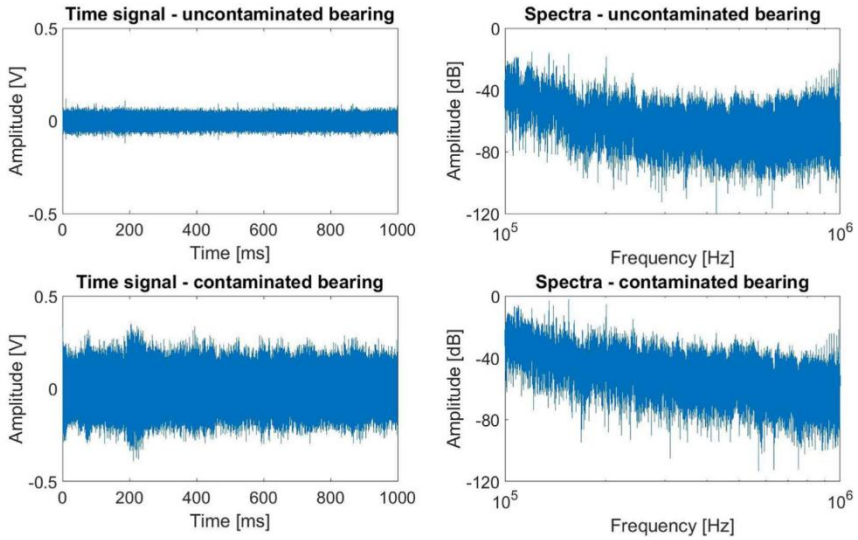

Figure 23. Time signal and spectra of acoustic emission measurements of a contaminated and an uncontaminated bearing at 100 rpm and 10 kN load [40].

The results of this paper indicate that the full scale bearing tests could be understood better by using component tests, studying isolated phenomena, such as plastic deformation or transient forces. This note should be considered in any future work.

One of the recent and famous studies in this field was done by Fuentes R. et al. [41] in which they presented a methodology for detecting sub-surface damage using AE measurements.

They relied on the idea that damage in bearing parts can be detected before it reaches the surfaces of those parts. In other words, sub-surface damage can be detected using AE.

The authors used probabilistic modelling, more specifically Gaussian mixture models as a principled statistical procedure for damage detection. They stated that damage in bearings starts under the surface, as a result of Hertzian contact mechanics. Sub-surface damage is harder to detect and has received much less attention. AE data were collected from many sensors and processed separately in order to evaluate the detectability of the different levels of defects at each location.

Detection of damage was carried out by first extracting three different damage-sensitive features from the raw AE data, and then fitting a probabilistic model to perform novelty detection. The features chosen in this investigation were hit summary statistics, Auto Regressive (AR) coefficients of the individual AE hit time histories, and the envelope spectra of the raw AE signals. These features all capture a different type of information contained in the AE data. The hit-based summary statistics contain information about the average energy, duration and the distance each individual stress wave has travelled. While the hit AR coefficients on the other hand provide a greater level of detail as to the spectral characteristics of the waveforms. Finally, the envelope spectra capture the amplitude modulation of the signal, so any periodic bursts of energy, which is a characteristic manifestation of damage in dynamic response data, should be evident in this feature.

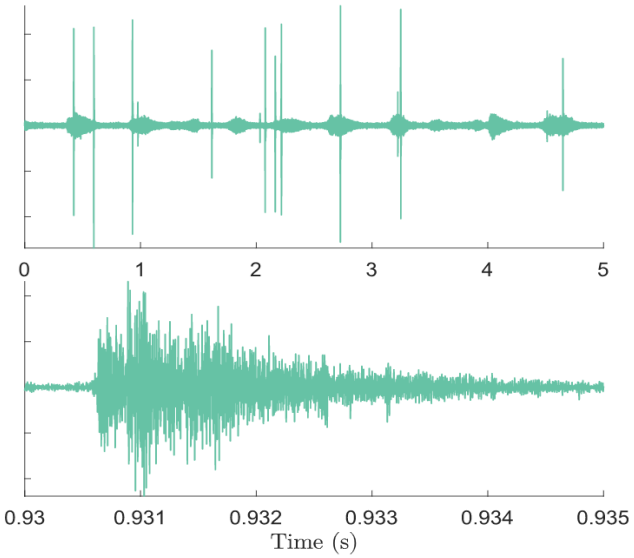

Figure 24. Example of a) an AE signal measured from an undamaged bearing in operation and b) a zoom-in to one of the "hits" characteristic of AE measurements.[39]

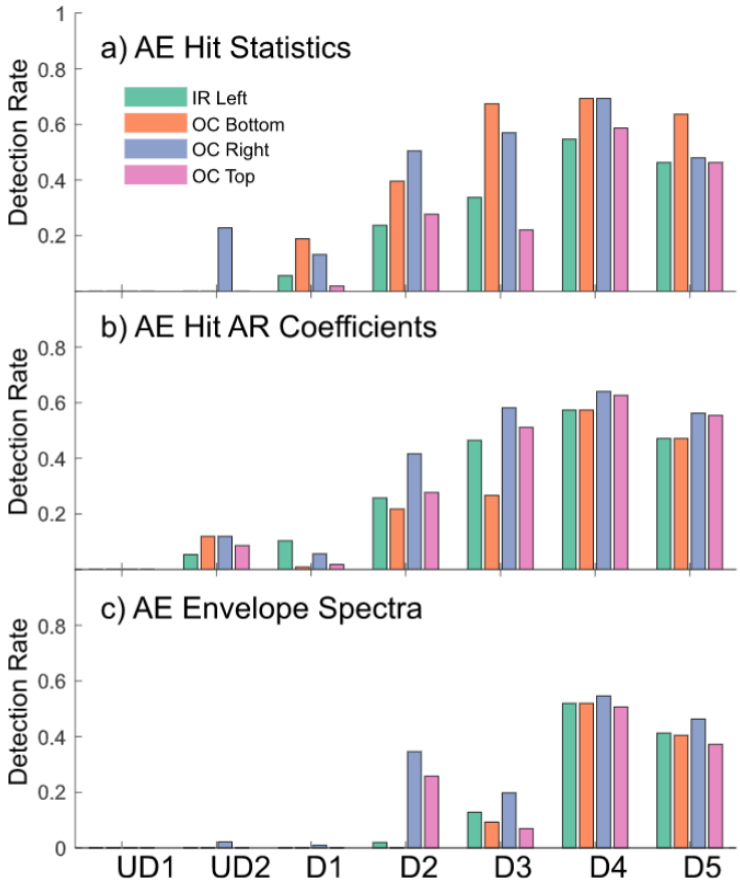

Figure 25. Detection rate for the four different AE sensor locations, and the three damage-sensitive feature considered.[39]

It is clear that the larger surface-level defects are evident through a clear change in the probability distribution of the features. This is easy to spot qualitatively. On the other hand, the change in all damage-sensitive features arising from sub-surface damage is not necessarily clear from visual examination. The early-stage surface defects were also investigated in this work. A total of five levels of damage were used, two sub-surface and three early-stage surface defects. This work provided a complete analysis for the prediction of sub-surface damage detection. And the methods developed here have proved to be robust against challenges like the changes in applied load and temperature. And we know that one of the key aspects of AE activity within a bearing environment is that it is highly dependent on applied load and temperature, as this affects the lubrication properties.

It also showed that it is possible to identify sub-surface damage from a practical measurement location (in their case, at the casing of a planetary gearbox bearing), which is very important statement for any future study concerned with the location of AE sensors when detecting damage in bearings.

The interest in the fault diagnosis of low speed rolling bearing using AE one of the most studied and researched subjects using different techniques and available technologies in combination with AE, as did Chen R. et al. [42] where they used the subspace embedded feature distribution alignment (SADA) with AE. Their method uses the FFT to preprocess the AE signal to obtain a spectral matrix transformed from time domain to frequency domain. Then using SADA to align the basis vectors of two domains to overcome the interference caused by different rotational speeds on data distribution.
They compared the fault diagnosis performance of AE signal and vibration signal at low-speed. Their results showed that AE signal had better performance than vibration signal at low-speed. Then they claimed that their proposed SADA method was compared with several transfer learning methods and deep learning methods and showed higher diagnostic accuracy.

It is important to mention at the end of this section that, the Institute of Machine and Industrial Design (IMID) - Brno University of Technology, where this work has been carried out, has been accumulating over the last three decades an extensive amount of experience and knowledge in the field of using AE as a NDT technique in detecting damage and condition monitoring of bearings and investigating the use of AE for detecting and predicting defects from different types of material fatigue. As a matter of fact, until recently, IMID has been the only institute in the Czech Republic that applied AE for such studies on mechanical materials.
Some of the outputs of this long tradition in IMID include the dissertation work of Petráš, Jiří 2004 on the detection and localization of defects in materials using AE. Then the work of Hort, Filip 2011 on the use of AE for detailed diagnostics of radial bearings damage. The work of Nohál, Libor 2014 on the correlation between AE and RCF in bearings. Other publications included Mazal, P. et al. [43], about the use of AE for the identification of fatigue micro-cracks creation, and Nohal, L et al. [44], about investigating RCF in steel using AE, and Mahmoud, H. et al. [45], about the use of AE for determining the relationship between loading and defects in pneumatic cylinders.

2.3 Application of DF of AE hits as a parameter for measurement

The Dominant Frequency (DF) of AE hit is defined as the frequency corresponding to the highest power in the PSD (Power Spectrum Density) of the AE hit waveform, and this is the reason it is sometimes called the Peak Frequency. This parameter of AE hit has been gaining a lot of attention in research recently, specifically in the geotechnical engineering field, not in mechanical engineering applications, and certainly not in bearings.
It is worth noting that there are other parameters for the AE hit in the frequency domain, such as average frequency, frequency centroid, and reverberation frequency, but dominant frequency is the most used and applied parameter.

In this section the spot light was turned on the research literature where the dominant frequency of AE hits was used as a parameter for detection of defects or for condition monitoring of studied materials. We could not find in the research literature any study that addressed the use of DF of AE hits in bearings or bearings' material. Therefore, this review of the literature concentrates on the use of DF of AE hits in other areas with the goal of noticing the way it has been used and the methods that have been applied.

Those research efforts started not long ago, almost just two decades ago after many advancements in AE signal acquisition and measurements took place, where it was possible to identify AE hits with extremely high sampling frequency and to apply sophisticated analyses. One of the prominent works that depended on the use of DF of AE hits was carried out by Woo S. and Goo N. [46], where they used DF bands of AE to analyze the bending fracture of piezoelectric composites actuators. They divided the distribution of DFs of AE hits to bands, this technique was used almost by every other study that followed.

Li, L. R. et al. [47] stated in their technical note that the spectral analysis methods are often used for signal waveforms analyses. Because frequency content in an AE is determined by the wave source, studying the DF characteristics provides significant controls on investigations of microscopic fractures. The authors presented the dominant frequency characteristics of AE waveforms of marble samples acquired during direct tensile tests, and then they discussed the relationship between the microscopic failure mechanism and the statistical characteristics. Their results associated specific DF bands to the number of observed AE events and to specific tensile conditions.

A statistical relationship between energy ratios of AE waveforms distributed in low and high DF bands and peak strengths of rocks under tension was built by Zhang, Z. et al. [48]. The authors statistically analyzed the distribution and evolution laws of DF of AE waveforms with normalized applied stress, and they built the statistical relationship between the energy ratios of AE waveforms distributed in low and high DF bands (L-type and H-type waveforms) and peak strengths of rock specimens. Among the results was a clear distinction between the DF bands of AE during direct tensile failure process of the rock which is reflected in the difference between Initial release moments of Low-type waveforms and the High-type waveforms.

Zhu, J. et al. [49] provided a reasonable explanation for the tensile strength reduction of water-bearing rock by connecting the rock micro-failure and the DF of AE waveform signals released. They used a very intriguing method of data processing for the extraction of the DF of an AE waveform using the Fast Fourier transformation (FFT), the principle of which is shown in Figure 26. As a result, all DF of AE waveforms and their amplitude were obtained and used to analyze the rock tensile failure process based on statistical analysis.

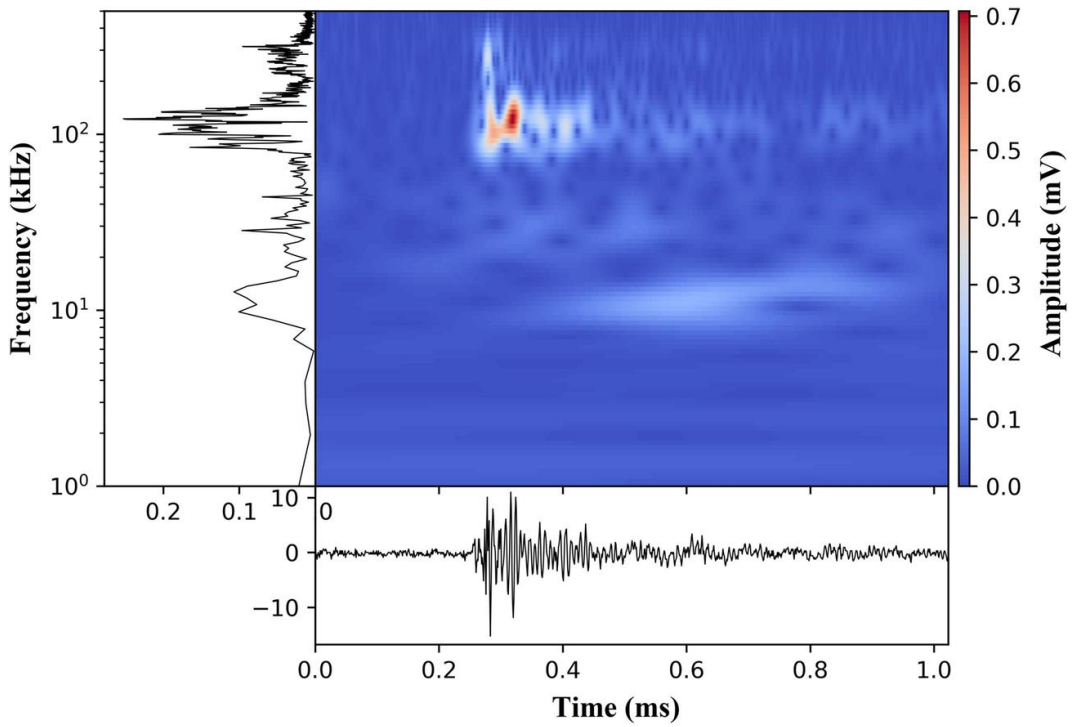

Figure 26. Extraction process of the DF of AE waveform [47]

In an experimental investigation Wang, Ch. et al. [50] analyzed the dynamic process of rock-burst, and the information entropy of the AE dominant frequency was determined to be an indicator of rock-burst. This meant to analyze the evolution of AE dominant frequency from a chaotic state to a relatively ordered state in different stages of rock-burst. As a result, the correlation between the evolution characteristics of AE dominant frequency entropy and rock-burst was established.

Similarly, in their comprehensive study of damage characteristics and AE response mechanism of sandstone, Zhang, H. et al. [51] explained the cause of the changes in the AE dominant frequency–amplitude signal characteristics according to the rock mineral composition and pore structure. They distinguished between four types of AE signals in the fracture process of sandstone: low-frequency and low-amplitude (LF–LA), low-frequency and high-amplitude (LF–HA), medium-frequency and low-amplitude (IF–LA), and high-frequency and low-amplitude (HF–LA) signals. They established the response mechanism of AE dominant frequency–amplitude signals from the angle of rock failure process combined with SEM fracture morphology, and found a clear correspondence between the type of the signal and the failure mode.

Niu Y. et al. [52] studied the temporal DF evolution characteristics during fracture process of sandstone, which means that they analyzed the time-varying DF and amplitude characteristics of AE waveforms during the real-time cracking process. They also used the division of DF distribution to bands and they classified the bands in to low and high and middle frequency bands and studied them statistically.

Many other studies followed the same approaches that have been summarized so far, such as the work of Zhu J. et al. [49], and Zheng-Hu et al. [53], and Lei R. et al. [54].

2.4 Toroidal Roller Bearings

Toroidal roller bearings are single row bearings with long, crowned rollers. The concave raceways in the inner ring and outer ring are concentric relative to the center of the bearing. The raceway profiles are matched to each other and ensure optimum distribution of stresses in the bearing as well as low operating friction.
The rollers are self-guiding. They will always automatically adopt the position at which the load is distributed over the length of the roller, Figure 27.

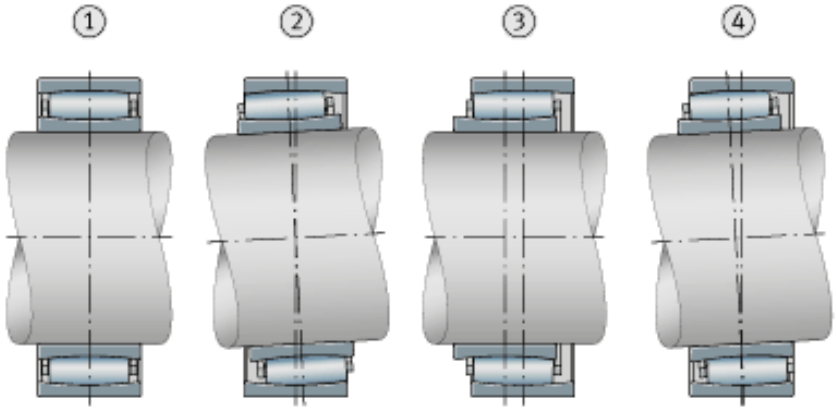

Figure 27. Toroidal roller bearing (angular and axial displacement) [55]

① Initial position ② inner ring with tilting ③ inner ring with axial displacement ④ inner ring with displacement and tilting

Where a shaft is liable to temperature-induced elongation and misalignment defects, the non-locating bearing is a particularly important concept. In this case, toroidal roller bearings have proved ideal as non-locating bearings, Figure 28.

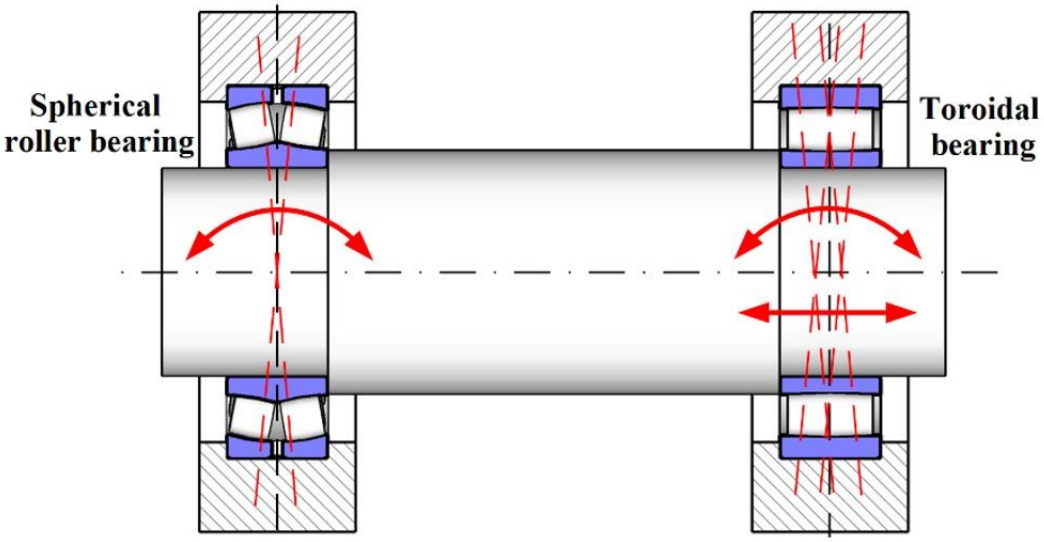

Figure 28. The Non-locating concept

In comparison with normal non-locating bearing arrangements, they offer significant advantages: Substantial changes in shaft length are compensated without constraint between the raceways and the rolling elements within the bearing.

The design work involved in other solutions is unnecessary. Even more considerable axial displacements have no effect on the locating bearing. There is no axial distortion of the bearing system. Figure 29 and Figure 30 show the application of this principle in real-life example, which is the main shaft of a wind turbine.

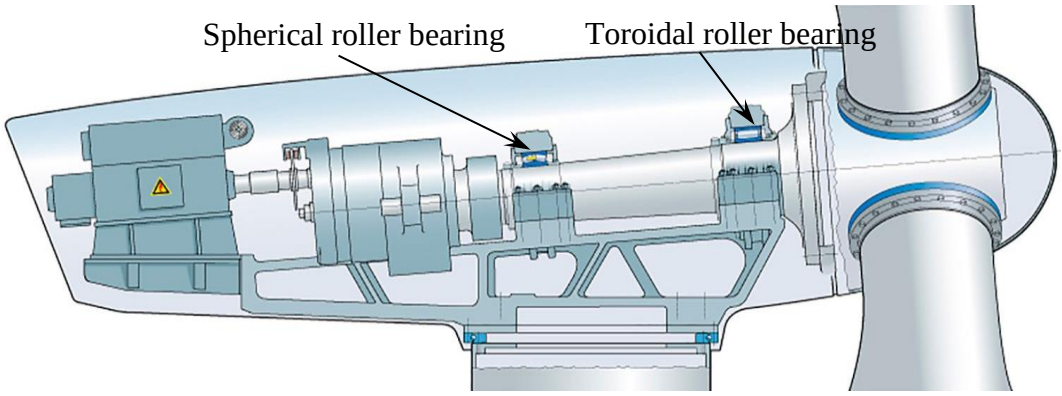

Figure 29. Use of TRB and SRB on the main shaft of wind turbine. (With permission from skf.cz)

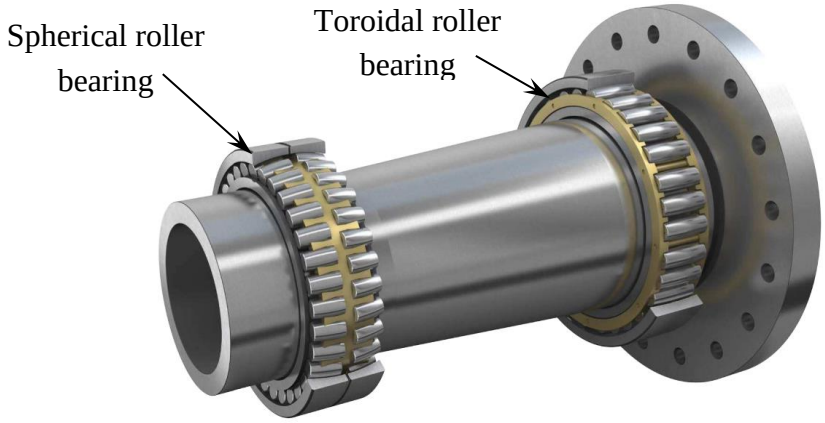

Figure 30. The main shaft of wind turbine with TRB and SRB [55]

In an experimental study, Laurian T. et al. [56], examined the functioning characteristics of the toroidal roller bearing from CARB® by means of a multibody dynamic simulation. They considered different conditions like load direction, races relative position and angular misalignment. They stated that load carrying capacity of the CARB bearing is very high even when it has to compensate for angular misalignment or axial displacement.

The results of the simulation and the experiments concluded that the TRB CARB® advantages can be summarized as following: axial displacement without inducing thrust (axial) loads; elimination of rotating outer ring and wear in the bore thanks to the toleration of angular misalignment of the bearing; which in total led to a decrease of vibration level, decrease of the operating temperature, increase of bearing service life and reduction of the maintenance costs.

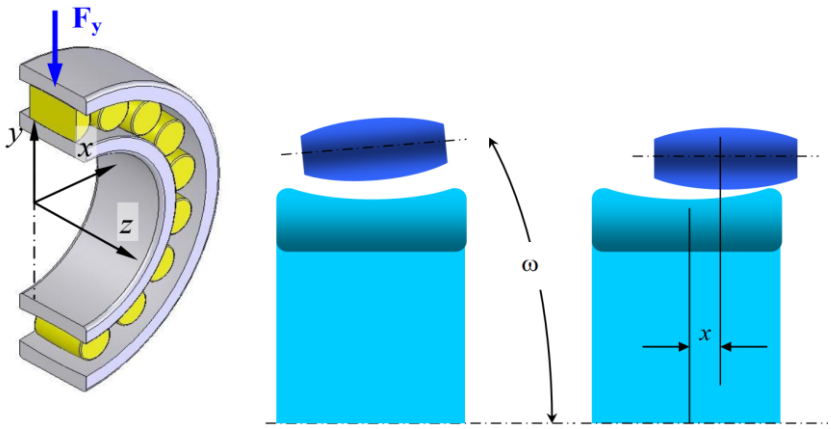

Figure 31. The toroidal bearing model with angular misalignment (ω), and axial displacement (x).[54]

Another effort by Zhang L. et al. [57], with regard to TRB concentrated on the mould design of the rollers. They considered cold rolling technology of the rollers, and after a thorough calculation of the elastic deformation and a comparison with traditional methods, they concluded that the advantages of mould in rolling process is high reliability, smooth movement, and good rolling effect, therefore, high economic efficiency.

In a simulation study by Fritzson D. et al. [58], the authors used TRB because bearing simulations are very computationally intensive, and they used the specific structure of TRB to develop suitable scheduling strategies.

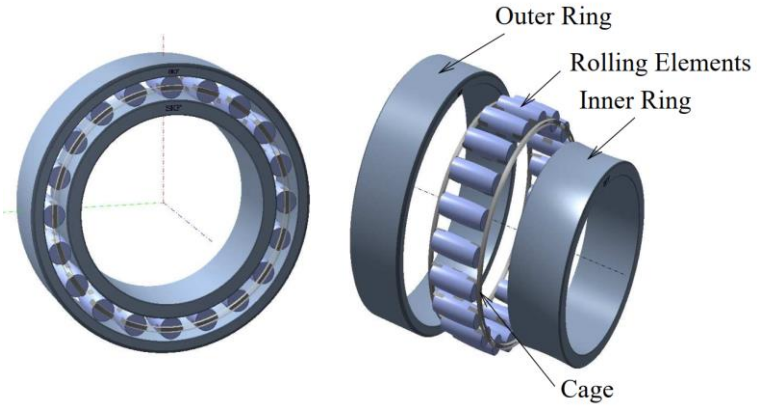

Figure 32. Exploded view of the tested toroidal bearing (CARB®) [55]

Other studies such as [59] by Benchea M. et al. used TRB as a specimen in their numerical study to investigate surface roughness influence, but the results were not specifically related to TRB, and they could have used other type of roller bearings without affecting the results.

It is noticeable that the number of studies in literature concerned TRB is very limited, even though their use has been in constant increase since their introduction in the mid-1990s.

Since TRB are roller bearings and they can withstand heavy loading and high vibration and oscillation without increased stress levels, they find application mostly in heavy industries such as paper production and casting or rolling of sheet metal. But the most important use of TRB recently is its successful application on the main shaft of wind turbines. The combination of a TRB as a non-locating bearing and a SRB (Spherical Roller Bearing) as a locating bearing proved to be very successful in this application.

3 ANALYSIS OF THE LITERATURE REVIEW

This section summarizes the acquired knowledge based on research papers from the field of AE usage for RCF detection and condition monitoring of bearings, then in the advancements in AE signal characteristics and parameters, and in the field of its application on roller bearings.

3.1 AE as an NDT technique

Historically, the field of Acoustic Emission (AE) traces back to J. Kaiser's work in 1950, where he tested metallic materials and discovered the Kaiser effect, which is the absence of detectable AE at a fixed sensitivity level, until previously applied stress levels are exceeded [16]. In 1961, B. H. Schofield officially used the term "Acoustic Emission", and subsequently, A. T. Green and H. L. Dunegan started developing standard procedures and devices. The paper of Yoshioka T. and Fujiwara T. in 1982 was the first to point out RCF detection in bearings using AE. They introduced an AE source locating system, showing the coincidence between AE sources and failure sources, establishing its precision in locating failure positions.

Physically, failure involves the release of stored strain energy, nucleating cracks, and generating elastic waves, detected as AE waves by transducers attached to the surface. Although modern AE devices are digital, detection systems remain analog. AE, a transient elastic wave phenomenon, occurs when materials are stressed, releasing strain energy as detectable elastic waves. Plastic deformation and crack growth generate AE giving it the advantage of detecting subsurface cracks, unlike vibration monitoring, which detects only surface defects.

AE signals are typically weak, therefore they undergo amplification by pre-amplifiers and main amplifiers, often providing over 1000 times gain. The band-pass filter eliminates noise, and a bandwidth of several to hundreds of kHz could be recommended for measurements depending on the tested materials, the environment, the nature of the test, among other parameters.

Jacobs L. J. et al.'s research in the early 1990s significantly influenced AE experimental usage, advancing its analytical characterization. Stress waves, influenced by factors like propagation velocities, attenuation, and geometry, make surface vibrations measurable by AE transducers. Various types of transducer, including piezoelectric, capacitance, electromagnetic, and optical, can be used. Piezoelectric transducers remain the most popular. They convert AE into electric signals, providing voltage-time representations of the detected displacement-time waves. Their sensitivity spectra is determined by ISO standard 24543:2022 [14].

Throughout its history, AE has transitioned to become a valuable NDT tool, particularly in detecting issues like RCF in bearings. As a results of this evolvement, its parameters have dramatically increased in number and in complexity.

3.2 Studying RCF in bearings using AE

The early work by Yoshioka T. and Fujiwara T. [7] [8] laid the foundation, showcasing AE's success in detecting RCF in bearings. Subsequent studies in the 1990s, including those by Yoshioka T. and Mano H. [19], explored AE's application in locating positions of spalling in radial rolling bearings.

Choudhury A. and Tandon N. [21] investigated AE signal changes for simulated defects, highlighting the efficacy of ringdown counts for defect detection. Schwach D. and Guo Y. [22] studied the impact of surface integrity on RCF, emphasizing AE amplitude's sensitivity to fatigue damage.

Rahman M., Yoshioka T. et al. [24] focused on incipient damage monitoring using AE, identifying AE hit counts rate as a crucial parameter for detecting early damage. Mba D. contributed significantly, validating AE parameters like RMS and Counts for robust bearing RCF damage detection [60].

Studies by Mba D. and Elforjani M. in the 1990s, [29] [28] [26] [27] [31] [30] gave insights into the crack initiation and propagation, showcasing the effectiveness of AE parameters in detecting RCF defects and determining their size.

Widodo A. et al. [33] used AE for fault diagnosis in low-speed bearings, emphasizing the importance of signal processing techniques. Van Hecke B. et al. [36] proposed a resampling approach for AE signals to diagnose RCF bearing faults at low shaft speeds. Cockerill A. et al. [37] explored the effects of speed and load on AE in cylindrical roller bearings, demonstrating AE's sensitivity to operating conditions and bearing failure.

Rycerz P. et al. [38] studied the growth of RCF cracks, identifying two distinct stages and key parameters controlling crack propagation. Sharma R. and Prey A. [39] developed a mathematical model correlating AE to bearing operating parameters for CM of RCF defects.

Schnabel S. et al. [40] investigated plastic deformation in rolling element bearings using AE, highlighting the importance of studying isolated RCF phenomena for a better understanding of full-scale bearing tests. Fuentes R. et al. [41] presented a methodology for detecting sub-surface damage from RCF using AE measurements, utilizing probabilistic modeling for damage detection. Chen R. et al. [42] used subspace embedded feature distribution alignment (SADA) with AE for fault diagnosis in low-speed rolling bearings, demonstrating superior diagnostic accuracy of RCF defects compared to vibration signals.

These studies and many others collectively contributed valuable insights into AE's potential for the RCF fault detection in bearings, paving the way for huge advancements in this field.

3.3 AE Frequency-domain parameters

This part of the literature review focuses on the Dominant Frequency (DF) of AE hits, a parameter defined as the frequency corresponding to the highest power in the Power Spectrum Density (PSD) of the AE hit waveform. While this parameter has gained attention, particularly in geotechnical engineering, its application in mechanical engineering is scarce.

The DF of AE hits has been extensively used in various fields outside mechanical engineering. Studies by Xie, Q. et al. [61], Li, L. R. et al. [47], Zhang, Z. et al. [53], Zhu, J. et al. [49], Wang, Ch. et al. [50], Zhang, H. et al. [51], and Niu Y. et al. [52] and many others, explored its application in areas such as analyzing bending fracture of piezoelectric composites, direct tensile tests on marble samples, tensile strength reduction of water-bearing rock, rock-burst indicators, damage characteristics of sandstone, and temporal evolution during fracture.

All the above-mentioned studies have been conducted during the last 5 years. Which indicates that it is quite a recent trend even in those fields, even though there have been studies mentioning the same approach long before.

These studies employed different techniques to extract the DF of AE waveforms, but the most popular one was Fast Fourier Transformation (FFT), and they all applied statistical analyses to assess correlation between the DF of AE hits with various material behaviors. The DF bands were categorized into low, intermediate and high-frequency bands, providing insights into microscopic fractures, peak strengths of rocks, and the evolution characteristics during different stages of the material burst or fracture processes.

In summary, while the DF of AE hits has found applications in various fields, its use in mechanical engineering, particularly in bearing analysis, remains very limited in the existing literature. Further exploration and research will definitely unveil potential applications and benefits of this parameter in the context of mechanical systems and bearings.

3.4 Toroidal Roller Bearings in research

Limited number of literature addressed TRBs in research, despite their increased use and success in a number of heavy industries because of their advantages in the ability to withstand heavy loads and tolerate axial and angular misalignment, i.e. high level of vibration and axial expansion together. The most successful usage was their application on the main shaft of wind turbines as a non-locating bearing. The studies that mentioned TRBs have used them as specimens most of the time, not as the subject of the study.

3.5 Blank spot in the Current State of Knowledge

Based on the analysis of the current state of knowledge, certain spots of lack of knowledge were identified. Some assumptions were also raised for the supplementation of knowledge.
Both are summarized in the following points:

- The use of AE frequency-domain parameters in research such as frequency centroid, the average frequency, the dominant frequency and reverberation frequency has been increasing lately as a result of the increased use of AE for detecting defects in materials. However, the use of some of those parameters, particularly DF in the field of mechanical applications is still very limited, and there is none in the studies of RCF in bearings.

- The temperature of the rings and of the lubricant as parameter has been used before, but not in combination with vibration and AE in laboratory and in the field. It might look intuitive that vibration and AE are more sensitive than the temperature of the bearing rings, nevertheless, it has not been stated based on experiments.

- Carrying out an experiment on a specific type of bearings in laboratory, and then applying the same approach on this type of bearings in the field, while they are in operation to verify the findings from the laboratory has not been addressed.

- Even though TRBs have been gaining popularity in the industrial arena, especially in heavy industries, the research literature that mentions them is very limited.

- The subject of testing toroidal bearings with regard to their ability to adapt to different working positions (angular and axial misalignments) was not studied before. Even other types of bearings, which allow only angular misalignment (like spherical bearings), or axial misalignment only (like cylindrical bearings), were not studied with regard to their different working positions.

4 AIMS OF THE THESIS

The main goal of the dissertation is to investigate the rolling contact fatigue behavior of toroidal bearings using AE technique. This investigation is intended to be mostly experimental, thus should include carrying out experiments in the laboratory of this type of bearing, as well as measurements in the field where those bearings are installed and are in operation.
To achieve the main goal of this dissertation, the following steps were taken into consideration:

- Identification and execution of the experimental procedures, which include selecting the suitable set of tools, equipment and devices that are required for the measurements, and setting the right parameters for those devices according to previous experience and to collected knowledge from reliable sources.
- The measurements and experiments deal with fatigue; therefore, time is an important factor, which could span from several days to months. This requirement should be taken into consideration when recording results and when monitoring, by setting up a remote control system (or a remote monitoring system) for the measurement/experiment.
- Concentrating on the analysis of the frequency-domain of AE signal, because many studies recently have highlighted the close correspondence between AE frequency-domain parameters and the condition of the studied material.
- Since the frequency-domain analysis is more demanding, computationally speaking, it might not be practical to carry it out on the whole experiment or measurement time. Therefore, specifying the relevant time intervals to be analyzed is essential. Another factor that should be taken into consideration with this regard is the flexibility to adjust the analysis parameter even after the end of the experiment or measurement, therefore a post-processing detectors should be set up.
- The use of toroidal bearings has proven to be most successful in its recent application as a non-locating bearing on the main shaft of the wind turbine, this application will be considered for the measurements. Therefore, finding the right site and setting up the equipment and the remote monitoring system is a priority.
- Designing and assembling a special test rig for bearings that allows angular and axial misalignments. Modifying an existing test rig that serves the same goal could be considered as a viable option if it satisfies the requirements.
- Special attention will be paid to studying the ability of the tested toroidal bearing to tolerate angular misalignment and axial displacement.

4.1 Scientific questions

Upon analysis and review of the literature, the following 3 scientific questions were identified:

Question 1**:**
How does the effect of operating parameters in the initiation of RCF cracks differ between TRBs from other types of bearings?

Question 2**:**
How the dominant frequency of AE hits, which is a quantifiable frequency-domain parameter of AE signal, could be used to evaluate or quantify the level of defects on the monitored bearings' raceways?

Question 3**:**
How does the shape of the toroidal rolling element affect the operation parameters of the bearing (vibration, temperature, noise...)?

4.2 Hypotheses

Each scientific question was tested through working hypothesis formulated based on the state of the knowledge and previous research.

Hypothesis 1:

Studying the propagation of surface initiated RCF cracks in bearing steel, Rycerz P. et al. [38] concluded that contact pressure was shown to be one of the main parameters controlling the propagation rate of surface initiated RCF cracks in bearing steel. The contact pressure is basically the ratio of normal load to the true contact area. Therefore, since the contact line (toroidal contour) between the rollers and the raceways in toroidal bearings is bigger (longer) than the contact line in other types of bearings, like ball bearings, this means a smaller contact pressure between the inner and outer rings and the rollers, when applying the same loading under the same conditions. However, contact pressure is not the only factor that is affecting the initiation of RCF in bearings, especially the bearings that are in real-life operation, not in experimental environment. The allowed rotation speed, for example, is a factor that runs against the contact pressure, so it increases with the decrease of the mutual contact. Vibration is also known to have a major influence on RCF, the operating internal clearance, as well as temperature. While lubrication in contact area is the major factor in subsurface initiated RCF cracks in bearings according to Santus, C [2]. Therefore, this hypothesis should take into consideration a comprehensive approach combined with experiments and measurements to provide supporting results, because of the complex relationships between the toroidal bearing geometry properties and the operating parameters.

Hypothesis 2:

The procedure that is applied to extract the DFs of AE hits could differ from analysis to another, but the common part is the transformation from the time-domain to frequency-domain, which is a procedure mostly achieved by applying FFT or/and similar transformations, as shown before in studies [50] [62] [54] [63] [64] [49].
After extracting the DFs of a number of AE hits that have been detected by a predefined threshold, those DFs could be visually represented on a plot where the horizontal axis represents the time (interval) when AE events took place, and the vertical axis represents the frequencies of the DFs. This visual representation could be called the DF map, which would be an image for the distribution of the DFs of all AE hits in the time-domain.
Since we are back to the time-domain, it would be possible based on a synchronous comparison to establish a correlation between the DF map and the condition of the monitored bearing, following similar procedures as in [65] [51] [52], just with different studied materials.
Reading this DF map statistically, by different means such as the ones demonstrated in [52] [61] [47], would give a quantifiable measurement of the level of defects in the monitored material, in this case it would be the bearings' raceways. However, the level of defects is still a wide term that does not indicate the size or the type of individual defects on the raceways. Repeating this process would be necessary, and it is achievable by automating the process, then by overlaying many DF maps for many consecutive time intervals in one 3D graph, would give confirmation of the results and a more comprehensive view of the condition of the bearings.

Hypothesis 3:

TRB are well-known for their ability to tolerate high level of vibration and thermal expansion in the shaft [66] [55], which means when combined with the results from the research work of Laurian, T. et al. [56], that the contact line between the barreled rolling elements and the raceway changes overtime. Another factor is the design consideration, which changes from one type of TRB to another according to the size and loading category of the bearing, or even the producer. Those factors that lead to the change of the length of the contact line with the raceways will definitely affect the RCF characteristics of the bearing. Another important factor in the operation of bearings, especially roller bearings, is the effect of operating internal clearance of the bearing, which hugely influences the load distribution in a bearing and influences whether the rolling elements move by rolling or sliding motion, leading ultimately to big effects on the operation parameters, such as noise, vibration, and temperature.
The complexity of the interactions between the many factors included here would require a careful design of experiments that can give observations and answers. A finite element analysis would be considered as a complementary option to support the findings.

5 MATERIAL AND METHODS

To test hypotheses formulated from the scientific questions, it was necessary to perform various types of experiments and measurements. This section describes the equipment, the experiments, and the methods used to test the hypotheses. This simplify the process of going through this section, it has been divided to two main parts. In the first part the experiments were described by detailing how the laboratory tests were conducted on toroidal bearings, and in the second part a description of the measurements that we performed on an application of the toroidal bearings in a wind turbine main shaft.

5.1 Laboratory Experiments:

The laboratory experiments that we conducted were all concerned with testing toroidal roller bearings. The specimens for the tests were provided by the manufacturer of those types of bearings, which is ZKL, one of the biggest producers of rolling bearings in the middle of Europe, especially for the wind turbine industry. The tests were carried out on a stand specially designed for this type of tests in the laboratories of ZKL. In our latest tests we added some modifications to the testing stand to accommodate a new and special type of AE sensors that allow the sensor to be in direct contact with the outer ring of the tested bearing (which is the stationary ring). Figure 33 shows the testing stand and the specimen bearing inside, which are toroidal bearings of the types C4030V and C4026V.
The procedures of the experiments, regarding the application of AE, were conducted in accordance with the standard ISO 22096:2007 (en) Condition monitoring and diagnostics of machines — Acoustic emission [67], which specifies the principles required for the application of AE for the CM and diagnostics of machinery operating under a range of conditions and environments. The standard states that AE in this context can be used as a stand-alone CM technique, or it may also be employed to complement other CM techniques based on other technologies (e.g. vibration, infrared, etc.) used for machine condition analysis and diagnosis and/or prognosis. AE can be employed as a permanently installed, semi-permanent or portable system, and fully understanding the mechanics of the monitored machine is not essential [67].

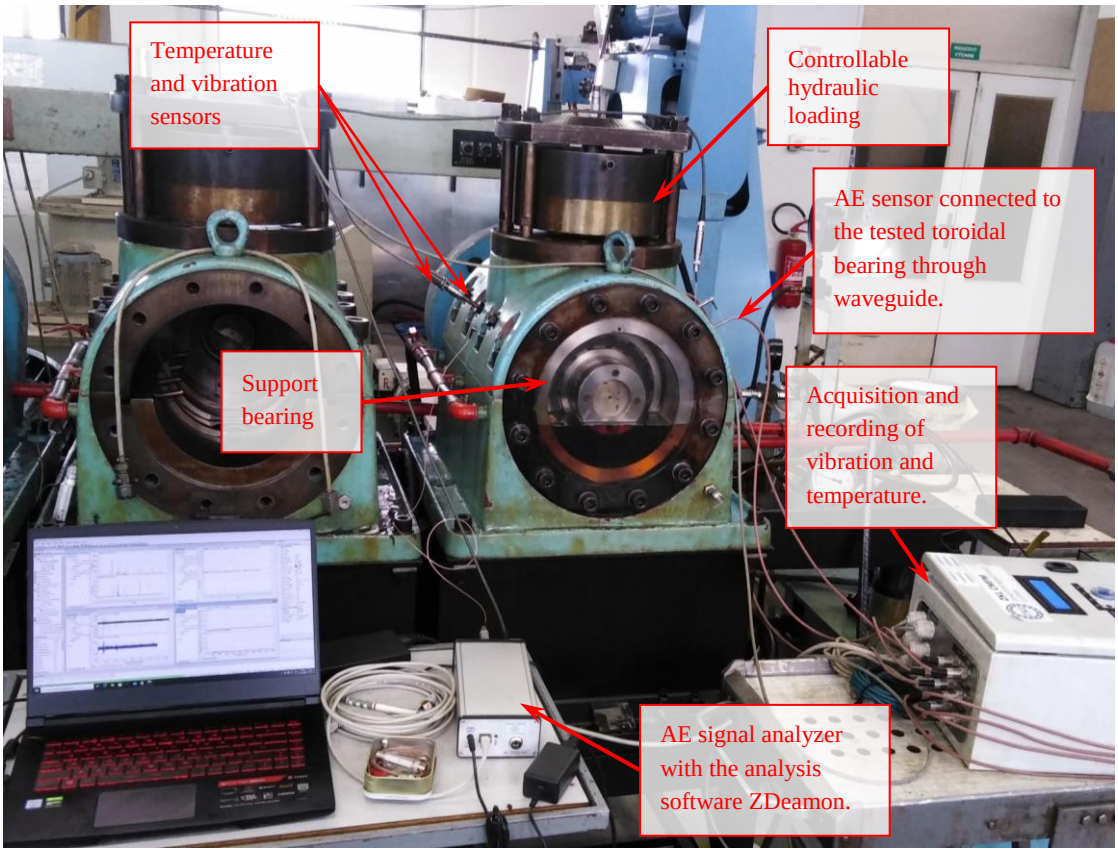

Figure 33. The experimental configuration for Toroidal Bearing testing in ZKL Laboratories

The materials of inner ring, outer ring and rollers are high-carbon chromium bearing steel $GCr_{15}SiMn$ which is hardened and tempered to hardness HRC 58 for the rings and HRC 61 for the rollers. The parameters of the two types of bearings are shown in Table 1 below.

Table 1. Parameters of the two main shaft bearings.

Property	C4030V	C4026V
Bore diameter	150	130
Outside diameter	225	200
Width	75	69
Permissible axial displacement 1	17	11
Permissible axial displacement 2	10	4

Figure 34 shows a schematic drawing illustrating the principle of the test.

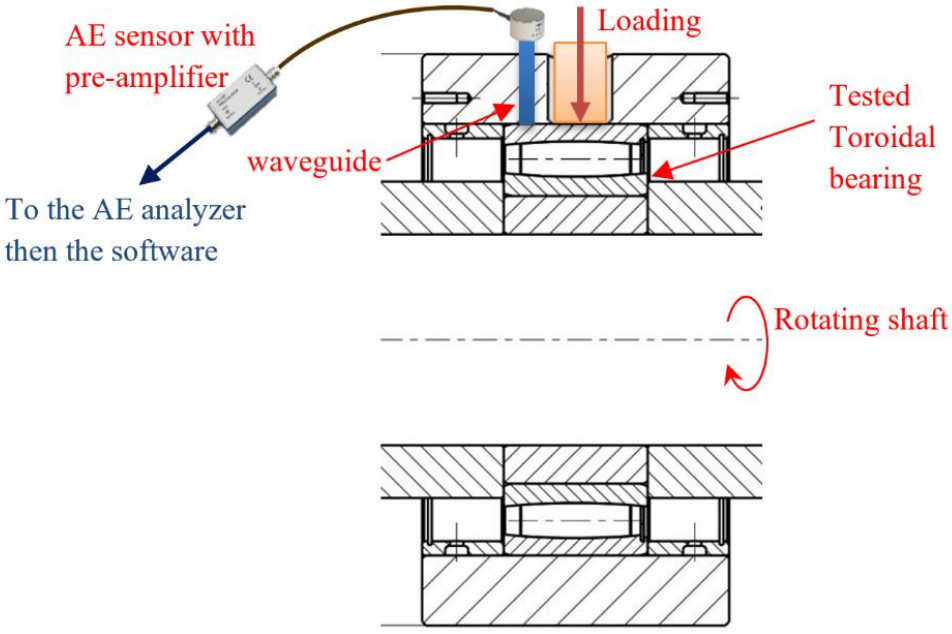

Figure 34. Schematic drawing for the principle of the experiment

The main part of the stand is the housing that contains the tested bearing with two support bearings (cylindrical bearings), and the hydraulic loading system is mounted on this housing. The upper part of the split housing contains two waveguides, which receive the AE signal from the surface of the outer ring of tested bearing and transmit it to the AE sensors that are firmly attached to those waveguides, as shown in the schematic drawing in Figure 34. Two AE sensors were employed in the tests. One of the AE sensors was attached to a waveguide in contact with the outer ring of the bearing, and the other to the housing of the bearing (which is supposed to act as a reference for the other signal). The AE sensors used in this experiment are from the type IDK-14 with a built-in preamplifier 20 dB, frequency range [10-500 kHz] and the AE monitoring system used is the analyzer DAKEL-ZEDO with two channels. The sampling frequency used for frequency spectrum computation is 5 MHz, and even though it is considered a high value, it was still a tradeoff, to be able to record longer periods of the signal without overloading the saving hardware. The frequency bandwidth was limited by digital filters: High-pass filter 50 kHz and Low-pass filter 400 kHz (software switchable). The global measurement period for AE parameters was set to 1 second, because it was anticipated that the test will run for many days.

5.1.1 Design and properties of the toroidal bearings

Permissible tilting (angular misalignment)

Toroidal roller bearings can be tilted by an angle of up to 0.5° (CARB® from SKF© and TORB® from Schaeffler©) between the center axes of the inner ring and outer ring without impairment of the function and rating life.

In this way, the toroidal roller bearing can compensate a slight geometrical deviation of the housing bore or a shaft that is not precisely aligned without difficulty. Depending on the series and size, tilting of more than 0,5° is also possible but may be associated with a reduction in the rating life.

Axial displacement (axial misalignment)

Toroidal roller bearings can accommodate axial offset and thus compensate thermal expansion or deviations from the required bearing position.

The maximum displacement distances S_1 and S_2, which are specific to the product type, apply only where a sufficiently large operating clearance is present and to untilted bearing rings. Axial displacement and tilting changes the position of the rolling element in the bearing, which affects the operating clearance. During the design process, it must always be checked whether the operating clearance required will be present if there is:

- Axial misalignment (displacement)
- Angular misalignment (tilting)
- Axial misalignment and tilting.

In the case of full complement bearings, the displacement distance S_2 is restricted on one side by the retaining ring. This ensures that the crowned roller does not come into contact with the retaining ring. In order to ensure that the axial displacement distance is available, it is necessary that the free space on both sides of the bearing is observed.

In order to ensure the function of the toroidal roller bearings, two different situations must be checked. On the one hand, it must be checked whether the axial displacement distance in combination with the tilting is still within the permitted displacement distance s1 or s2 respectively. Since axial displacement and tilting affect the bearing clearance, it must also be checked whether sufficient operating clearance will be present in the application.

The resulting bearing clearance can be determined using the following equation 3:

$$S_{res} = S_{ini} - K_{\delta} \cdot \left(\delta_{ax} + K_{\varphi} \cdot \varphi\right)^2 \qquad (3)$$

Where:

S_{res} [µm] Resulting bearing clearance after tilting and axial displacement

S_{ini} [µm] Radial internal clearance after mounting

K_{δ} Operating clearance factor, (from dimension table)

δ_{ax} [mm] Axial displacement from central position

K_{φ} Tilting factor, (from dimension table)

φ ° Tilting between inner ring and outer ring (angular misalignment ± shaft deflection).

Geometrical restriction of the axial displacement:

Tilting causes axial displacement of the rollers from the central position. This means that the axial displacement facility of the bearing rings relative to each other is reduced by S_{φ}.

This reduction in the axial displacement facility due to tilting can be calculated as follows:

$$S_{\varphi} = K_{\varphi} \cdot \varphi \qquad (4)$$

Where:

S_{φ} [mm] Reduction in axial displacement facility as a result of tilting

K_{φ} Tilting factor, (from dimension tables)

φ ° Tilting between inner ring and outer ring (angular misalignment ± shaft deflection).

When tilting occurs at the same time, the maximum possible axial displacement facility is calculated as follows:

$$S_{red} = S_1 - S_\varphi \quad (5)$$

In the case of full complement bearings, there is an additional effect as follows:

$$S_{red} = S_2 - S_\varphi \quad (6)$$

Where:

S_{red} [mm] Maximum axial displacement facility under tilting

S_1 [mm] Maximum axial displacement facility from dimension table, in the case of full complement bearings this is in the opposing direction to the retaining ring

S_φ [mm] Reduction in axial displacement facility as a result of tilting

S_2 [mm] Maximum axial displacement facility from dimension table, in the case of full complement bearings this is in the direction of the retaining ring.

5.1.2 Restriction due to reduction in radial bearing clearance

The bearing clearance is reduced in the following cases:

- axial displacement
- tilting of the bearing from the central position
- axial displacement and tilting of the bearing from the central position.

Depending on the necessary operating clearance, it must be checked whether the required axial displacement is possible under the tilting present.

The reduction in operating clearance is calculated as follows:

$$\Delta S = K_\delta \,.\left(\delta_{ax} + K_\varphi.\varphi\right)^2 \quad (7)$$

Where:

ΔS [µm] Reduction in radial bearing clearance

K_δ Operating clearance factor, (according to dimension)

δax [mm] Axial displacement

Kφ Tilting factor, (from dimension tables)

φ ° Tilting between inner ring and outer ring (misalignment ± shaft deflection).

5.2 AE measurements on the bearings of the Wind Turbine

The measurements took place in a real-life environment on a WT of the type VESTAS 90/2,0MW wind turbine in South Moravia, the Czech Republic. This type of WTs with the 2-megawatt production is the most popular in that region, and it operates in a wind speed range between 4-25 m/s. The drivetrain of this WT is of the four-point suspension type, which is characterized by a main shaft supported by two separate roller bearings. In the four-point suspension drivetrain, the weight forces, the yawing and nodding moments from the rotor are completely transmitted to the nacelle's main frame, which means that the gearbox is protected against those effects, it also makes the replacement of the gearbox relatively simpler.

The WT that accommodates our investigation has been in service since 2006. The main shaft and its bearings have not been replaced. So statistically speaking, the main bearings are supposed to be getting closer to the end of their service life, since they have been in service for 16 years. The parameters of the WT are given in Table 2.

Table 2. Operation parameters of the wind turbine.

Property	Value
Model VESTAS	V90/2,0MW
Rated power	2,000.0 kW
Cut-in wind speed	4.0 m/s
Rated wind speed	13.0 m/s
Cut-out wind speed	25.0 m/s
Rotor Diameter	90.0 m
Swept area	6,362.0 m²
Specific area	3.19 m²/kW
Rotor speed, max	14.9 r.p.m
Tip-speed	70 m/s
Power density	1:314.4 W/m²
Weights	Nacelle: 68 tons, Rotor + hub: 36 tons.
Number of blades	3
Power control	Pitch

The procedure of the measurement is shown in the schematic diagram in Figure 29.

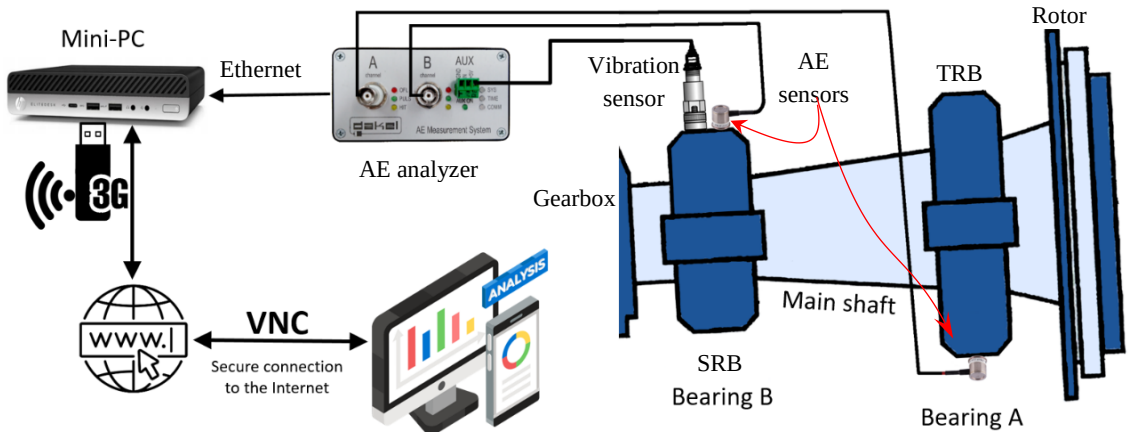

Figure 35. Schematic diagram of the measurement

The two bearings under investigation are from the types:
Bearing A: SKF C 30/630 KM/C4, which is a toroidal roller bearing.
Bearing B: SKF 24188 ECA/W33, which is a spherical roller bearing.
Some of the main parameters of the bearings were given in Table 3.

Table 3. Parameters of the two main shaft bearings.

Property	SKF C 30/630 KM/C4	SKF 24188 ECA/W33
Bore diameter	630	440
Outside diameter	920	720
Width	212	280
Number of rollers	28	21 x2
Roller diameter	69.4	74.6

5.2.1 The application of AE as a CM Technique

For the purpose of monitoring the condition of the two main shaft bearings of the WT we (as a research group) applied the same CM system that we used in the laboratory experiments, which is an AE based CM system. We continuously recorded and analyzed the AE activities using the same AE analyzer Zedo (Dakel) which has a high dynamic range and a sampling frequency. We even tried to use the same version that was applied in the experiments, which is equipped with two AE channels and one auxiliary input channel that was connected to the vibration accelerometer. Figure 36 (Equipment) shows the analyzer fixed to the frame of the nacelle, and connected to the mini-Pc using Ethernet cable. The analyzer is also connected to two AE sensors with coaxial cables. The two AE sensors that were used are from the model MDK-13, which is a relatively small AE sensor with internal preamplifier (MDK13AS) and built-in magnetic holder. Each sensor contains an internal impedance converter and preamplifier with a 35 dB

gain. The sensitivity of the sensor is at its best between 100-400 kHz (according to the manufacturer recommendations). AE sensor that is connected to channel A is fixed to the lowest point on the housing of bearing A, and AE sensor that is connected to channel B is fixed to the top of the housing of bearing B, as shown in the schematic diagram in Figure 35.

The sampling frequency that we chose for frequency spectrum computation is 2 MHz, which was chosen after considering the long expected time the measurements are going to take. The frequency bandwidth was limited by digital filters as follows: High-pass filter 50 kHz and Low-pass filter 500 kHz (software switchable). The global measurement period for AE parameters was set to 1 second, which is a suitable compromise for long-term measurements, according to our own experience, since we planned from the beginning for a long-term measurement that could take many months. However, since we have continuous online access to the monitoring system, we were able to increase those values in specific times of interest if required. Some basic configurations on the AE analysis software included saving the full signal twice a day for a period of 30 seconds, and simultaneously recording the full vibration signal for those 30 seconds (twice a day, at 8:00:00 a.m. and at 04:00:00 p.m.).

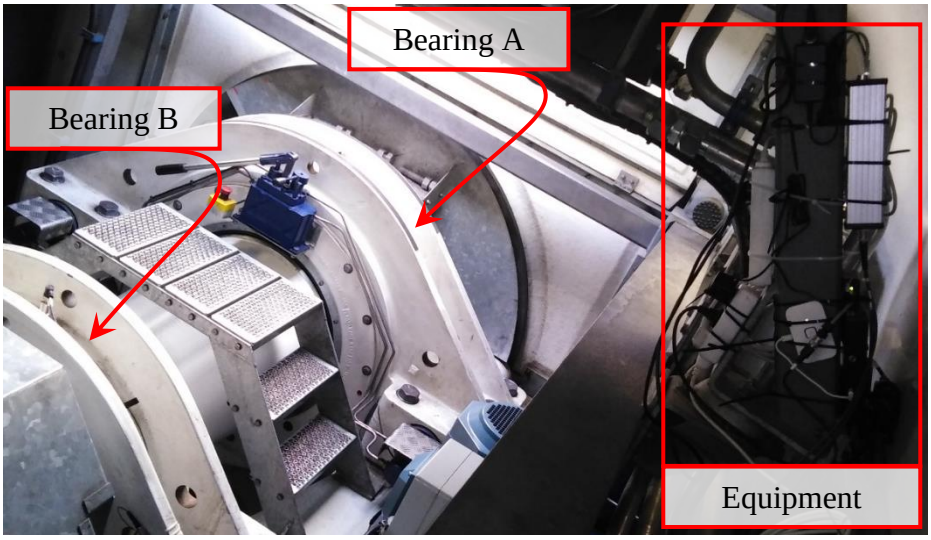

Figure 36. Position of the measuring equipment inside the nacelle

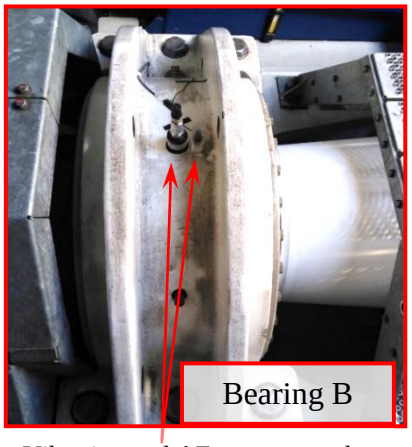

(b) Vibration and AE sensors on the housing of bearing B

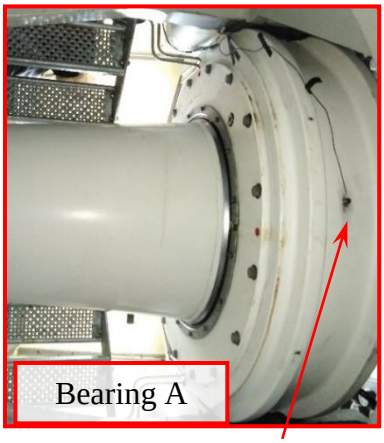

(a) AE sensor on the lower half of the housing of bearing A

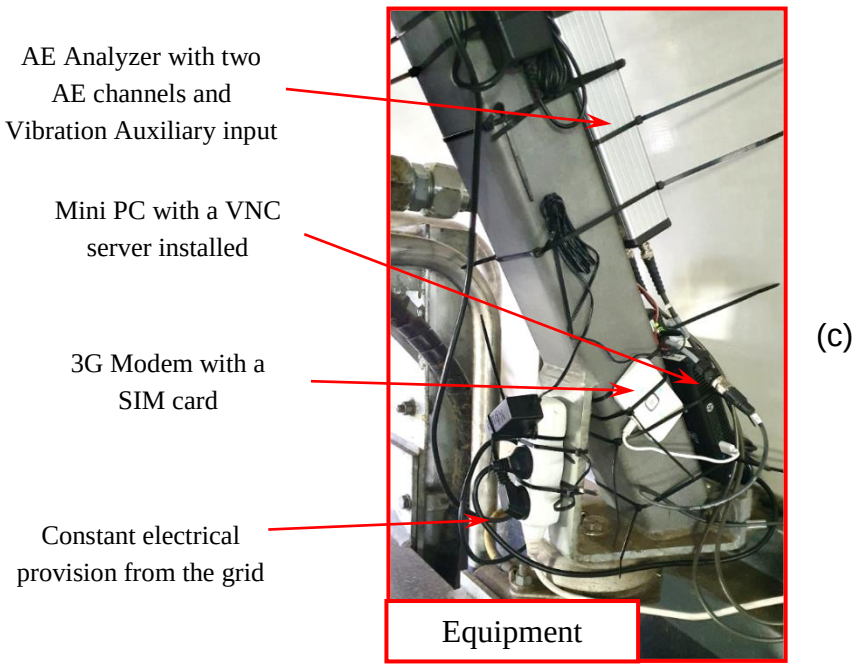

Figure 37. (a) & (b) Positions of AE sensors on the housings, (c) Equipment for data acquisition, analysis and transmission from WT nacelle.

The AE analyzer that we used provides all the required AE parameters. As specified earlier, since our main focus in this study will be on the analysis of frequency domain, we chose to use RMS of the signal and ASL. RMS is the most commonly used time-domain parameter of AE is RMS, and it is defined as:

$$RMS = \sqrt{\sum_{i=1}^{N} \frac{X(i)^2}{N}} \qquad (8)$$

Where N is the number of measurements (related to the sampling frequency), and X(i) is the voltage values of the signal from the sensor.

Another commonly used AE parameter is the Average Signal Level (ASL), defined as:

$$ASL = \frac{1}{T} \int_{t_0}^{t_0+T} |v(t).dt| = \frac{1}{N} \sum_{n=1}^{N} |v(n)| \qquad (9)$$

Where t_0 is the initial time, T is the integration time of the signal and N is the number of discrete AE data within the interval T. v(t) is time-varying signal voltage. ASL value from this equation is in volts.

Since we could not get information from the SCADA system of the WT, we applied our own real-time online monitoring system, by installing a mini PC (it has all the capabilities of a regular PC, but with compact design) connected to AE analyzer inside the nacelle of the WT. The AE analyzer captures high-frequency AE signals emitted by the bearings during operation via AE sensors that are fixed firmly to the housings of the two main bearings. The mini PC acts as a local data processing unit, performing primary signal analysis and feature extraction processes. More demanding and advanced analyses on the extracted data are then performed after transmission to our Lab computers.

To ensure seamless and secure data transmission, a 3G (3rd generation of digital mobile networks) internet connection was employed, by using a modem with a 3G SIM card connected to the PC, allowing continuous remote access to the mini PC within the WT's nacelle. Furthermore, a VNC (Virtual Network Computing) server software was installed (RealVNC®) on the PC to establish a secure and encrypted connection between the PC and any VNC viewers software on our office PCs. The electricity supply for the PC was provided by a cable from the electric grid, not from the WT, to guarantee a continuous provision of electricity.

This integration of a 3G internet connection and a VNC facilitates real-time data transmission wirelessly, and yet ensures secure remote access to the monitoring system.

It is important here to distinguish between the case of wind farms and individual isolated WTs. The use of a highly sophisticated SCADA system in the case of wind farms consisting of big number of WTs pays off on the long run. However, in the case of individual stand-alone WTs, utilizing a VNC server installed on a mini PC equipped with a reliable 3G connection, the monitoring process becomes significantly streamlined and cost-effective. This approach eliminates the need for a complex and resource-intensive SCADA system that is required in the case of wind farms, and it allows direct access to real-time turbine data from anywhere, on any device that has access to the internet. It is worth noticing that we are not suggesting this application as a replacement of SCADA, but as a complementary application to reduce the complexity of SCADA.

The vibration transducer (accelerometer) that we used is from the type IEPE (Integrated Electronics Piezo-Electro); it has a built-in integrated circuit with a charge to voltage converter. It requires 18 – 24 V DC power supply with constant current, which was not a problem in our installation to provide it from the analyzer itself. The accelerometer is connected to Analog-to-Digital Converter (ADC) in the auxiliary card of the AE analyzer. It has a sensitivity value of 97.6 [mV/(m/s^2)], and Bias = 11.5 [V]. The data that are received from the vibration transducer (accelerometer) are raw acceleration data. This signal is digitally processed and presented in the time domain, and then it is transformed to the frequency domain.

The sampling frequency of the vibration data is: $F_{s\text{-}v}$ = 1000 [Hz]

Since the measurements are continuous, it is not reasonable nor realistic to record the whole period of the measurement especially with such high sampling frequency, so we are recording two times a day for 30 seconds (two slices a day).

We started the measurement procedure in April 2022, and since then we have been monitoring and recording data about the condition of the main shaft bearings in the WT. Therefore, by the time of preparing this paper, we already have data for one year. We divided the recorded data into weeks, so for each week we have a block of data ready to be analyzed separately.

Figure 38 shows the recorded data for two weeks in April 2022, as an example. It includes some of the most relevant operation parameters of the WT, such as the wind speed, rotor r.p.m, and the produced power to the grid, as well as some of AE parameters such as RMS and ASL from both channels A and B, which are connected to AE sensors on bearings A and B respectively.

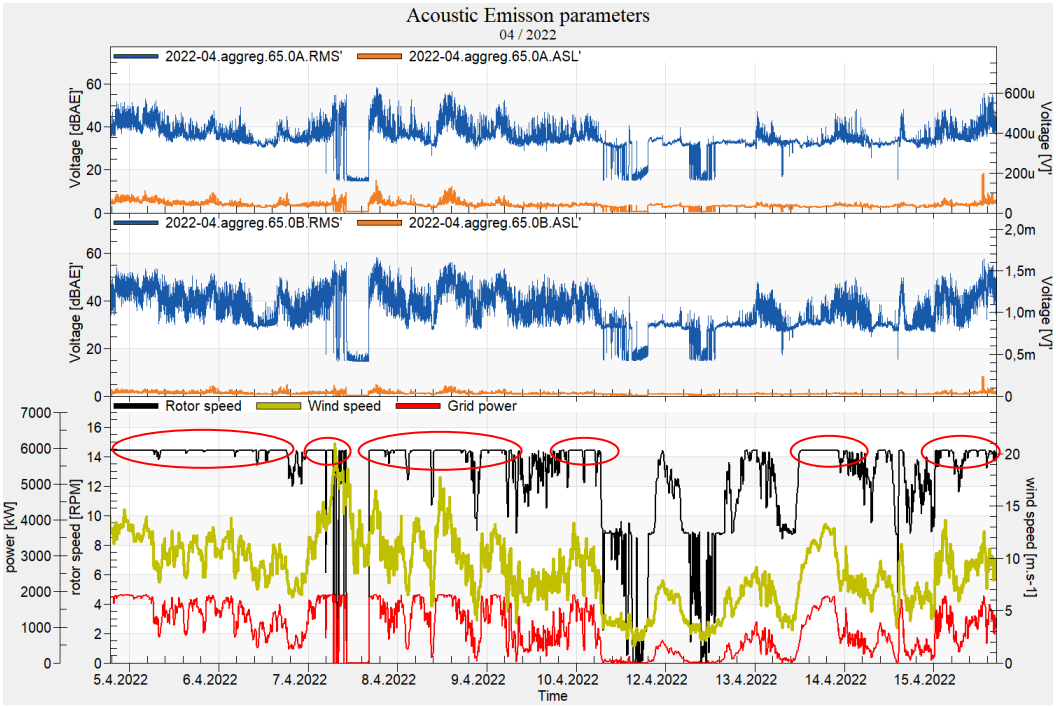

Figure 38. Operation data for the first two weeks in April 2022 (as an example).

(a) RMS and ASL (aggregated) of AE from channel A. (b) RMS and ASL (aggregated) of AE from channel B. (c) WT operation parameters, rotor speed, wind speed, output power. Red ellipses are the places of the cut-out rotor speed, where data were picked to be analyzed.

We then sliced each block of data to segments where the full data was recorded, which means twice a day, each time segment consists of 25 seconds of fully recorded AE and vibration data, we call them time slices. We concentrated on analyzing the time slices where the rotation of the rotor was at its highest (at the cut-out value of 14.9 r.p.m). Because as it is shown in Figure 38 (c), marked by red ellipses, it is obvious that at these times the signal was the strongest, and the AE parameters were at their highest values.

This fixed highest speed for the rotor is considered as an advantage for monitoring the main shaft bearings in WT, because it helps fix one of the main parameters, which is the rotation speed, for a period of time as long as the wind speed is above its cut-out value, which is 25 (m/s). In our case, the cut-out rotation speed was set at 14.9 r.p.m. Therefore, we applied all the analyses to the signals just in these cut-out periods.

The duration of 1 cycle during the cut-out speed is: $60/14.9 \approx 4$ seconds.

5.2.2 The AE signal analysis method

We applied similar sequence of actions for the analysis of AE signal that was received from both sensors fixed to the bearings. Those steps are shown in the diagram in Figure 39. Which consists of signal acquisition in the time domain, transforming the signal to the frequency domain using FFT, and identifying the DF for each AE hit in the time slice to create a DF map for all AE hits in that time slice. Many AE parameters were also extracted, but we chose to present just the RMS in correlation with the DFs in the time domain, since RMS is the mostly

used AE parameter according to the literature, and because we are aiming at a signal-based analysis rather than a parameters-based one.

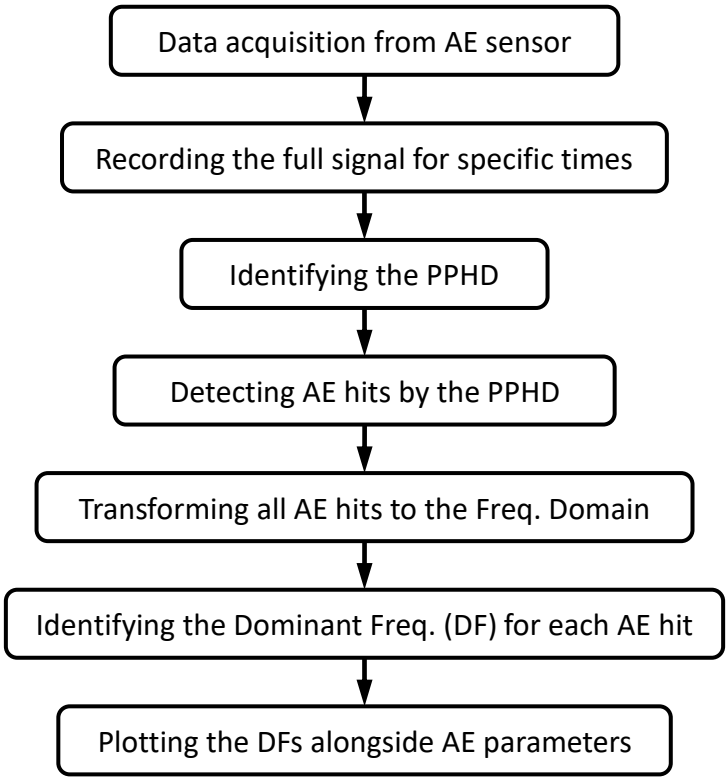

Figure 39. Sequence of steps for AE signal analysis

Figure 40 shows one AE hit in the time domain that is detected by a PPHD. The PPHD was established to get more versatility in determining the parameters for detecting AE hits, even on the recorded signal (offline). Table 4 summarizes some of the main parameters of the PPHD.

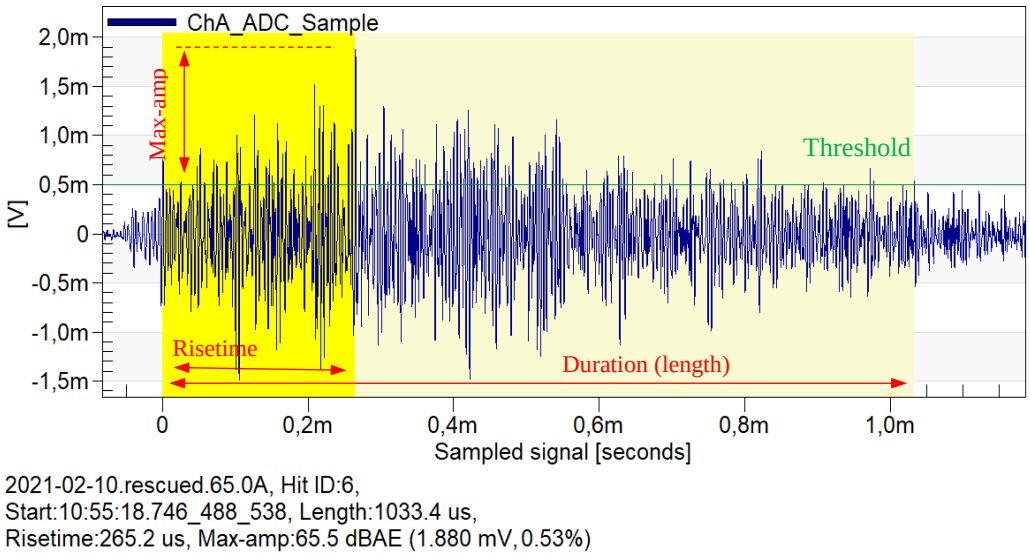

Figure 40. AE hit from channel A

Table 4. The main setup parameters for PPHD in WT measurement

Parameter	Value
Detection threshold	1 mV (60 dBAE)
Separation time	1 ms
Dead time	10 ms
Minimum hit length	1 us
Maximum hit length	500 ms
FFT Calculation method	Welch estimate
Window size	8192
Window overlap	50%

The signal is then transformed to the frequency domain using FFT-based method (Welch method) to create the power spectrum shown in Figure 41. From this figure, the frequency corresponding to the highest power in the power spectrum is defined as the dominant frequency of the waveform. We can see from Figure 41 that DF for this AE sample is around 170 kHz.

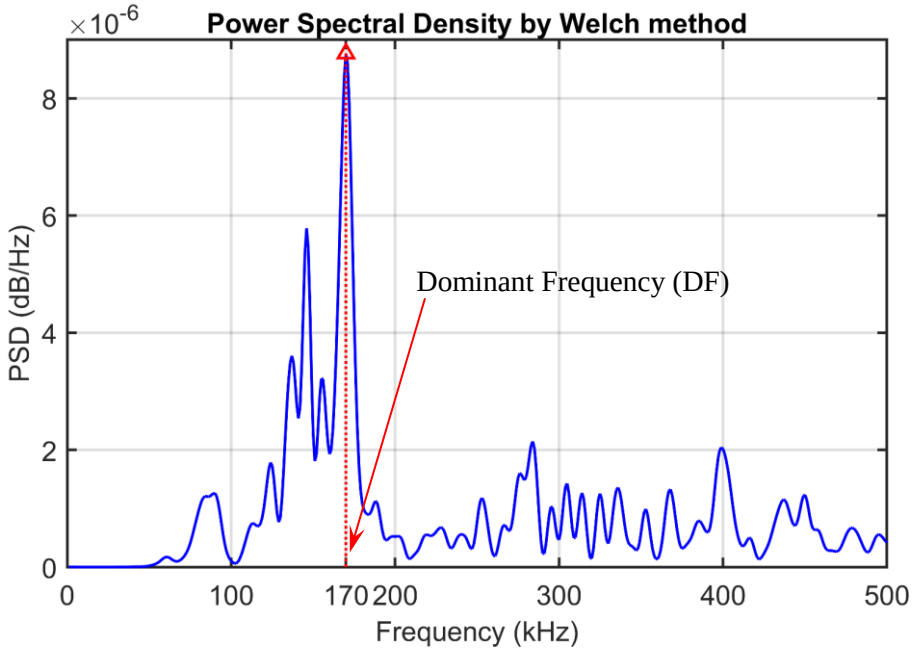

Figure 41. Frequency domain of the AE hit shown in Figure 40 above

This could have been done using the Sort-Time Fourier Transform (STFT) to produce the spectrogram shown in Figure 42, then getting the index (the frequency) at the point with the highest energy. This would give the same 170 kHz as a dominant frequency for this particular AE hit shown in Figure 40. The STFT is well-known for being used to analyze the changes in frequency content of a nonstationary signal over time, such as AE signal. However, since the Welch method would give the same result, and it would reduce the number of computations, it has been chosen for the analysis of AE signal in these measurements.

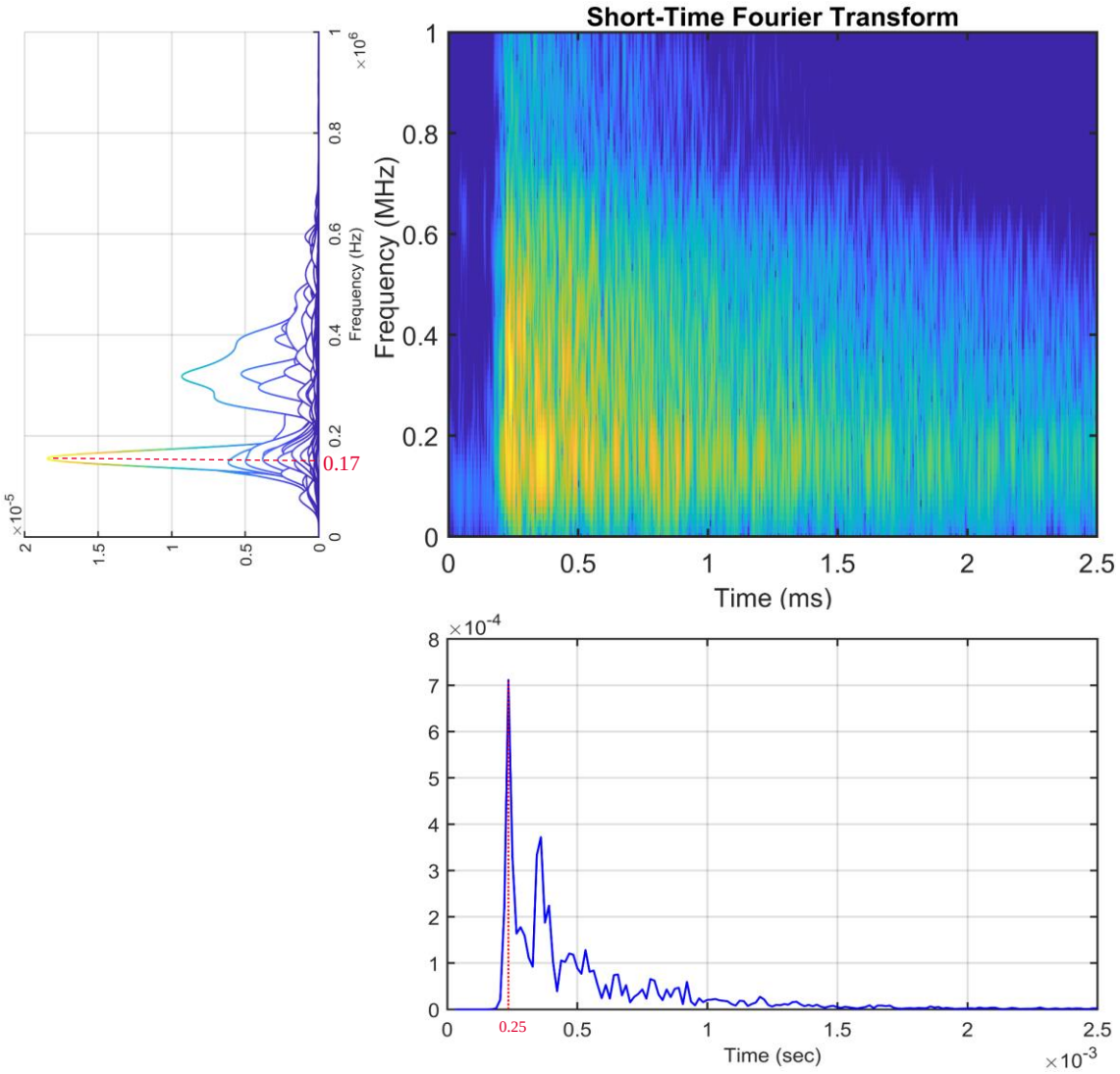

Figure 42. The STFT spectrogram of the AE hit in Figure 40, with its time and frequency components

The same process was then applied for each AE hit detected by the PPHD. The DFs for all the detected hits in one time slice were then collected in one graph as shown in Figure 43 (a) and (b) which are called the DF maps for bearing A (TRB) and B (SRB), respectively. Figure 43 also shows the RMS of AE from both channels A and B.

It is work mentioning here that the application of AE was carried out according to the standard ISO 22096:2007 [67]. While other procedures for CM and diagnostics of the drivetrain of the WT were carried out in accordance with the standards ISO 16079-1:2017(en) [68], which covers the application of CM to wind turbines, including recommendations and best practices described in the generic standards. And ISO 16079-2:2020(en) [69], which prescribes the methodology for making an FMSA (Failure Mode Symptoms Analysis) with the purpose of defining symptoms and related descriptors to detect a particular failure mode.

6 RESULTS AND DISCUSSION

This section is related to the previous section (Materials and Methods), therefore, it follows the same division to two parts, the first part describes the results of the laboratory experiments and the second outlines the results from the field measurements.

6.1 Results of laboratory experiments

The result of this analysis is shown in the Figure 43, where Figure 43 (a) shows the temperature and vibration levels on the outer ring of the tested bearing, and Figure 43 (b) shows the AE RMS value and the DF of AE hits that were detected by PPHD. The green curve represents the incremental number of AE hits during the full test.

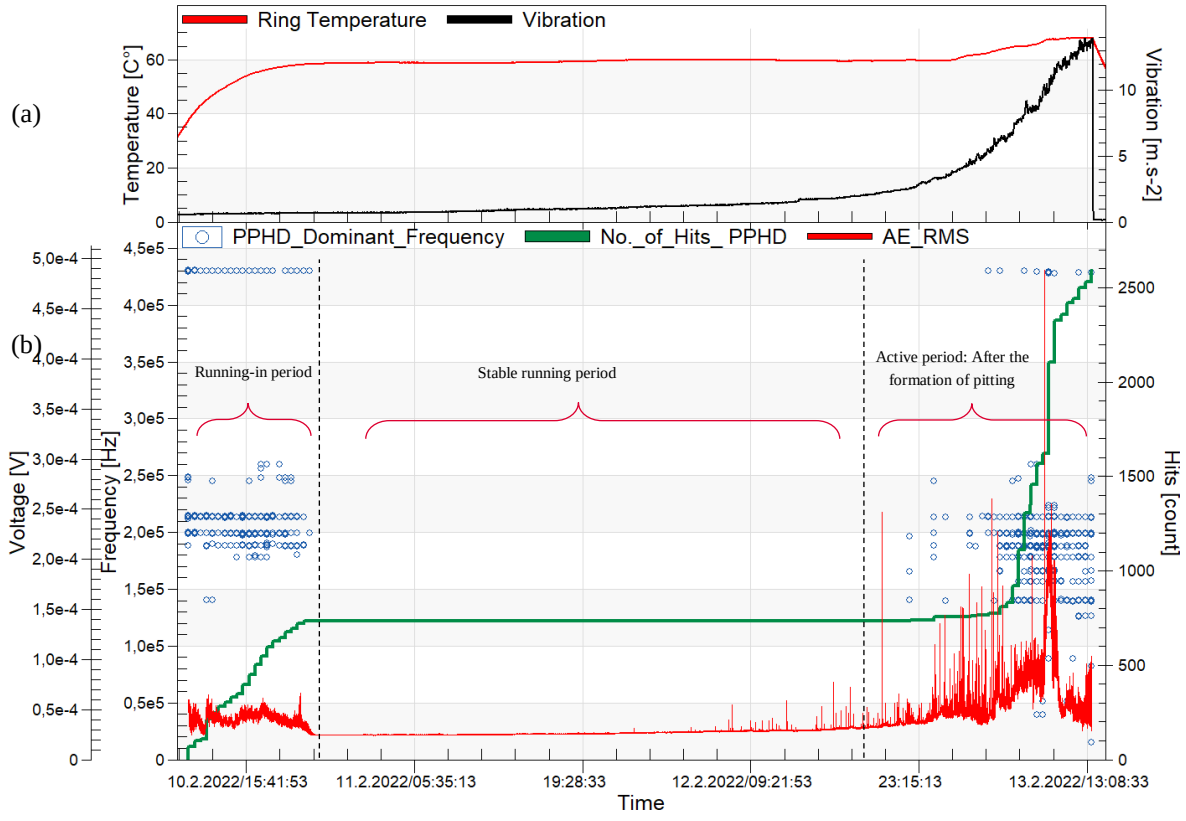

Figure 43. Temperature, Vibration, RMS_{AE}, and AE DFs for the whole period of the measurement

From Figure 43 (a), we can see that the vibration signal, which represents the raw acceleration value received from the vibration transducer, reflected the changes in the condition of the bearing during the test. While the temperature of the outer ring was not responsive enough, and the range of change in temperatures is small and cannot be depended upon. On the other hand, Figure 43 (b) gives an obviously more detailed picture of the same measurement using AE. The red line that represents the RMS_{AE} shows at the first couple of hours the running-in period, which is the initial process that occurs when solid surfaces are brought together under a non-zero normal force. It clearly shows an increase in AE activity because of the breaking of the tips and abnormality that are left on the surface of the bearing raceways and rollers as a result of the machining. The removal of those abnormalities because of the big pressure between the rollers and loading zone on the raceways makes the raceways surface smoother as shown in Figure 44, which we took for the bearing rings after the end of running-in period.

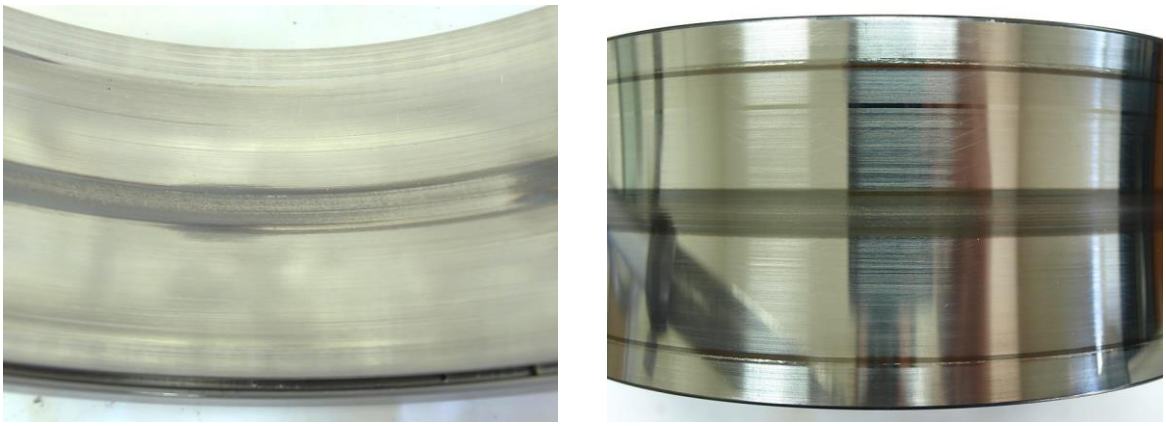

Figure 44. The smoothness of the raceways of the outer and inner rings after the running-in period.

The RMS_{AE} curve in Figure 43, then shows the stable running period which continues for a couple of days. This is the useful period of the bearing, and it is preferred to be as long as possible while the bearing is service, but it is not useful in our experiment since it is inactive, as the graph of RMS_{AE} shows. Figure 43 also shows the DF of AE hits as small blue circles, and we can see that they disappear almost completely during the stable running period. This is in part because of the parameter that were chosen for the DF, which are given in Table 4. However, since those parameters are applied the same on the whole experiment, the values that DF give during the running in period take more credibility. Those DF values during the running-in period show that all DFs of AE hits fall in 8 separate and well-defined bands. Since this period continues for couple of hours then disappears, it is not important per se, but it is a proof of the effectiveness of using AE over vibration, since vibration curve did not reflect obviously the existence of it in its curve. The analysis of the signal in this period is also important for comparison purposes, since we know for sure that this is the running in period, hence we know the origin of AE hits is in this period.

Figure 45 shows a concentration “magnification” on the first 10 hours of the whole experiment where the running in takes place.

The figure shows 20 columns of blue circles, each column represents 10 seconds out of 30 minutes of the fully recorded signal, which means 10 hours. Those columns are the places where the signal was fully recorded and then analyzed by producing the list of DFs of all PPHD hits. Each column continues for just 10 seconds out of 30 minutes because recording the full signal continuously is impractical and it does not provide extra information.
Sample number 4 from those 20 columns was chosen for further analysis because it contains the highest increased number of PPCD hits, which is represented on the figure by the DFs of those hits.

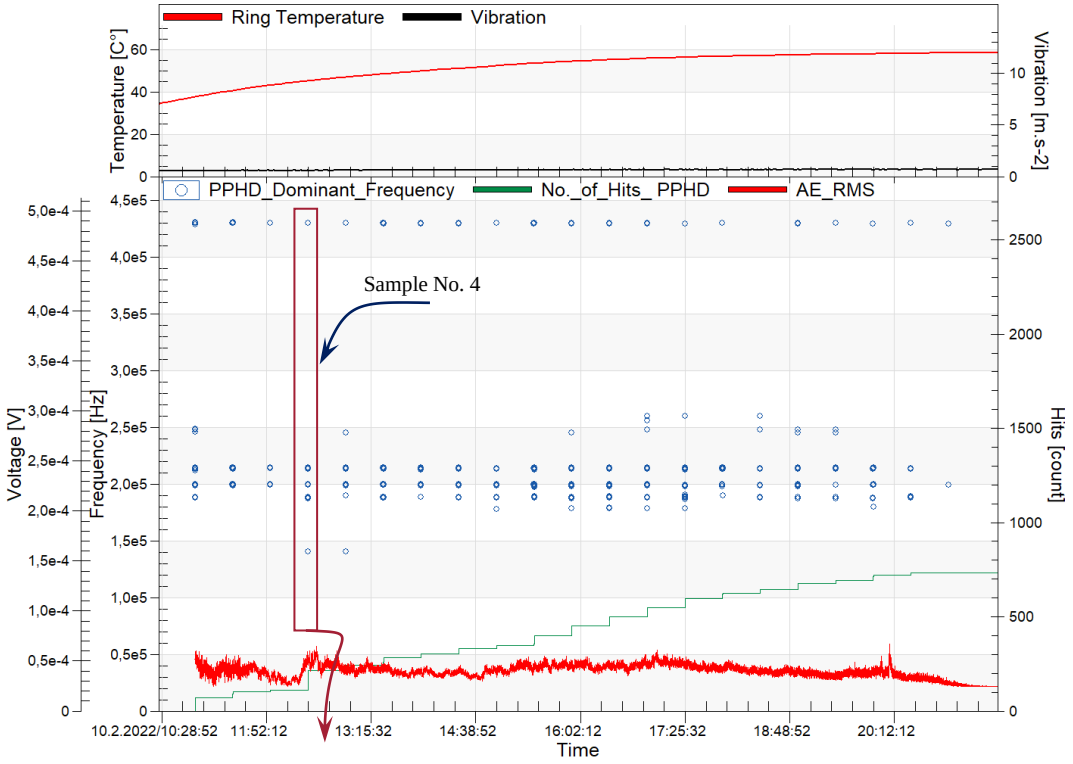

Figure 45. Temperature, Vibration, RMS_{AE} and AE DFs for the period of first 10 hours (the running-in period)

The magnification of column number 4 from Figure 45 is shown in Figure 46. The time slice for this sample lasted from 10.02.2022/12:25:18 to 10.02.2022/12:25:28.

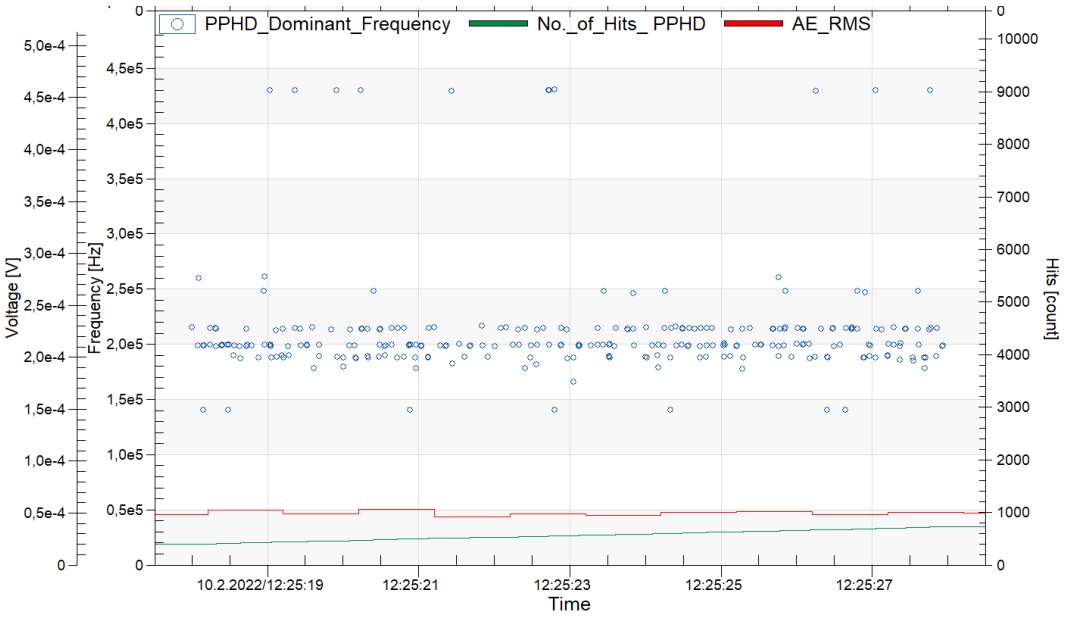

Figure 46. Temperature, Vibration, RMS_{AE} and AE DFs for the period of the 4th time slice with the highest number of AE hits in the running-in period

From this figure we can obviously see the 7 frequency bands that are separate and distributed to ranges shown in Table 5. This specific distribution of DFs of AE hits was repeated in all other time slices (columns of blue circles on the figure). The sum of all DFs of AE hits in the running-in period is then summarized and analyzed statistically later.

After the running-in period, comes a long stable running period, where the set-up PPHD did not capture any hit, but once the pitting started to formulate on the raceways of the bearing, this period is considered as finished, and the PPHD started recording. Hence started the so-called active period, which is the period that starts with the beginning of first signs of pitting and continues until the end of the experiment when the vibration level exceeds a specific safety value, which is a point where the bearing is rendered unusable anymore. This active period in this particular experiment continued for almost 11 hours, therefore we concentrated on analyzing the signal during this period, as shown in Figure 47, which can be considered as a magnified part of Figure 43. In (a) part it shows the same as before, that vibration increased steadily until a specific value that is preset to stop the test while the temperature's increase was very small. In Figure 47 (b) we see the 22 columns of blue circles that represent the DFs of AE hits.

From those columns the sample number 14 was chosen for further analysis because, as the curve of the number of PPHD hits shows, this sample has the highest number of hits. The time slice for this sample lasted from 13.02.2022/09:59:17 to 13.02.2022/09:59:27.

So "magnifying" this time slice further gives Figure 48. This figure shows clearly the separate DF bands of AE hits. The frequency ranges of the bands are given in Table 5.

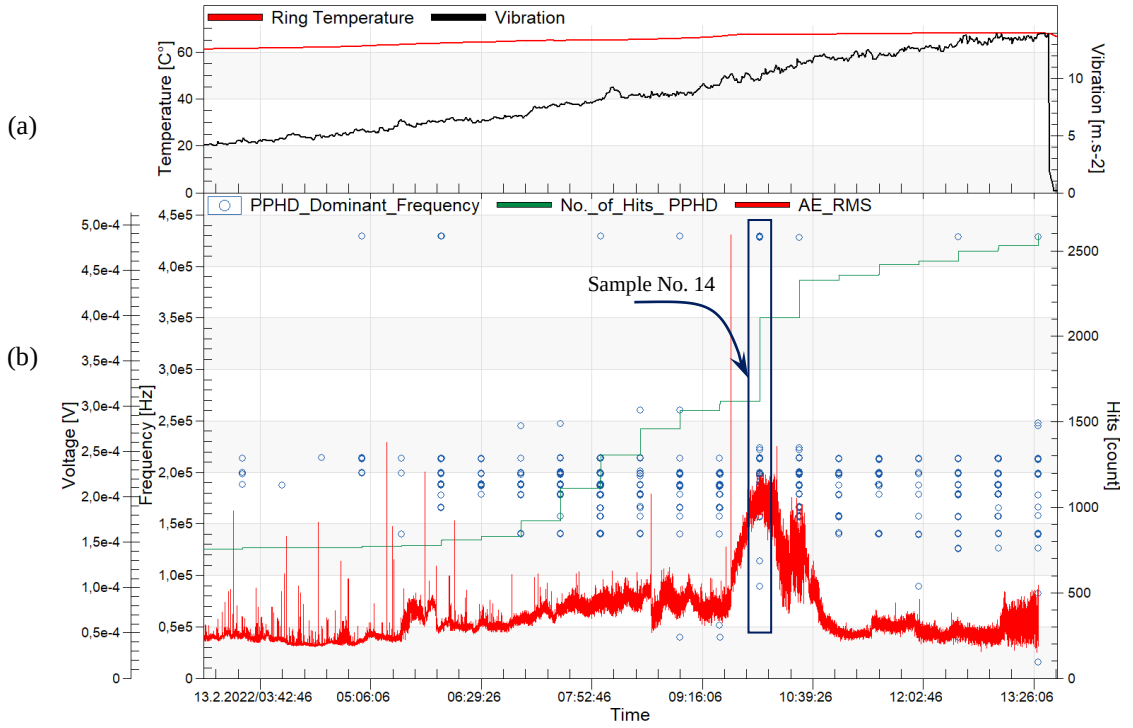

Figure 47. Temperature, Vibration, RMS_{AE} and AE DFs for the period of last 11 hours of the measurement

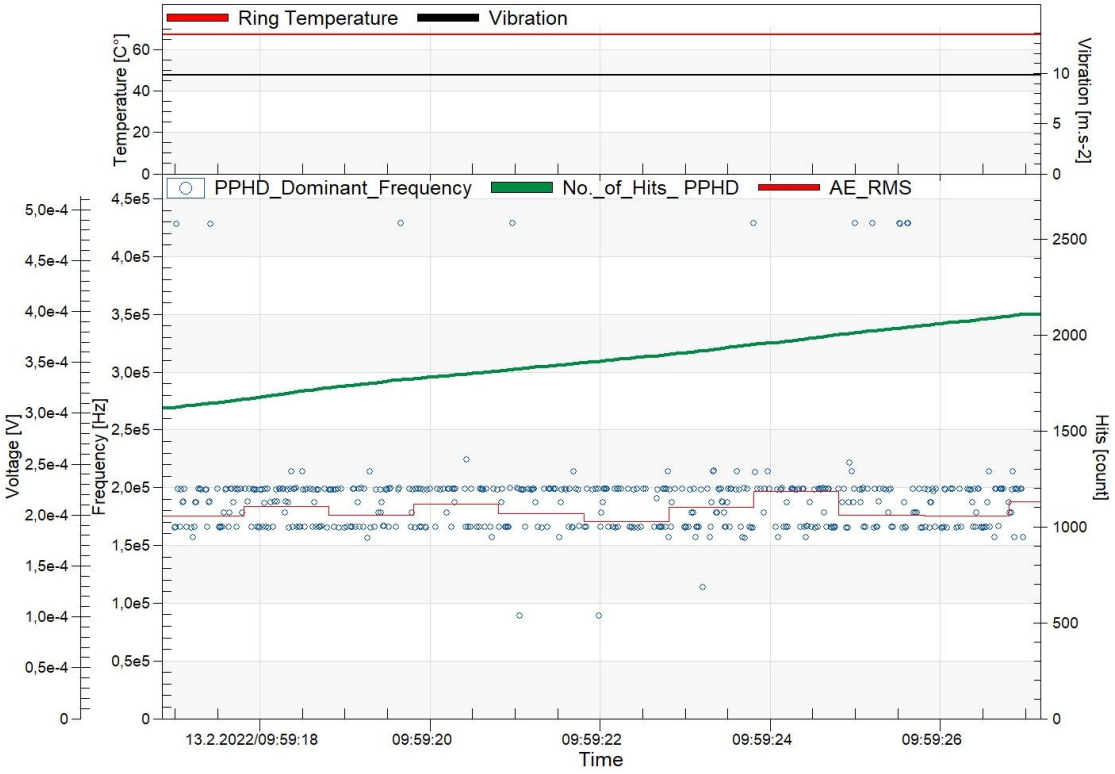

Figure 48. Temperature, Vibration, RMS_{AE} and AE DFs for one time slice with the highest increase in AE hits

Table 5 also includes the number of AE hits that fall inside each range (frequency band).

Table 5. The distribution of AE hits in the specified DF bands

	DF bands in the running-in period (first 10 h.) (kHz)		DF bands in the active period (last 12 h.) (kHz)		
	Range	Number of hits	Range	Number of hits	Sum
1	429 – 431	104	427 – 429	21	125
2	260 – 263	3	260 – 261	5	8
3	245 - 248	17	245 – 248	5	22
4	222 – 225	0	222 – 225	5	5
5	212 – 216	318	213 – 216	144	462
6	197 – 200.5	182	196 - 200.5	495	677
7	186 – 190	98	186 – 190	275	373
8	177 – 180	8	177 – 179	424	432
9	165 – 166	0	165 – 166	243	243
10	156 – 157	0	155 – 158	52	52
11	139.5 – 140	4	190 – 141	168	172
12	125 – 127	0	125 – 127	5	5
13	80 – 83	0	80 – 83	6	6
14	30 – 40	0	30 - 40	12	12
		734		1860	2594

Total sum = 2594 AE hit. The visual presentation of the results in Table 5 is in Figure 49

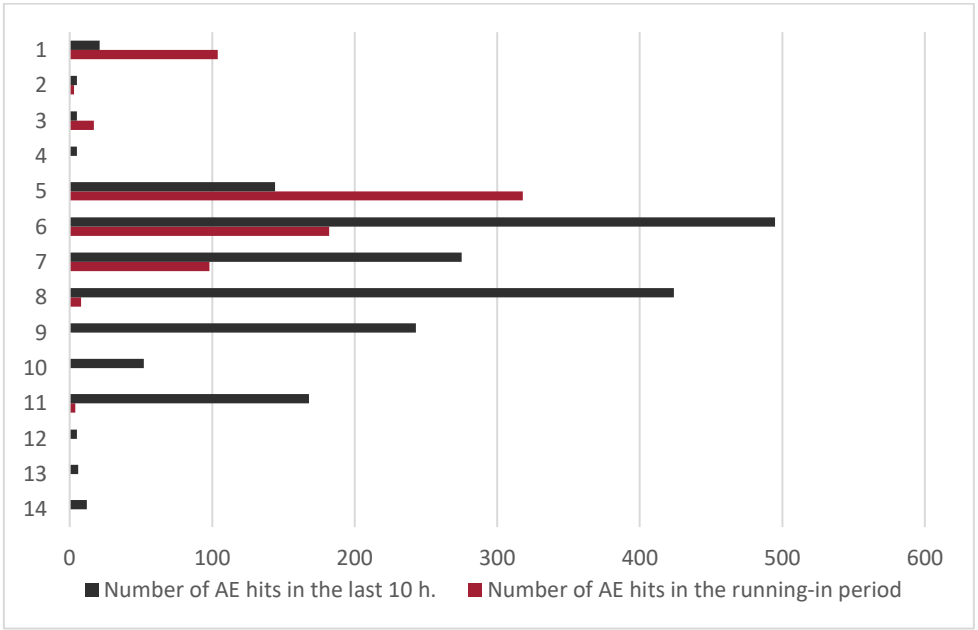

Figure 49. Comparison between the number of AE hits in the two periods where AE hits took place

From the statistical analysis of this specimen's results, which is demonstrated in Figure 49, we can find that the number of AE hits that appear during pitting and/or scalling is higher in the lower DF ranges (lower than 200 kHz), and the number of the AE hits that appear during the running-in period is higher in the high DF range (above 200 kHz). This pattern is repeated when we repeat the statistical analysis of the PPHD AE hits for other time slices, and it could be seen even in a visual comparison as the one presented in Figure 50 which is the same as Figure 43 after removing the stable running period in the middle, and where the DF bands where specified by yellow lines.

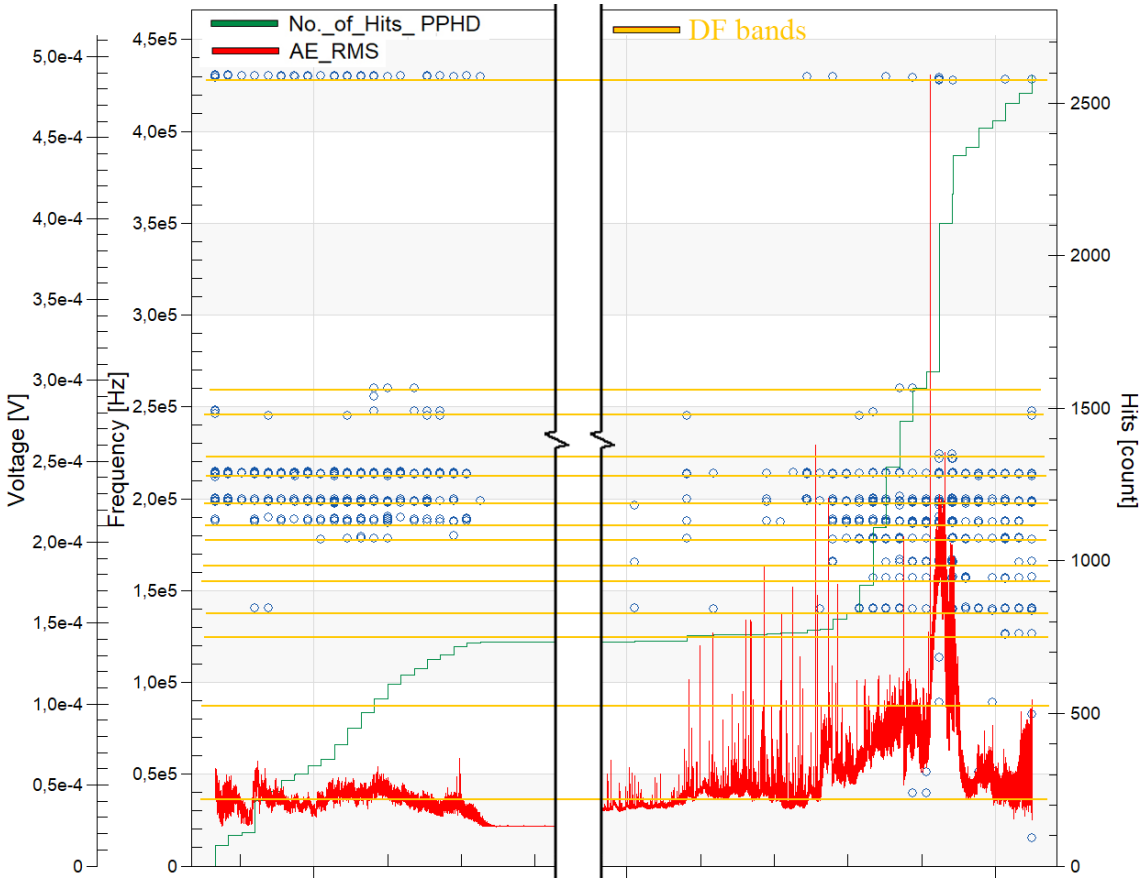

Figure 50. A comparison between the discrete AE DFs bands (the yellow lines) in the two periods at the beginning and at the end of the test.

The visual inspection of the tested bearings parts showed no pitting on the rolling elements, a few pits on the inner ring (the rotating ring), and big amount of pitting and even scaling in the outer ring (the fixed ring) specifically in the loading zone. The following figures, Figure 51, Figure 52, and Figure 53 show the rolling elements, the inner ring, and the outer ring of the tested bearing, respectively.

Figure 51. Number of the rolling elements of the toroidal bearing after the test.

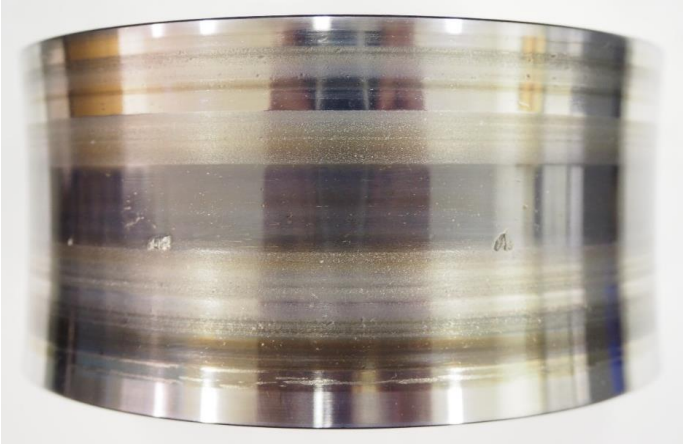

Figure 52. The scattered pitting on the inner ring of the toroidal bearing after the test.

Figure 53. The spalling in the loading zone on the outer ring of the toroidal bearing after the test (with permission from jakub.nemecek@zkl.cz).

6.2 Results of the measurements on WT bearings

6.2.1 Analysis of the Vibration signal:

The vibration signal was received from an accelerometer that is fixed to the upper part of the housing of the tested bearing, as shown in Figure 35. The signal then converted to digital by ADC in the analyzer and sent to the software to be presented in the time domain, as shown in Figure 54, which presents the fully recorded time slice (25 seconds) of the vibration data. It contains many overlapping signals from different sources, and a lot of noise, which cannot be distinguished. Therefore, we transform it to the frequency domain using Fast Fourier Transform (FFT). To produce the spectrum of frequencies in the signal we used Welch method [70], which is a method based on sectioning the recorded signal, taking modified periodograms of these sections, and averaging these short modified periodograms using FFT for the estimation of power spectra. It is essentially an improvement of the periodogram spectrum estimating method, and its main advantage is the reduction of noise in the estimated power spectra.

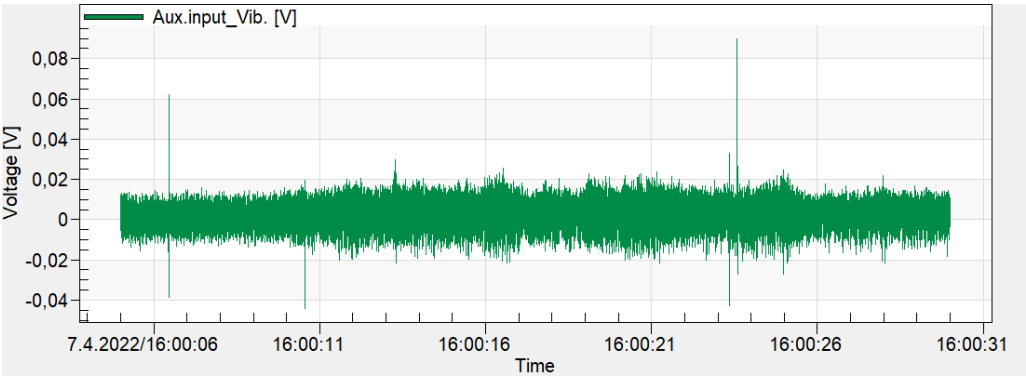

Figure 54. Fully recorded 25 seconds of vibration signal in the time domain

The procedure of the method goes by splitting up the original data segment into L data segments of length M, overlapping by D points. So, if D = M/2, the overlap is 50%, and if D = 0, the overlap is 0%. We chose the overlap between welch windows to be 50%, and the size of each window to be equal to the sampling rate, which is 1000 points.

To apply welch method and get the power spectrum of the signal, we extracted the data from the time domain and applied the procedure of Welch estimation in MatLab®. The result is shown in Figure 55. It shows the spectrum of frequencies of the signals that are combined in the vibration, and it distinguishes the frequencies that are dominant. We can tell from this figure that there are many signals received by the accelerometer with different frequencies, but the DF of vibration in this time interval is around 60 Hz.

The Y axis in Figure 55 is in logarithmic scale, so we remove this logarithmicity of Y, to get a more definitive curve for the DFs in the signal, as shown in Figure 56.

We can see from Figure 56 that the fundamental frequency of the vibration signal is around 60 Hz, and we can see the smaller peaks at its harmonics, the 120 Hz and 180 Hz. We can see also a peak at 0.25 Hz (=15 rpm), which is equal to the rotational speed of the main shaft. These results indicate a bearing fault, we can assume that there is a defect in raceways of bearing B.

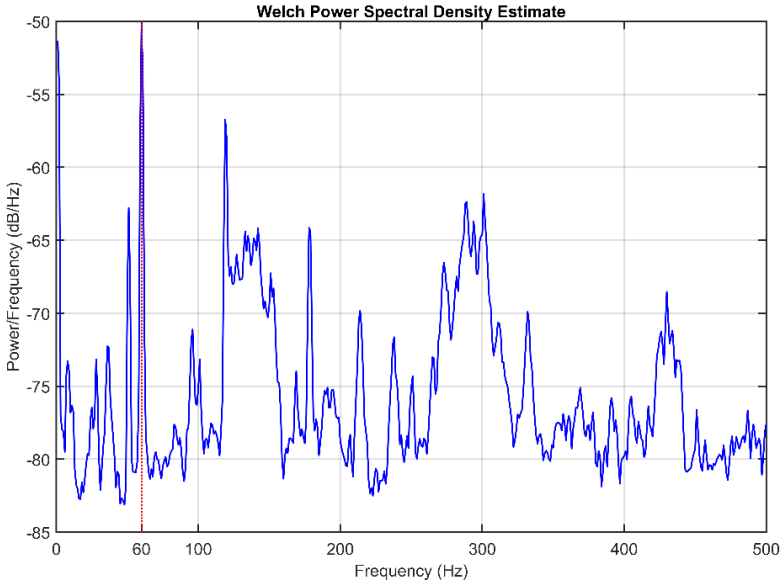

Figure 55. Spectrum of the vibration signal using Welch estimate

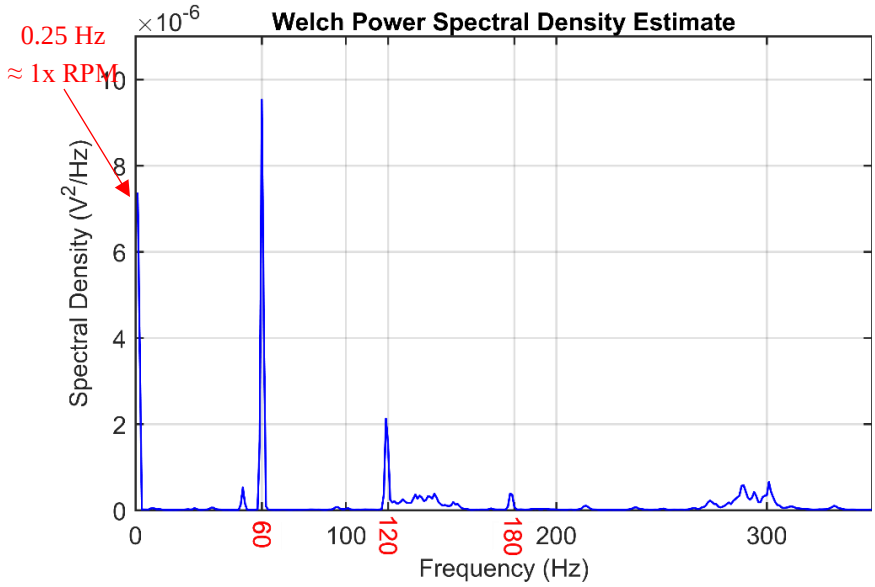

Figure 56. Spectrum after removing the logarithmicity of Y-axis

6.2.2 Reading the spectrogram:

We produced the spectrogram of the signal to estimate the power of the signal at different frequencies and at different times. The spectrogram in Figure 57 (a) shows the frequencies in time for this signal, while the intensity of yellow colour represents the power of the signal. Figure 57 (b) is the same as Figure 55 rotated by 90 degrees, because it represents the side view of the 3D spectrogram.

To find which timestamps contain the highest frequencies, we sum the power across all frequencies for each timestamp. As shown in Figure 58, we summed all the spectral power values at each timestamp from the spectrogram (a) to make up the graph (b) in the time domain.

Then we specify the maximum 10 values of the sum of signal's PSDs, or the 10 local maxima, as they are called in Figure 58 (b). Then we superimpose those values back on the time domain, as shown in Figure 59.

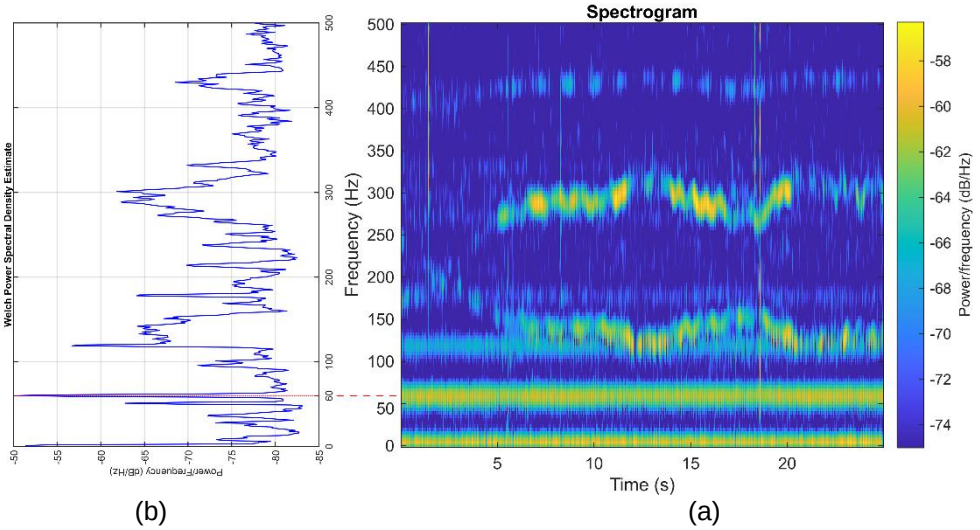

Figure 57. (a) Spectrogram of vibration signal, (b) with PSD of the signal.

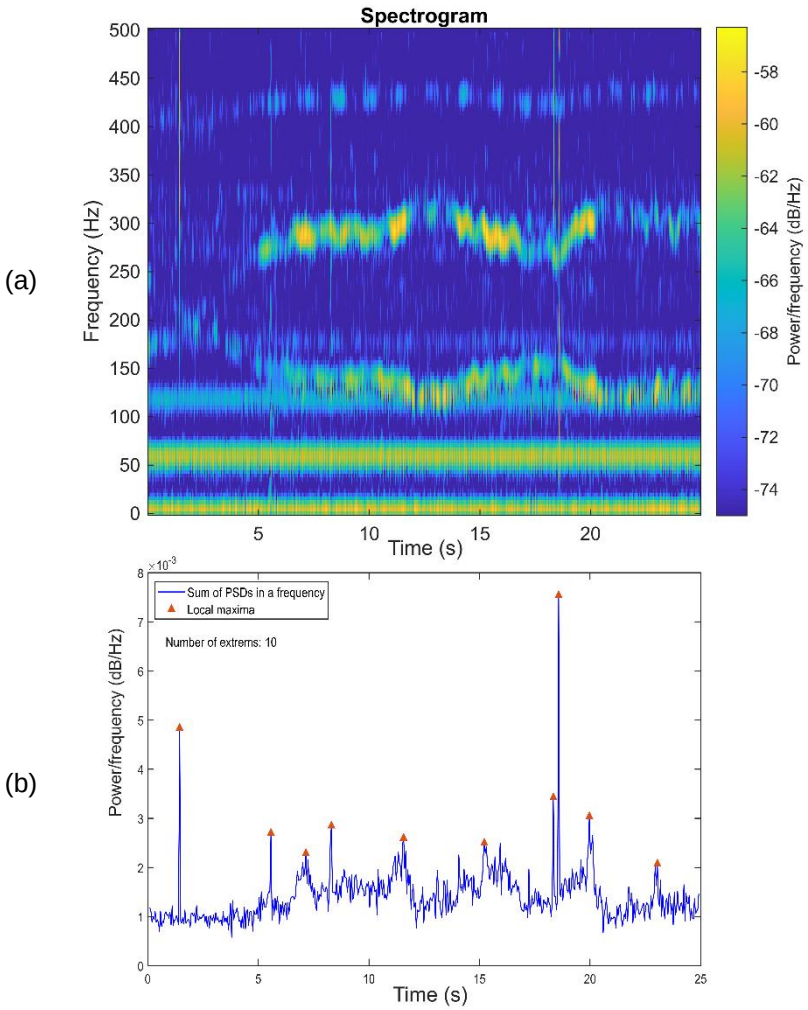

Figure 58. (a) Spectrogram, (b) The sum of power densities

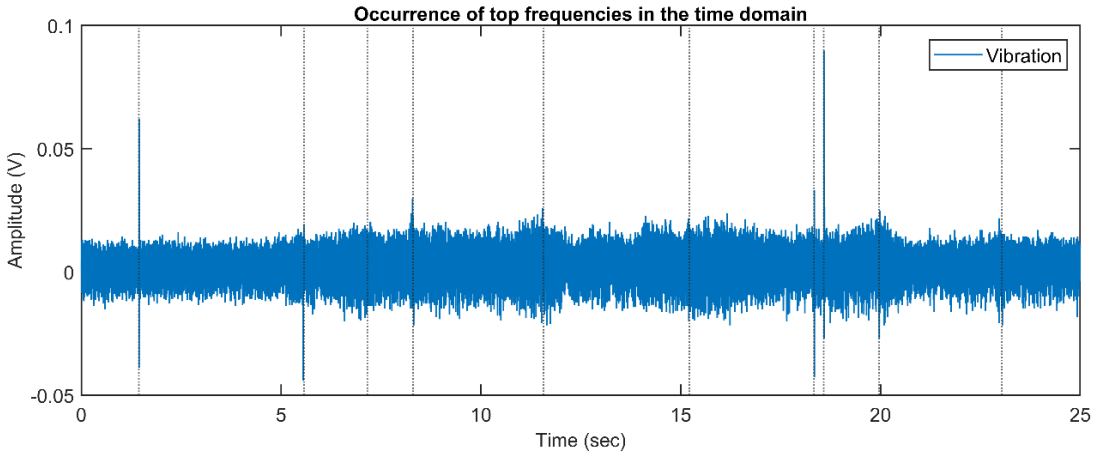

Figure 59. Superimposing the maximum 10 sums of PSDs on the time domain

When comparing Figure 59 with Figure 54, we can see that some of the occurrences of the 10 maxima of PSD sums take place at the times where there is sudden increase in the vibration amplitude, and some do not, those are buried in the noise. In addition, we notice from the distribution of the maxima of PSD in Figure 59 that the occurrences have a kind of periodicity. When taking into consideration the previous discussion on Figure 56, this periodicity of PSD maxima supports our previous assumption of existing defects on the bearing raceways.

6.2.3 Analysis of AE signal

We applied similar sequence of actions for the analysis of AE signal that was received from both sensors fixed to the bearings. Those steps are shown in Figure 60.

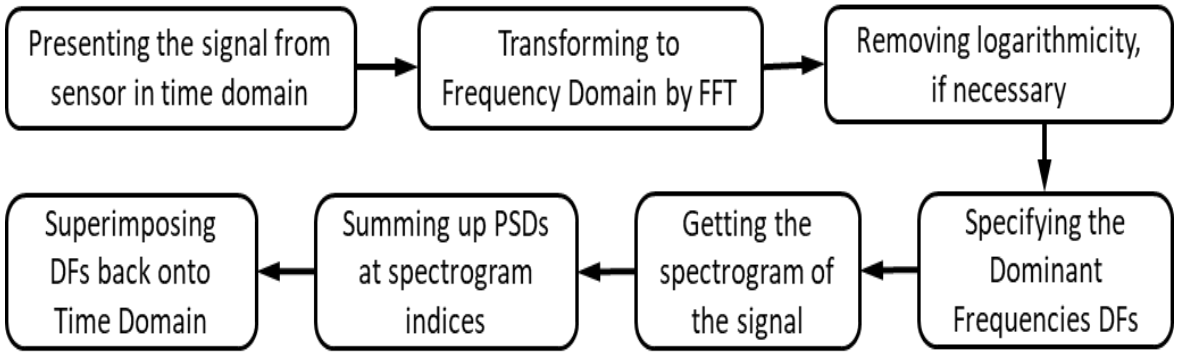

Figure 60. Sequence of steps for vibration signal analysis

The steps of analysis for AE signal consists of getting the signal in the time domain, getting the AE parameters, which gives an indication of the bearing situation, then using FFT, transforming the signal to the frequency domain, and identifying the DF for each AE hit in the time slice to create a DF map for that time slice.

Figure 40 shows one AE hit in the time domain that is detected by a PPHD. We established the PPHD to get more flexibility in specifying AE hit detector, and to be able to modify it constantly even on the recorded signal (offline). PPHD parameters are given in Table 6.

Table 6. The main setup parameters for the PPHD in TRB experiments

Parameter	Value
Detection threshold	1 mV (60 dBAE)
Separation time	1 ms
Dead time	10 ms
Minimum hit length	1 us
Maximum hit length	500 ms
FFT Calculation method	Welch estimate
Window type	Welch window
Window size	8192
Window overlap	50 %

The signal is then transformed to the frequency domain using FFT, as shown before in Figure 41. From this figure, we can identify the DF, which is shown to be around 68 kHz.

We apply the same process for each hit detected by the PPHD. Therefore, we get from each graph the DF of that hit. The DFs for all the detected hits in one time slice were then collected in one graph as show in Figure 61 (a) and (b) which we call the DF map for bearing A (TRB) and B (SRB) respectively. Figure 61 also shows the RMS of AE from both channels A and B.

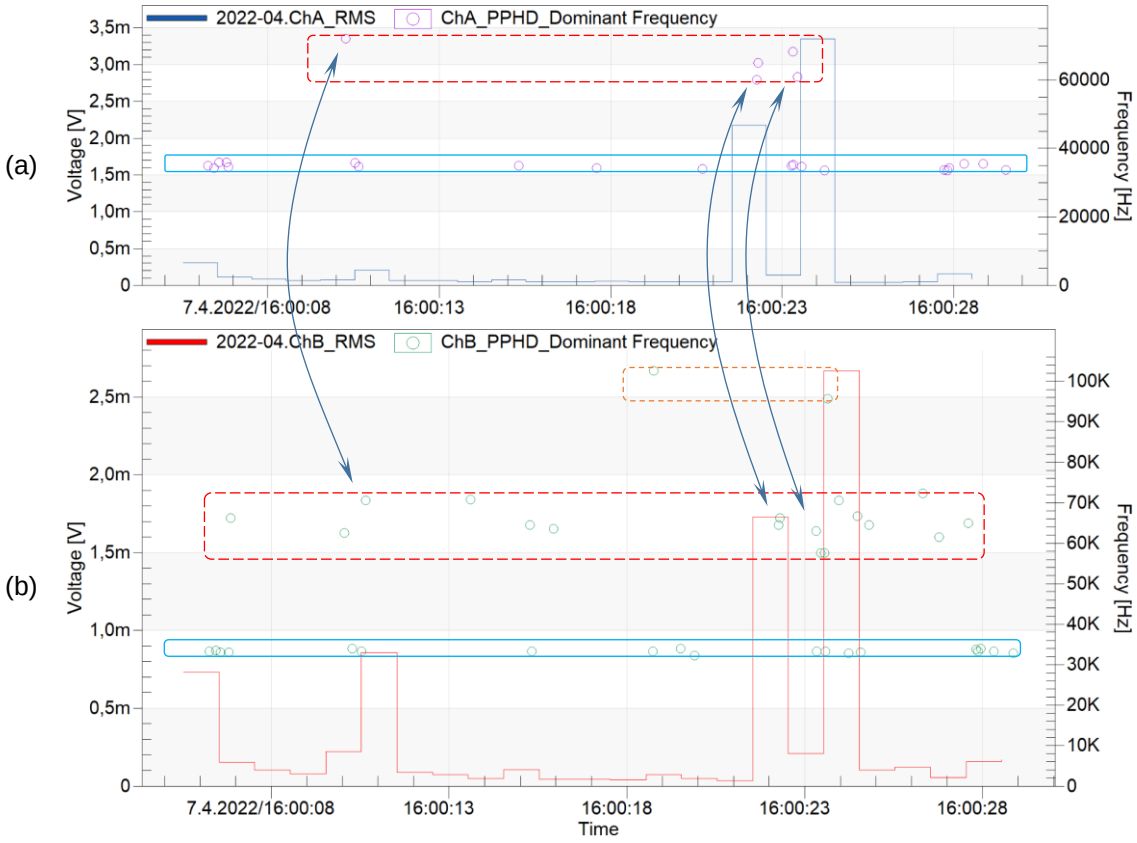

Figure 61. DF map for bearings A and B.

(a) DFs of the PPHD hits from bearing A, (b) DFs of the PPHD hits from bearing B.

Figure 61 (a) shows that all DFs of the PPHD hits from bearing A fall inside two ranges, the first range is [33 - 36] kHz which is a narrow specific range (enclosed inside a blue rectangle on the figure), and the second range spans from [60 - 77] kHz (enclosed inside a dashed red rectangle).

And Figure 61 (b) shows that all DFs of the PPHD hits from bearing B fall inside almost the same two ranges. A narrow range [33 - 36] kHz (inside a blue rectangle) and another range [60 - 77] kHz (inside a dashed red rectangle).

When comparing the two ranges of DFs between the two bearings, we can see that most of the hits that have DFs in the lower frequency range [33 - 36] are shared between the two bearings. They happen at the same time. Therefore, we can assume that most of those hits, the synchronous ones, are the result of outside sources affecting both bearings at the same time causing the received hits with these DFs inside this range.

While when looking at the upper range of DFs [60 - 70], we can see that the number of hits differ greatly between the two bearings. Bearing B produces many more hits at these frequencies than bearing A. Bearing A produces hits at these frequencies just when AE RMS has an abrupt increase, and similar hits can be seen at this time from bearing B, as shown by the curved double-arrows on the figure.

On the other hand, when comparing the DFs of hits from both channels with the RMS from both channels in this time slice, we see some hits with similar DFs taking place even when the values of RMS are relatively low. Which imply that RMS as an AE parameter did not capture or react to all the sources of the hits, so it cannot be depended upon solely for describing the status of the monitored bearing.

Another intriguing aspect of the DFs from channel B is their patterned occurrence; they exhibit periodicity and repeat every 4-6 seconds. When taking into consideration the rotational speed of the shaft, which is about 4 seconds for one full rotation at the time of measuring, and considering the inevitable sliding effect of the rollers in their raceways, we can assume that those DFs belong to AE hits that represent defects in the raceways of the bearings.

We also see in Figure 61 (b) a number of hits which were received just from channel B, whose DFs are in a range between [95 - 105] kHz (enclosed inside a dashed orange rectangle). They have no counterpart from channel A on Figure 61 (a) or on any other DF map. Figure 62 (a) and (b) are just another DF maps for bearings A and B taken in different time slice. Figure 62 (b) shows a group of hits with high DFs that range between 195 and 215 kHz (enclosed in a purple rectangle). From Figure 61(b) and Figure 62(b) we can tell that those groups of hits that have the highest DFs are not connected strictly to the RMS values.

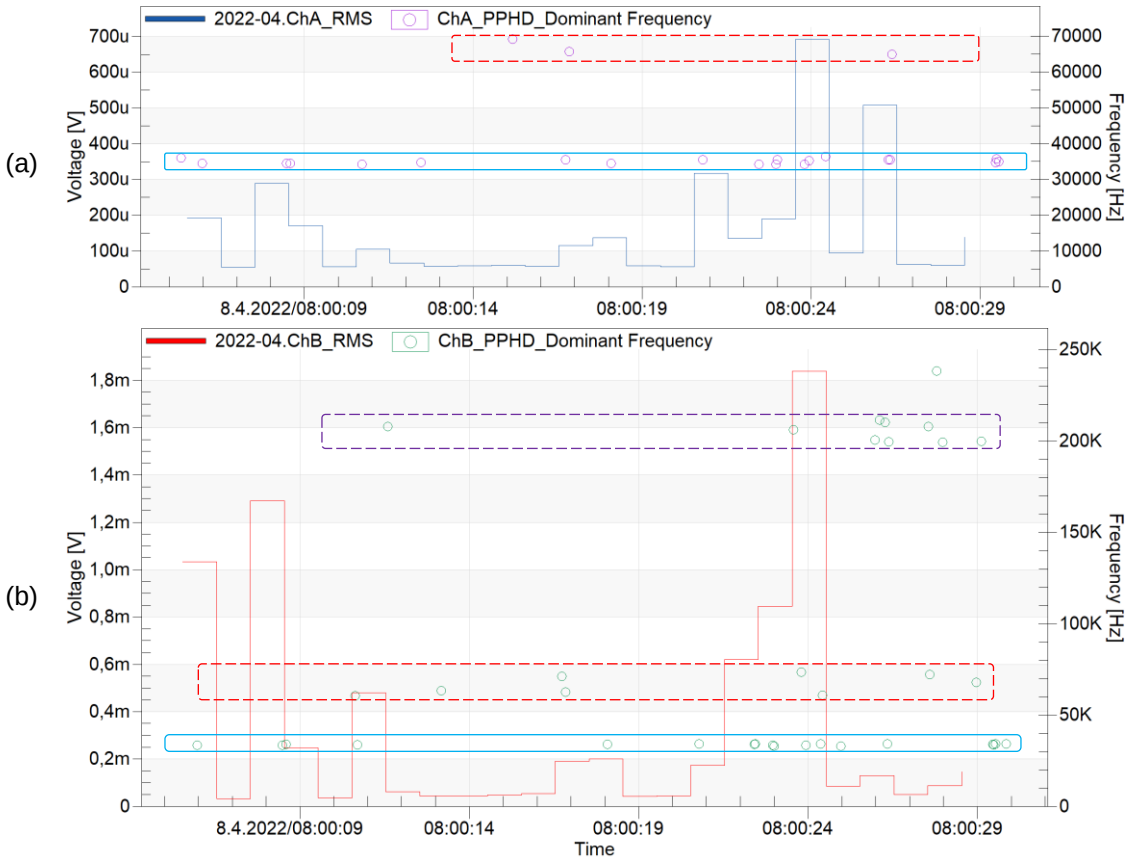

Figure 62. (a) DF map for bearing A, (b) DF map for bearing B.

6.2.4 Combining a number of subsequent DF maps

The preceding findings were observed in all other analysed time slices. Therefore, we produced the DF maps for many consecutive time slices in consecutive days and combined (overlaid) them in one graph for each bearing, as shown in Figure 63 for bearing A, and Figure 64 for bearing B. (Note: The DF maps are not distributed regularly, because we chose the time slices where the rotation speed was fixed at its maximum (i.e. the cut-out value of 14.9 rpm).

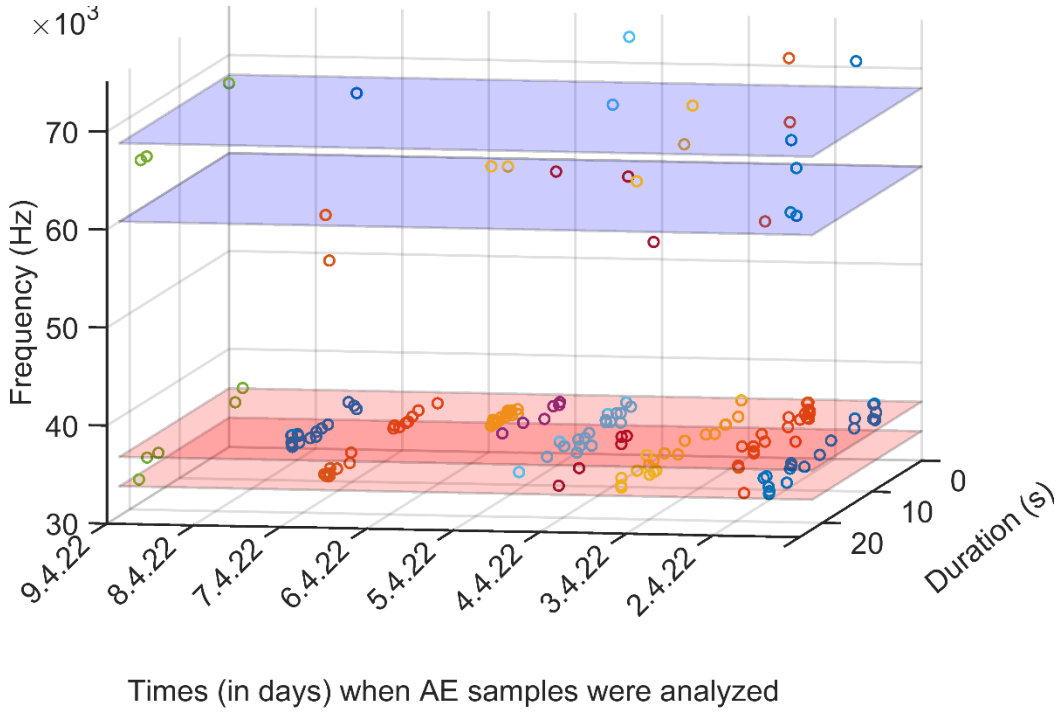

Figure 63. The overlay of some consecutive DF maps for bearing A

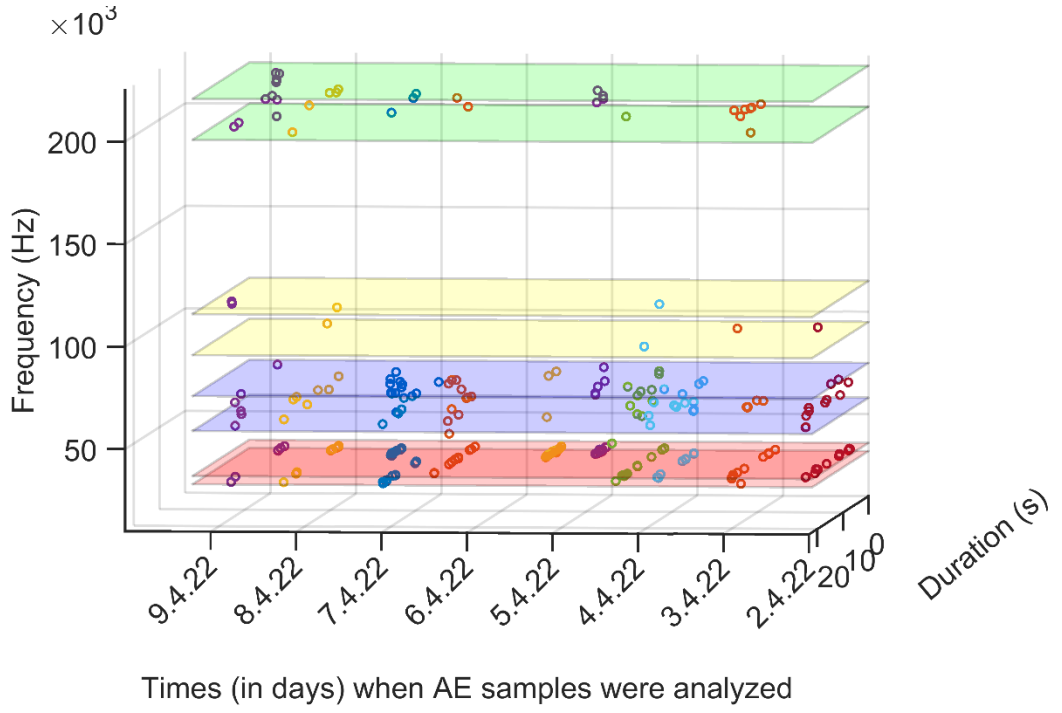

Figure 64. The overlay of some consecutive DF maps for bearing B.

The overlays of DF maps for bearing B in Figure 64 confirm the existence of the two ranges of high DFs, [95 - 105] kHz and [195 - 215] kHz, that were not shown in any of the DF maps of bearing A. Combining this fact with the conclusion that we reached after the vibration analysis of bearing B, we can presume that the defects on the raceways of bearing B are from different types and sizes; therefore, they caused AE hits with different ranges of DFs.

The comparison between the two overlays of DF maps for the two bearings leads to the conclusion that bearing B is in a much worse situation than bearing A. It does not give an accurate description of the situation of bearing A, as long as we cannot interpret the exact representation of the DFs in the lower ranges, [33 - 36] kHz and [60 - 77] kHz. Since most of the AE hits with DFs in those lower two ranges are common between the two bearings, ignoring those simultaneous hits in both bearings, especially when they are accompanied with abrupt change of AE parameters, will contribute to removing the hits that result from outside effects (which effect both bearings simultaneously). And we will be left with the hits that are the result of internal defects in each bearing.

To predict the precise remaining useful life (RUL) of the bearing, we would need access to historical data of similar bearing types. Such data is currently unavailable to us, since this method of using DF of AE hits and DF maps to estimate the health of bearings is a new method, to the best of our knowledge as authors. With that limitation in mind, our study aims to leverage the available data and analytical techniques to provide valuable insights into the condition and potential lifespan of the bearing. By utilizing and improving our existing algorithms and employing advanced predictive approaches, we aim, as future step, to approximate the RUL to the best of our ability and contribute to the understanding of bearing performance and maintenance optimization.

7 CONCLUSIONS

This dissertation work has focused on the experimental investigation of RCF behavior in TRBs using AE. It started by giving a brief background about TRB, AE technique and its use in detecting RCF in bearings. The analysis of the state of knowledge established the basis for forming scientific questions and hypotheses. The investigation work started by testing newly produced TRB on a special stand that is designed for this purpose in the production facility. Some recommendations were introduced, while the conclusion from the early experiments showed that AE was a reliable tool for detecting the beginning of crack initiations in this type of bearings, and it proved to be more sensitive and reactive to RCF than the widely used vibration method [71]. The temperatures of the rings were tested in this stage, but the results demonstrated that the range of change in temperatures is small, hence it was not indicative enough. Therefore, temperature was excluded as an option for later measurements.

The analysis of the state of knowledge led to the observation that AE time-domain parameters have been extensively used for most of the work that applied AE as a NDT technique for defect detection or CM in mechanical applications, while the use of frequency-domain parameters is very limited. The research for the use of AE frequency-domain parameters led to the fact that it had been gaining popularity and getting attention in the field of Geotechnical Engineering [46 - 54] but not in Mechanical applications, and certainly not in bearings studies. Therefore, the use of DF of AE hits was considered to be explored and utilized for the rest of the studies. It has been shown by a big body of research recently, that DFs of AE hits have a strong correlation with the defect initiation and propagation in the monitored material. The experiments on TRB were performed again, using several specimens, with concentration on the frequency-domain parameters, especially on the DF of AE hits.

For the sake of full control of the analysis, a post processing hit detector (PPHD) was created, which gives a higher level of flexibility in the analysis by allowing to change the settings of the analysis even after the experiment. The drawback of PPHD is that it requires the recording of the full signal, which is very demanding in the case of AE, since it requires a huge amount of space. Therefore, some tradeoffs had to be made with regard to the periods and frequencies of recording. Another aspect of PPHD is that changing the values of its parameters affects the number of detected AE hits, but it does not affect the monitored trend of the events.

For the transformation from the time domain to frequency domain, FFT was used for the whole AE signal analysis except when extracting the DF of AE hit that were detected from PPHD, in that case Welch method was used, because it reduced the variance by dividing to small manageable windows and averaging them.

The DFs of AE hits for the tests on 5 different specimens were recorded and presented using MatLab®. Different Matlab codes were created to automate the process and compare all the results from different time slices during the whole experiment.

The result of this analysis was a so-called DF map, which is a visual representation of the DFs of all detected AE hits in specific time intervals. The DFs of AE hits on the DF map fell inside separate well-defined ranges that were called bands.

The statistical analysis on the output of DF extraction gave consistent results which led to the conclusion that there is a strong correlation between DF bands of AE hits with the type of

defect as well as with the amount (magnitude) of defects. The discrete nature of the resulting DF bands made it possible to use these distinctively separate DF bands to identify the type and the amount of defects based on previous knowledge of the defect, which in turn helps in predicting the source of defects later just by examining the DF bands map. For example, knowing the distinct pattern of DF bands from the running-in period, which peaked and had big number of hits in the range [185 – 216] kHz, but had a distinct narrow range of DFs in [429 – 431] kHz that was related to it. The source of AE hits that have these DFs is supposedly known, which is the breaking of asperities and abnormalities on the surfaces between the machined raceways and the rollers. Combining those two pieces of information leads to predict the source of AE events when seeing similar DF band pattern on a DF map, especially when such pattern is repeated. Applying a basic statistical analysis on the whole period of DF map results demonstrated that the number of AE hits that appear during pitting and/or scaling is higher in the lower DF ranges (lower than 200 kHz), and the number of the AE hits that appear during the running-in period is higher in the high DF range (above 200 kHz). However, the most important aspect of the analysis was not the number by themselves, but **the ability to link the numbers to the RCF defects in the bearings**, by correlating them to a quantifiable parameter, which is the number of DFs of AE hits.

With the results of the lab experiments in mind, the application of the same approach on TRBs in operation in the field gave similar results. The ideal example was the main shaft of wind turbine where TRB was used as non-locating bearing, and SRB as a locating bearing.

Similar AE based CM system was applied on both WT bearings along with an integrated vibration monitoring system. In this application, the vibration analysis gave a preliminary assumption of the condition of the bearing, which was that defects have developed in the SRB.

The AE signal analysis that produced DF maps for both bearings showed supporting results, but to confirm the findings, a more advanced effort was carried out to overlay many DF maps for many consecutive time intervals together, to give more confirmation of the results and a more comprehensive view of the condition of the two bearings. This overlaying was achieved by exporting the results to Matlab© and then applying a snippet code.

When comparing the two overlays of DF maps for the two bearings in a 3D graph, it has been noticed that the two high DF bands, [95 - 105] and [195 - 215] kHz, appeared only in DF maps for the SRB and did not exist in DF maps for TRB. Another observation is that the number of AE hits in the middle DF band [60 - 77] kHz for the SRB is bigger than the number of AE hits for bearing A in that frequency band. Those hits show patterned appearance, where each 4 seconds we see at least one hit. It has been also noticed that both bearings have the highest number of AE hits in the lowest DF band [33 - 36] kHz, which indicates from the number of those hits and their distribution, that most of them are attributed to noise and external sources.

Combining those observations with the vibration analysis of the SRB gave more support to the presumption of the existence of defects on the raceways of the SRB. And it indicated that those defects are of different types and sizes. It showed that **the SRB bearing on the WT main shaft is in a worse condition than the TRB**.

One of the outputs was the number of Matlab® snippet codes that were created, because they can be combined and integrated in a CM system, then used externally for the development of a predictive maintenance strategy to mitigate the potential risks of bearing failure.

One of the conclusions of this work that contradicts with previous findings in literature, especially the early studies, like the work of Mba, D. et al. [25] [71] [31], was that AE time-domain parameters, such as RMS and ASL, did not completely correspond to the events that were represented by the occurrence of AE hits. In other words, **AE time-domain parameters cannot be depended upon solely for the determination of the condition of a bearing**.

Another output of this work is the successful application of a remote CM system using a VNC server, a 3G internet connection and a PC in the nacelle. This system was motivated by the need for monitoring the long measurements that take days or months in places that are not always accessible. Having such a system was essential for giving not just access to the measurement data, but also to the ability to change some of the parameters or thresholds in cases of necessity. Even though the components of this system are available and relatively cheap, no previous study of similar nature has reported using such system. The reason for that could be partly attributed to the availability of the SCADA system in WTs, which is resource-extensive and expensive. The new monitoring system that is suggested, applied and verified here is an easy-to-apply and easy-to-use method for continuous online monitoring of not just bearings, but any critical asset that requires long time of monitoring. It has been in use for more than a year and still reliably used for monitoring and recording data.

To the best knowledge of the author, the principle of DF maps has not been used before for CM or fault detection of mechanical materials, let alone for bearings. It has been shown that it has promising potential as a method for representing the condition of a bearing. It is apparent from the DF maps that the DFs of AE hits are grouped in well-defined discrete ranges (frequency bands). Those ranges/bands represent different types and sizes of defects. However, the exact correlation between the sizes of the defects and the DFs requires further investigation. More specifically, it requires building a database that could be depended upon to link each type of defect to its relevant DF band in the DF map.

Any future work in this direction is bound to focus on this specific aspect with building databases that further proves and consolidate the relationship between DFs of AE hits and the defect types and sizes on the monitored bearing. The size of such databases and the complicated relationships between its elements will create the need to use Artificial Intelligence (AI) in managing this process. The use of AI in CM of bearing has been used in an ever-increasing number of studies recently, and it has become an essential part of any new effort to classify results. The increasing availability of AI tools and software made this and will continue to make it more accessible and achievable.

8 LIST OF PUBLICATIONS

8.1 Papers in journals with impact factor:

MOHAMMAD, H.; MAZAL, P.; VLAŠIC, F.; MAYA, B. Active Monitoring of RCF in Toroidal Bearings using Acoustic Emission. LNME. **IF: 0.45**
Link

MOHAMMAD, H.; VLAŠIC, F.; Zacek, J.; MAZAL, P.; MAYA, B.
Using acoustic emission for condition monitoring of the main shaft bearings in 4-point suspension wind turbine drivetrains. Nondestructive Testing & Evaluation. **IF: 2.6**
Link

MOHAMMAD, H.; VLAŠIC, F.; SHEHADEH, M.; MAYA, B.; MAZAL, P.
New Evaluation Method for Defects Propagation Using Dominant Frequency of Acoustic Emission Hits in Toroidal Bearings. Nondestructive Testing & Evaluation. **IF: 2.6** (In process)

MOHAMMAD, H.; VLAŠIC, F.; MAYA, B.; MAZAL, P.
New Method for Condition Monitoring of Slow-Speed Bearings Using Peak Frequency of Acoustic Emission Hits. BINDT-INSIGHT. **IF: 0.9** (In process)

ŽÁČEK, J.; ŠEBESTA, K.; MOHAMMAD, H.; JENIŠ, F.; STRECKER, Z.; KUBÍK, M. Experimental Evaluation of Modified Groundhook Car Suspension with Fast Magnetorheological Damper. Actuators, 2022, s. 1-14. ISSN: 2076-0825. **IF: 2.4**
Link

8.2 Papers in conferences:

MOHAMMAD, H.; VLASIC, F.; MAZAL, P. a MAYA, B.. Active Diagnosis of Toroidal Bearings using Acoustic Emission Technique. NDE for Safety Proceedings: Czech Society for NDT, 2019. ISBN 978-80-214-5799-7. Link

MOHAMMAD, H.; V., Frantisek a MAZAL, P.. Condition Monitoring of Toroidal Roller Bearings Using Acoustic Emission Technique. Online. European NDT & CM. 2021. Link

MOHAMMAD, H., MAZAL, P., VLASIC, F. a MAYA, B.. Active Monitoring of RCF in Toroidal Bearings Using Acoustic Emission. In: Proceedings of the 5th International Conference on Maintenance, Condition Monitoring and Diagnostics 2021, Oulu, Finland. Springer Nature Singapore, 2023, s. 73-81. ISBN 978-981-99-1987-1. Link

Springer Lecture Notes in Mechanical Engineering

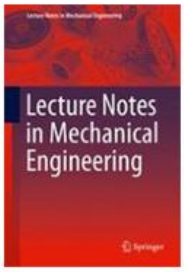

Active Monitoring of RCF in Toroidal Bearings Using Acoustic Emission

Housam Mohammad, Pavel Mazal, Frantisek Vlasic, and Baraah Maya

Abstract This paper demonstrates the results of testing toroidal bearings using the parameters extracted from Acoustic Emission testing. The aim is to find the characteristics of the Rolling Contact Fatigue (RCF) in these special bearings during testing. Toroidal bearings are characterized by their special design, which combines the self-aligning capability with the axial displacement ability, which contributed to the significant increase in their applications, especially in the wind turbine industry. The main concentration of this paper has been on the period of test before the appearance of pitting. We believe that analyzing and studying the Acoustic Emission (AE) signal in the period before pitting will make it possible to specify the pattern of the signal that can be later used to predict the initiation of pitting. The experiments took place in a specially designed stand for this type of bearing to obtain the best results from AE sensors. This study is an initial step toward other more advanced steps to better understand the crack initiation and pitting mechanisms in the especially important toroidal bearings.

Keywords Acoustic emission · Rolling contact fatigue · Toroidal bearings · Pitting

1 Introduction

Toroidal roller bearings are single-row bearings with long, crowned rollers. The concave raceways in the inner and outer rings are concentric relative to the center of the bearing. The raceway profiles are matched to each other and ensure optimum distribution of stresses in the bearing as well as low operating friction.

H. Mohammad (✉) · P. Mazal · F. Vlasic · B. Maya
Faculty of Mechanical Engineering, Brno University of Technology, Technicka 2, Brno 61669, Czech Republic
e-mail: Housam.mohammad@vutbr.cz

E. Juuso and D. Galar (eds.), *Proceedings of the 5th International Conference on Maintenance, Condition Monitoring and Diagnostics 2021*,
Lecture Notes in Mechanical Engineering,
https://doi.org/10.1007/978-981-99-1988-8_6

NONDESTRUCTIVE TESTING AND EVALUATION
https://doi.org/10.1080/10589759.2023.2283511

Taylor & Francis
Taylor & Francis Group

Using acoustic emission for condition monitoring of the main shaft bearings in 4-point suspension wind turbine drivetrains

Housam Mohammad [a], Frantisek Vlasic [a], Jiri Zacek [a], Baraah Maya [b] and Pavel Mazal [a]

[a]Institute of Machine and Industrial Design, Brno University of Technology, Brno, Czechia; [b]Institute of mathematics, Brno University of Technology, Brno, Czechia

ABSTRACT

The continuous growth of wind power technology makes condition monitoring of wind turbine components crucially important for their operational efficiency. The main shaft bearings in wind turbines have been identified as one of the most critical components in the system, especially with the ongoing increase in rotor size and weight. This increase made the 4-point suspension drivetrain more preferable. In this study, we present a novel approach for condition monitoring of the main shaft bearings in a 2 Megawatt wind turbine with 4-point suspension drivetrain using primarily acoustic emission (AE). The focus was on the analysis of time and frequency domains of the AE signal, where the dominant frequency of each AE hit was identified and plotted back in the time domain to create the so-called dominant frequency map in specific time intervals for each bearing. A comparison between the two dominant frequency maps of the two bearings gives valuable insights into the condition of the two bearings. The distinctive nature of the dominant frequency bands in the dominant frequency maps presented promising potential for this method. The presented method is straightforward and can be automated and then integrated into a planned predictive maintenance programme for this wind turbine.

ARTICLE HISTORY
Received 6 August 2023
Accepted 5 November 2023

KEYWORDS
Acoustic emission (AE); wind turbine (WT); main shaft bearing; condition monitoring (CM); dominant frequency (DF)

1. Introduction

With the rise of green energy, wind power has become the fastest-developing renewable energy in the world. As the Global Wind Report [1] shows, 2022 was another record year for wind installations and particularly for the fast-growing offshore wind sector. However, the report also points out that new installations must still quadruple by the end of this decade to achieve the goal of net zero emissions by 2050. The total global wind power capacity is now up to 837 GW, helping the world avoid over 1.2 billion tons of CO_2 annually [1].

The efficient operation of WTs heavily relies on the reliable performance of their critical components. Any failure of these components can lead to downtime and

CONTACT Housam Mohammad Housam.mohammad@vutbr.cz

actuators

MDPI

Article

Experimental Evaluation of Modified Groundhook Car Suspension with Fast Magnetorheological Damper

Jiří Žáček *, Karel Šebesta, Housam Mohammad, Filip Jeniš, Zbyněk Strecker and Michal Kubík

Institute of Mechanical and Industrial Design, Faculty of Mechanical Engineering, Brno University of Technology, 616 69 Brno, Czech Republic

* Correspondence: jiri.zacek@vut.cz; Tel.: +420-54114-3216

Abstract: The car suspension setting is always a trade-off between comfort and handling. The semi-active damper system seems to be an option for reducing the compromise between the two demands. This paper deals with the effect of the magnetorheological damper setting on a car's suspension performance, especially tire grip, which was directly measured. A unique test rig was developed, and an experimental trolley with a fast magnetorheological damper (response time of 3 μs) was used in the paper. The damper was controlled by a modified Groundhook algorithm. Compared with the passive regime, the experiments showed a 30% improvement when using the Groundhook algorithm and when the damper was adequately set. The experiments proved the trends that were set by simulations.

Keywords: magnetorheological damper; semi-active damper; Groundhook; adaptive suspension

check for updates

Citation: Žáček, J.; Šebesta, K.; Mohammad, H.; Jeniš, F.; Strecker, Z.; Kubík, M. Experimental Evaluation of Modified Groundhook Car Suspension with Fast Magnetorheological Damper. *Actuators* **2022**, *11*, 354. https://doi.org/10.3390/act11120354

Academic Editor: Hai Wang

Received: 18 October 2022
Accepted: 25 November 2022
Published: 29 November 2022

Publisher's Note: MDPI stays neutral with regard to jurisdictional claims in published maps and institutional affiliations.

1. Introduction

Modern cars (and all vehicles) still have to catch up with higher customer demands. Modern cars are requested to carry the vehicle over bumps as smoothly (minimalizing sprung mass vibrations) as possible while maintaining a good level of car handling (keeping the wheel grip stable). Because the passive damping system design is always a trade-off between comfort and ride quality, a semi-active (S/A) damper has been put into action.

The semi-active (S/A) damper system seems to be a solution for reducing the compromise between those two demands [1]. This system works on a feedback mechanism which is composed of sensors, a control algorithm, and an adjustable damper [2]. The S/A system reacts in real-time on the road situation and adjusts its damping parameters to improve both ride quality and comfort. The suspension system is controlled by an algorithm, which switches the damping force depending on the signals from the sensors and control strategy. The force switching time (response time) and dynamic force range of the damper was shown to affect the semi-active control efficiency [3]. The selection of the damper response time and dynamic force range are always connected to the parameters of the dynamic system (suspension) and control strategy (algorithm).

Magnetorheological (MR) technology is widely used [4] in controllable mechanical devices (clutches [5], brakes [6], and seals [7]), and it appears to be a good option for the semi-active control of dampers [8]. The MR damper uses MR fluid, which is a suspension of ferromagnetic particles in the carrier fluid [9]. When the MR fluid is subjected to an external magnetic field, the ferromagnetic particles form chain structures in the direction of the magnetic field, and the apparent viscosity rapidly increases [10]. This phenomenon is fully reversible and is essential for MR damper function. The MR damper usually has a monotube design with one or more electromagnetic coil piston configurations [11]. As the electric current in the coil changes, the magnetic field changes as well. The viscosity of the MR fluid changes with the magnetic field, and in this way, the damping force is controlled. Typical dynamic force range values (the ratio of the damping force in the activated

9 REFERENCES

[1] HARRIS, Tedric a KOTZALAS, Michael. *Rolling bearing analysis*. 5th ed. Boca Raton, FL: CRC/Taylor & Francis, 2007. ISBN 0849381673.

[2] SANTUS, C.; BEGHINI, M.; BARTILOTTA, I. a FACCHINI, M. Surface and subsurface rolling contact fatigue characteristic depths and proposal of stress indexes. online. *International Journal of Fatigue*. 2012, roč. 45, s. 71-81. ISSN 01421123. Dostupné z: https://doi.org/10.1016/j.ijfatigue.2012.06.012. [cit. 2023-12-24].

[3] SADEGHI, Farshid; JALALAHMADI, Behrooz; SLACK, Trevor; RAJE, Nihar a ARAKERE, Nagaraj. A Review of Rolling Contact Fatigue. online. *Journal of Tribology*. 2009, roč. 131, č. 4. ISSN 0742-4787. Dostupné z: https://doi.org/10.1115/1.3209132. [cit. 2023-12-22].

[4] LIU, Zepeng a ZHANG, Long. A review of failure modes, condition monitoring and fault diagnosis methods for large-scale wind turbine bearings. online. *Measurement*. 2020, roč. 149. ISSN 02632241. Dostupné z: https://doi.org/10.1016/j.measurement.2019.107002. [cit. 2023-12-21].

[5] SUN, Jun; WOOD, R.J.K.; WANG, L.; CARE, I. a POWRIE, H.E.G. Wear monitoring of bearing steel using electrostatic and acoustic emission techniques. online. *Wear*. 2005, roč. 259, č. 7-12, s. 1482-1489. ISSN 00431648. Dostupné z: https://doi.org/10.1016/j.wear.2005.02.021. [cit. 2023-11-29].

[6] GROSSE, Christian; OHTSU, Masayasu; AGGELIS, Dimitrios a SHIOTANI, Tomoki (ed.). *Acoustic Emission Testing*. online. Springer Tracts in Civil Engineering. Cham: Springer International Publishing, 2022. ISBN 978-3-030-67935-4. Dostupné z: https://doi.org/10.1007/978-3-030-67936-1. [cit. 2023-08-13].

[7] YOSHIOKA, Takeo a FUJIWARA, Takashi. A new acoustic emission source locating system for the study of rolling contact fatigue. online. *Wear*. 1982, roč. 81, č. 1, s. 183-186. ISSN 00431648. Dostupné z: https://doi.org/10.1016/0043-1648(82)90314-3. [cit. 2020-03-28].

[8] YOSHIOKA, T. a FUJIWARA, T. Paper II(i) Measurement of propagation initiation and propagation time of rolling contact fatigue cracks by observation of acoustic emission and vibration. online. In: *Interface Dynamics, Proceedings of the 14th Leeds-Lyon Symposium on Tribology*. Tribology Series. Elsevier, 1987, s. 29-33. ISBN 9780444704870. Dostupné z: https://doi.org/10.1016/S0167-8922(08)71045-9. [cit. 2020-04-15].

[9] JACOBS, L.; SCOTT, W.; GRANATA, D. a RYAN, M. Acoustic Emission from a Growing Crack. online. In: THOMPSON, Donald O. a CHIMENTI, Dale E. (ed.); THOMPSON, Donald; CHIMENTI, Dale. *Review of Progress in Quantitative Nondestructive Evaluation*. Boston, MA: Springer US, 1990, s. 1749-1756. ISBN 978-1-4684-5774-2. Dostupné z: https://doi.org/10.1007/978-1-4684-5772-8_225. [cit. 2023-12-09].

[10] MBA, D. Acoustic Emissions and Monitoring Bearing Health. online. *Tribology Transactions*. 2003, roč. 46, č. 3, s. 447-451. ISSN 1040-2004. Dostupné z: https://doi.org/10.1080/10402000308982649. [cit. 2023-08-12].

[11] JACOBS, Laurence J. Characterization of Acoustic Emission Signals from Mode I Crack. online. *Journal of Engineering Mechanics*. 1991, roč. 117, č. 8, s. 1878-1889. ISSN 0733-9399. Dostupné z: https://doi.org/10.1061/(ASCE)0733-9399(1991)117:8(1878). [cit. 2023-12-09].

[12] JACOBS, Laurence; SCOTT, William; GRANATA, Dianne a RYAN, Martin. Experimental and analytical characterization of acoustic emission signals. online. *Journal of Nondestructive Evaluation*. 1991, roč. 10, č. 2, s. 63-70. ISSN 0195-9298. Dostupné z: https://doi.org/10.1007/BF00568101. [cit. 2023-12-09].

[13] UNNORSSON, Runar. Hit Detection and Determination in AE Bursts. online. In: SIKORSKI, Wojciech (ed.); SIKORSKI, Wojciech. *Acoustic Emission - Research and Applications*. InTech, 2013. ISBN 978-953-51-1015-6. Dostupné z: https://doi.org/10.5772/54754. [cit. 2023-08-12].

[14] ISO. online. In: Iso.org. 2022. Dostupné z: https://www.iso.org/obp/ui/en/#iso:std:iso:24543:ed-1:v1:en. [cit. 2023-12-28].

[15] UNNORSSON, Runar. Hit Detection and Determination in AE Bursts. online. In: SIKORSKI, Wojciech (ed.); SIKORSKI, Wojciech. *Acoustic Emission - Research and Applications*. InTech, 2013. ISBN 978-953-51-1015-6. Dostupné z: https://doi.org/10.5772/54754. [cit. 2020-04-22].

[16] online. In: Iso.org. 2001. Dostupné z: https://www.iso.org/obp/ui/en/#iso:std:iso:12716:ed-1:v1:en. [cit. 2023-12-28].

[17] UNNORSSON, Runar. Hit Detection and Determination in AE Bursts. online. In: SIKORSKI, Wojciech (ed.); SIKORSKI, Wojciech. *Acoustic Emission - Research and Applications*. InTech, 2013. ISBN 978-953-51-1015-6. Dostupné z: https://doi.org/10.5772/54754. [cit. 2023-07-27].

[18] SAUSE, Markus G.R. *In Situ Monitoring of Fiber-Reinforced Composites*. online. Springer Series in Materials Science. Cham: Springer International Publishing, 2016. ISBN 978-3-319-30953-8. Dostupné z: https://doi.org/10.1007/978-3-319-30954-5. [cit. 2023-12-13].

[19] YOSHIOKA, T. a MANO, H. Relationship between Acoustic Emission Source Position and Spalling Position in Radial Rolling Bearings. online. In: *Tribology for Energy Conservation, Proceedings of the 24th Leeds-Lyon Symposium on Tribology*. Tribology Series. Elsevier, 1998, s. 413-422. ISBN 9780444500335. Dostupné z: https://doi.org/10.1016/S0167-8922(98)80097-7. [cit. 2023-08-13].

[20] MANO, Hiroki; YOSHIOKA, Takeo; KORENAGA, Atsushi a YAMAMOTO, Takashi. Relationship between Growth of Rolling Contact Fatigue Cracks and Load Distribution. online. *Tribology Transactions*. 2000, roč. 43, č. 3, s. 367-376. ISSN 1040-2004. Dostupné z: https://doi.org/10.1080/10402000008982352. [cit. 2020-02-23].

[21] CHOUDHURY, A. a TANDON, N. Application of acoustic emission technique for the detection of defects in rolling element bearings. online. *Tribology International*. 2000, roč. 33, č. 1, s. 39-45. ISSN 0301679X. Dostupné z: https://doi.org/10.1016/S0301-679X(00)00012-8. [cit. 2023-08-12].

[22] SCHWACH, D a GUO, Y. A fundamental study on the impact of surface integrity by hard turning on rolling contact fatigue. online. *International Journal of Fatigue*. 2006, roč. 28, č. 12, s. 1838-1844. ISSN 01421123. Dostupné z: https://doi.org/10.1016/j.ijfatigue.2005.12.002. [cit. 2020-02-22].

[23] RAHMAN, Md.; OHBA, Hiroaki; YAMAMOTO, Takashi a YOSHIOKA, Takeo. A Study on Incipient Damage Monitoring in Rolling Contact Fatigue Process Using Acoustic Emission. online. *Tribology Transactions*. 2008, roč. 51, č. 5, s. 543-551. ISSN 1040-2004. Dostupné z: https://doi.org/10.1080/10402000801888911. [cit. 2023-08-11].

[24] RAHMAN, Ziaur; OHBA, Hiroaki; YOSHIOKA, Takeo a YAMAMOTO, Takashi. Incipient damage detection and its propagation monitoring of rolling contact fatigue by acoustic emission. online. *Tribology International*. 2009, roč. 42, č. 6, s. 807-815. ISSN 0301679X. Dostupné z: https://doi.org/10.1016/j.triboint.2008.10.014. [cit. 2020-02-22].

[25] AL-GHAMD, Abdullah a MBA, David. A comparative experimental study on the use of acoustic emission and vibration analysis for bearing defect identification and estimation of defect size. online. *Mechanical Systems and Signal Processing*. 2006, roč. 20, č. 7, s. 1537-1571. ISSN 08883270. Dostupné z: https://doi.org/10.1016/j.ymssp.2004.10.013. [cit. 2020-04-16].

[26] ELFORJANI, M. a MBA, D. Assessment of natural crack initiation and its propagation in slow speed bearings. online. *Nondestructive Testing and Evaluation*. 2009, roč. 24, č. 3, s. 261-275. ISSN 1058-9759. Dostupné z: https://doi.org/10.1080/10589750802339687. [cit. 2023-07-20].

[27] ELFORJANI, M. a MBA, D. Accelerated natural fault diagnosis in slow speed bearings with Acoustic Emission. online. *Engineering Fracture Mechanics*. 2010, roč. 77, č. 1, s. 112-127. ISSN 00137944. Dostupné z: https://doi.org/10.1016/j.engfracmech.2009.09.016. [cit. 2023-07-31].

[28] ELFORJANI, M. a MBA, D. Condition Monitoring of Slow-Speed Shafts and Bearings with Acoustic Emission. online. *Strain*. 2011, roč. 47, s. 350-363. ISSN 00392103. Dostupné z: https://doi.org/10.1111/j.1475-1305.2010.00776.x. [cit. 2023-07-10].

[29] ELFORJANI, M. a MBA, D. Natural mechanical degradation measurements in slow speed bearings. online. *Engineering Failure Analysis*. 2009, roč. 16, č. 1, s. 521-532. ISSN 13506307. Dostupné z: https://doi.org/10.1016/j.engfailanal.2008.06.005. [cit. 2023-07-10].

[30] ELFORJANI, M.; MBA, D. a CHARNLEY, B. Observations of a naturally degrading slow-speed shaft. online. *Nondestructive Testing and Evaluation*. 2010, roč. 25, č. 4, s. 267-278. ISSN 1058-9759. Dostupné z: https://doi.org/10.1080/10589750903473625. [cit. 2023-07-20].

[31] ELFORJANI, M. a MBA, D. Monitoring the Onset and Propagation of Natural Degradation Process in a Slow Speed Rolling Element Bearing With Acoustic Emission. online. *Journal of Vibration and Acoustics*. 2008, roč. 130, č. 4. ISSN 1048-9002. Dostupné z: https://doi.org/10.1115/1.2948413. [cit. 2023-12-06].

[32] YOSHIOKA, Takeo a SHIMIZU, Shigeo. Monitoring of Ball Bearing Operation under Grease Lubrication Using a New Compound Diagnostic System Detecting Vibration and Acoustic Emission. online. *Tribology Transactions*. 2009, roč. 52, č. 6, s. 725-730. ISSN 1040-2004. Dostupné z: https://doi.org/10.1080/10402000902913345. [cit. 2020-04-24].

[33] WIDODO, Achmad; YANG, Bo-Suk; KIM, Eric; TAN, Andy a MATHEW, Joseph. Fault diagnosis of low speed bearing based on acoustic emission signal and multi-class relevance vector machine. online. *Nondestructive Testing and Evaluation*. 2009, roč. 24, č. 4, s. 313-328. ISSN 1058-9759. Dostupné z: https://doi.org/10.1080/10589750802378974. [cit. 2023-08-03].

[34] HASE, Alan; MISHINA, Hiroshi a WADA, Masaki. Correlation between features of acoustic emission signals and mechanical wear mechanisms. online. *Wear*. 2012, roč. 292-293, s. 144-150. ISSN 00431648. Dostupné z: https://doi.org/10.1016/j.wear.2012.05.019. [cit. 2023-08-11].

[35] FERRANDO CHACON, Juan; KAPPATOS, Vassilios; BALACHANDRAN, Wamadeva a GAN, Tat-Hean. A novel approach for incipient defect detection in rolling bearings using acoustic emission technique. online. *Applied Acoustics*. 2015, roč. 89, s. 88-100. ISSN 0003682X. Dostupné z: https://doi.org/10.1016/j.apacoust.2014.09.002. [cit. 2023-08-11].

[36] VAN HECKE, Brandon; YOON, Jae a HE, David. Low speed bearing fault diagnosis using acoustic emission sensors. online. *Applied Acoustics*. 2016, roč. 105, s. 35-44. ISSN 0003682X. Dostupné z: https://doi.org/10.1016/j.apacoust.2015.10.028. [cit. 2023-08-11].

[37] COCKERILL, A; CLARKE, A; PULLIN, R; BRADSHAW, T; COLE, P et al. Determination of rolling element bearing condition via acoustic emission. online. *Proceedings of the Institution of Mechanical Engineers, Part J: Journal of Engineering Tribology*. 2016, roč. 230, č. 11, s. 1377-1388. ISSN 1350-6501. Dostupné z: https://doi.org/10.1177/1350650116638612. [cit. 2023-08-11].

[38] RYCERZ, Pawel; OLVER, Andrew a KADIRIC, Amir. Propagation of surface initiated rolling contact fatigue cracks in bearing steel. online. *International Journal of Fatigue*. 2017, roč. 97, s. 29-38. ISSN 01421123. Dostupné z: https://doi.org/10.1016/j.ijfatigue.2016.12.004. [cit. 2023-08-11].

[39] SHARMA, Ram a PAREY, Anand. Modelling of acoustic emission generated in rolling element bearing. online. *Applied Acoustics*. 2019, roč. 144, s. 96-112. ISSN 0003682X. Dostupné z: https://doi.org/10.1016/j.apacoust.2017.07.015. [cit. 2023-08-11].

[40] SCHNABEL, S.; MARKLUND, P.; LARSSON, R. a GOLLING, S. The detection of plastic deformation in rolling element bearings by acoustic emission. online. *Tribology International*. 2017, roč. 110, s. 209-215. ISSN 0301679X. Dostupné z: https://doi.org/10.1016/j.triboint.2017.02.021. [cit. 2023-08-11].

[41] FUENTES, R.; DWYER-JOYCE, R.S.; MARSHALL, M.B.; WHEALS, J. a CROSS, E.J. Detection of sub-surface damage in wind turbine bearings using acoustic emissions and probabilistic modelling. online. *Renewable Energy*. 2020, roč. 147, s. 776-797. ISSN 09601481. Dostupné z: https://doi.org/10.1016/j.renene.2019.08.019. [cit. 2023-08-11].

[42] CHEN, Renxiang; TANG, Linlin; HU, Xiaolin a WU, Haonian. Fault Diagnosis Method of Low-Speed Rolling Bearing Based on Acoustic Emission Signal and Subspace Embedded Feature Distribution Alignment. online. *IEEE Transactions on Industrial Informatics*. 2021, roč. 17, č. 8, s. 5402-5410. ISSN 1551-3203. Dostupné z: https://doi.org/10.1109/TII.2020.3028103. [cit. 2023-12-09].

[43] MAZAL, P.; VLASIC, F. a KOULA, V. Use of Acoustic Emission Method for Identification of Fatigue Micro-cracks Creation. online. *Procedia Engineering*. 2015, roč. 133, s. 379-388. ISSN 18777058. Dostupné z: https://doi.org/10.1016/j.proeng.2015.12.667. [cit. 2023-12-19].

[44] NOHÁL, L; HORT, F; DVOŘÁČEK, J a MAZAL, P. An experimental investigation of rolling contact fatigue of steels using acoustic emission method. online. *Insight - Non-Destructive Testing and Condition Monitoring*. 2013, roč. 55, č. 12, s. 665-669. ISSN 13542575. Dostupné z: https://doi.org/10.1784/insi.2012.55.12.665. [cit. 2020-07-18].

[45] MAHMOUD, Houssam; MAZAL, Pavel a VLASIC, Frantisek. Relationship between acoustic emission signal and loads on pneumatic cylinders. online. *Nondestructive Testing and Evaluation*. 2020, roč. 35, č. 2, s. 222-238. ISSN 1058-9759. Dostupné z: https://doi.org/10.1080/10589759.2019.1662900. [cit. 2021-03-15].

[46] WOO, S a GOO, N. Analysis of the bending fracture process for piezoelectric composite actuators using dominant frequency bands by acoustic emission. online. *Composites Science and Technology*. 2007, roč. 67, č. 7-8, s. 1499-1508. ISSN 02663538. Dostupné z: https://doi.org/10.1016/j.compscitech.2006.07.023. [cit. 2023-12-10].

[47] LI, L.; DENG, J.; ZHENG, L. a LIU, J. Dominant Frequency Characteristics of Acoustic Emissions in White Marble During Direct Tensile Tests. online. *Rock Mechanics and Rock Engineering*. 2017, roč. 50, č. 5, s. 1337-1346. ISSN 0723-2632. Dostupné z: https://doi.org/10.1007/s00603-016-1162-2. [cit. 2023-11-22].

[48] ZHANG, Zhenghu; MA, Ke; LI, Hua a HE, Zhiliang. Microscopic Investigation of Rock Direct Tensile Failure Based on Statistical Analysis of Acoustic Emission Waveforms. online. *Rock Mechanics and Rock Engineering*. 2022, roč. 55, č. 4, s. 2445-2458. ISSN 0723-2632. Dostupné z: https://doi.org/10.1007/s00603-022-02788-w. [cit. 2023-11-22].

[49] ZHU, Jun; DENG, Jianhui; PAK, Ronald; LIU, Jianfeng a LYU, Cheng. Experimental study on the failure process of water-bearing rock under uniaxial tension based on dominant frequency analysis of acoustic emission. online. *Bulletin of Engineering Geology and the Environment*. 2023, roč. 82, č. 6. ISSN 1435-9529. Dostupné z: https://doi.org/10.1007/s10064-023-03246-9. [cit. 2023-11-22].

[50] WANG, Chunlai; CAO, Cong; LIU, Yubo; LI, Changfeng; LI, Guangyong et al. Experimental investigation on synergetic prediction of rockburst using the dominant-frequency entropy of acoustic emission. online. *Natural Hazards*. 2021, roč. 108, č. 3, s. 3253-3270. ISSN 0921-030X. Dostupné z: https://doi.org/10.1007/s11069-021-04822-6. [cit. 2023-11-22].

[51] ZHANG, Hexing; LU, Kunpeng; ZHANG, Wuzhou; ZHOU, Yu; YANG, Gui et al. A comprehensive study of damage characteristics and acoustic emission response mechanism of sandstone with different water contents. online. *Engineering Fracture Mechanics*. 2023, roč. 288. ISSN 00137944. Dostupné z: https://doi.org/10.1016/j.engfracmech.2023.109392. [cit. 2023-11-22].

[52] NIU, Yong; ZHOU, Xiao-Ping a BERTO, Filippo. Temporal dominant frequency evolution characteristics during the fracture process of flawed red sandstone. online. *Theoretical and Applied Fracture Mechanics*. 2020, roč. 110. ISSN 01678442. Dostupné z: https://doi.org/10.1016/j.tafmec.2020.102838. [cit. 2023-12-10].

[53] ZHANG, Zheng-Hu a DENG, Jian-Hui. A new method for determining the crack classification criterion in acoustic emission parameter analysis. online. *International Journal of Rock Mechanics and Mining Sciences*. 2020, roč. 130. ISSN 13651609. Dostupné z: https://doi.org/10.1016/j.ijrmms.2020.104323. [cit. 2023-12-10].

[54] LEI, Ruide; ZHANG, Zhenyu; BERTO, Filippo; RANJITH, P.G. a LIU, Li. Cracking process and acoustic emission characteristics of sandstone with two parallel filled-flaws under biaxial compression. online. *Engineering Fracture Mechanics*. 2020, roč. 237. ISSN 00137944. Dostupné z: https://doi.org/10.1016/j.engfracmech.2020.107253. [cit. 2023-12-10].

[55] SKF GROUP, . Valivá Ložiska. In: . PUB BU/P1 17000/1 CS, 2019, s. 842 - 875.

[56] LAURIAN, Tiberiu; TUDOR, Andrei; MAFTEI, Costel; TURCAN, Doru a KRAFT, Gabriel. SKF TOROIDAL ROLLER BEARING CARB – PRODUCTIVITY IMPROVEMENT AND MAINTENANCE COST REDUCTION THROUGH RELIABILITY AND SUSTAINABILITY. *Academica Brancusi*. 2010, roč. 1, č. 5, s. 7-14. ISSN 1844-640X.

[57] ZHANG, Luo; MA, Bo a FU, Jing. Design of Mould on Cold Rolling for CARB Bearing's Arc Roller. online. *Advanced Materials Research*. 2012, roč. 424-425, s. 838-843. ISSN 1662-8985. Dostupné z: https://doi.org/10.4028/www.scientific.net/AMR.424-425.838. [cit. 2023-12-12].

[58] FRITZSON, Dag; FRITZSON, Peter; NORDLING, Patrik a PERSSON, Tommy. Rolling Bearing Simulation On Mimd Computers. online. *The International Journal of Supercomputer Applications and High Performance Computing*. 1997, roč. 11, č. 4, s. 299-313. ISSN 1078-3482. Dostupné z: https://doi.org/10.1177/109434209701100404. [cit. 2023-12-12].

[59] BENCHEA, M a CREţU, S. Surface roughness influence on active surfaces geometry and modified rating life of rolling contacts. online. *IOP Conference Series: Materials Science and Engineering*. 2020, roč. 724, č. 1. ISSN 1757-8981. Dostupné z: https://doi.org/10.1088/1757-899X/724/1/012025. [cit. 2023-12-13].

[60] MBA, D. Acoustic Emissions and Monitoring Bearing Health. online. *Tribology Transactions*. 2003, roč. 46, č. 3, s. 447-451. ISSN 1040-2004. Dostupné z: https://doi.org/10.1080/10402000308982649. [cit. 2020-02-23].

[61] XIE, Qiang; WU, Zhihui; BAN, Yuxin; FU, Xiang; CAO, Zhilin et al. The Experimental Investigation on Progressive Deformation of Shear Slip Surface Based on Acoustic Emission Measurements. online. *Arabian Journal for Science and Engineering*. 2022, roč. 47, č. 4, s. 5125-5138. ISSN 2193-567X. Dostupné z: https://doi.org/10.1007/s13369-021-06454-1. [cit. 2023-12-26].

[62] ZHANG, Zheng-Hu a DENG, Jian-Hui. A new method for determining the crack classification criterion in acoustic emission parameter analysis. online. *International Journal of Rock Mechanics and Mining Sciences*. 2020, roč. 130. ISSN 13651609. Dostupné z: https://doi.org/10.1016/j.ijrmms.2020.104323. [cit. 2023-07-30].

[63] NIU, Yong; ZHOU, Xiao-Ping a BERTO, Filippo. Temporal dominant frequency evolution characteristics during the fracture process of flawed red sandstone. online. *Theoretical and Applied Fracture Mechanics*. 2020, roč. 110. ISSN 01678442. Dostupné z: https://doi.org/10.1016/j.tafmec.2020.102838. [cit. 2023-07-30].

[64] LI, L.; DENG, J.; ZHENG, L. a LIU, J. Dominant Frequency Characteristics of Acoustic Emissions in White Marble During Direct Tensile Tests. online. *Rock Mechanics and Rock Engineering*. 2017, roč. 50, č. 5, s. 1337-1346. ISSN 0723-2632. Dostupné z: https://doi.org/10.1007/s00603-016-1162-2. [cit. 2023-07-30].

[65] ZHANG, Zhenghu; MA, Ke; LI, Hua a HE, Zhiliang. Microscopic Investigation of Rock Direct Tensile Failure Based on Statistical Analysis of Acoustic Emission Waveforms. online. *Rock Mechanics and Rock Engineering*. 2022, roč. 55, č. 4, s. 2445-2458. ISSN 0723-2632. Dostupné z: https://doi.org/10.1007/s00603-022-02788-w. [cit. 2023-11-22].

[66] SKC GROUP, . *CARB toroidal roller bearings*. online. In: Couldn't find publisher. 2022. Dostupné z: https://cdn.skfmediahub.skf.com/api/public/094bdeafb6b4ce5c/pdf_preview_medium/094bdeafb6b4ce5c_pdf_preview_medium.pdf#cid-600128. [cit. 2023-12-26].

[67] ISO. online. In: Couldn't find publisher. 2007. Dostupné z: https://www.iso.org/obp/ui/en/#iso:std:iso:22096:ed-1:v1:en. [cit. 2023-12-28].

[68] ISO. 1. 2017. Dostupné také z: https://www.iso.org/obp/ui/en/#iso:std:iso:16079:-1:ed-1:v1:en.

[69] ISO. 2. 2020. Dostupné také z: https://www.iso.org/obp/ui/en/#iso:std:iso:16079:-2:ed-1:v1:en.

[70] WELCH, P. The use of fast Fourier transform for the estimation of power spectra: A method based on time averaging over short, modified periodograms. online. *IEEE Transactions on Audio and Electroacoustics*. 1967, roč. 15, č. 2, s. 70-73. ISSN 0018-9278. Dostupné z: https://doi.org/10.1109/TAU.1967.1161901. [cit. 2023-12-15].

[71] MOHAMMAD, Housam; MAZAL, Pavel; VLASIC, Frantisek a MAYA, Baraah. Active Monitoring of RCF in Toroidal Bearings Using Acoustic Emission. online. In: JUUSO, Esko a GALAR, Diego (ed.). *Proceedings of the 5th International Conference on Maintenance, Condition Monitoring and Diagnostics 2021*. Lecture Notes in Mechanical Engineering. Singapore: Springer Nature Singapore, 2023, s. 73-81. ISBN 978-981-99-1987-1. Dostupné z: https://doi.org/10.1007/978-981-99-1988-8_6. [cit. 2023-12-12].

[72] AL-GHAMDI, A; COLE, P; SUCH, R a MBA, D. Estimation of bearing defect size with acoustic emission. online. *Insight - Non-Destructive Testing and Condition Monitoring*. 2004, roč. 46, č. 12, s. 758-761. ISSN 13542575. Dostupné z: https://doi.org/10.1784/insi.46.12.758.54491. [cit. 2020-04-16].

10 LIST OF FIGURES AND TABLES

10.1 List of Figures

10.2 List of Tables

10.3 List of abbreviations

#	Abb.	Name
	AE	Acoustic emission
	NDT	Non-Destructive testing
	RCF	Rolling contact fatigue
	TRB	Toroidal roller bearing
	SRB	Spherical roller bearing
	DF	Dominant frequency
	CM	Condition monitoring
	WT	Wind Turbine
	PPHD	Post processing hit detector
	RMS	Root mean squared
	ASL	Average signal level
	FFT	Fast Fourier transformation
	STFT	Short Time Fourier Transformation
	PSD	Power spectral density
	SCADA	Supervisory control and data acquisition system

IEPE	Integrated Electronics Piezo-Electro
VNC	Virtual Network Computing
3G	Third generation of digital mobile networks
ADC	Analog-to-Digital Converter
$< F >$	Average frequency
PF	peak frequency
CF	central frequency
$F_{centroid}$	Frequency centroid
F_{rev}	Reverberation frequency
F_{init}	Initiation frequency
t_0	Time of first threshold crossing (arrival time)
N_{AE}	Number of threshold crossings (Counts)
t_{AE}	Time between first and last threshold crossing of signal
U_{max}	Maximum signal voltage
t_{peak}	Time of maximum signal voltage
f_{peak}	Frequency of maximum signal contribution
N_{peak}	Number of threshold crossings between t0 and t_{peak}
W_{AE}	Absolute energy
N_{peak}	Count to peak
t_{AE}	Duration
dB_{AE}	Amplitude of AE
ΔS	Reduction in radial bearing clearance
K_δ	Operating clearance factor, (according to dimension)
δax	Axial displacement
Kφ	Tilting factor, (from dimension tables)
φ °	Tilting between inner ring and outer ring.
ΔS	Reduction in radial bearing clearance
S_φ	Reduction in axial displacement facility as a result of tilting.
S_{res}	Resulting bearing clearance after tilting and axial displacement
S_{ini}	Radial internal clearance after mounting
S_1	Maximum axial displacement facility, in the case of full complement bearings, this is in the opposing direction to the retaining ring.
S_2	Maximum axial displacement facility, in the case of full complement bearings, this is in the direction to the retaining ring.
k_δ	Operating clearance factor, (from dimension table)
δ_{ax}	Axial displacement from central position
$V(t)$	Time-varying signal voltage
CARB™	Compact Aligning Roller Bearing – a product of SKF
HRC	Rockwell scale hardness
FMSA	Failure Mode Symptoms Analysis